Numerical Simulations and Optimization Analysis of the Heat Transfer in Piezoelectric Fans

Siming Zhang

Queen Mary University of London

Submitted in partial fulfilment of the requirements of the Degree of Doctor of Philosophy

School of Engineering and Materials Science
Queen Mary University of London

September 2018

Declaration

I, Siming Zhang, confirm that the research included within this thesis is my own work or that where it has been carried out in collaboration with, or supported by others, that this is duly acknowledged below and my contribution indicated. Previously published material is also acknowledged below.

I attest that I have exercised reasonable care to ensure that the work is original, and does not to the best of my knowledge break any UK law, infringe any third party's copyright or other Intellectual Property Right, or contain any confidential material.

I accept that the College has the right to use plagiarism detection software to check the electronic version of the thesis.

I confirm that this thesis has not been previously submitted for the award of a degree by this or any other university.

Signature:

Date:

Abstract

A combined theoretical/computational study is performed to investigate an innovative cooling technology using piezoelectric actuators. The piezoelectric fan is an ultra-low energy air mover which induces unsteady periodic flow. This study focuses on the characteristics of the fluid flow and heat transfer as well as system optimisation in terms of the operational parameters of the piezoelectric fan blade. Regarding the dynamics of piezoelectric fan movements, the fan blades vibrate as a wave-like motion. The fan blade can be simplified as a homogeneous viscoelastic beam with uniform cross-section. In the theoretical analysis, the method of complex orthogonal decomposition is adopted to analyse the blade motions, and the travelling index is proposed to evaluate the curvature of piezoelectric fan blade. The unsteady fluid flow and heat transfer have been studied by computational fluid dynamics based on three-dimensional large-eddy simulation. A parametric study has been performed to investigate the effects of three dynamic parameters of the blade oscillation: oscillating frequency, oscillating amplitude and wave number. In the heat transfer study, a heat source represented by a high temperature wall is added to the computational model. The temperature and the surface Nusselt number of the hot wall serve the purpose of evaluating the characteristics of heat transfer. It is found that the oscillation frequency and amplitude have significant impacts on the fluid flow and heat transfer. In addition, the response surface method facilitates the process of finding the optimal operational parameters of piezoelectric fans. Considering practical limitations imposed by fan geometries and materials, factors determining the optimal operational parameters are outlined as the theoretical optimal operational parameters may not be achievable in practical applications. The results and analyses provide fundamental knowledge to guide the design of a piezoelectric fan system for cooling applications.

Acknowledgements

First of all, I would like to thank my supervisor Prof. Xi Jiang with the opportunity to undertake such an interesting project, and for his invaluable guidance and help throughout my studies. I learnt from him not only about academic research but also life experiences, and I really appreciate all his great supports and encouragements.

I would also like to thank Dr. Alastair Hales, who has helped me with research methods and we always had great discussions for progressing the research.

I am very grateful for the assistance provided by my colleagues and staffs both from the Queen Mary, University of London and Lancaster University. They helped me especially when I had problems. It was a pleasure to work with all of them.

Finally, I sincerely appreciate the support and encouragement offered by my friends and family, particularly for my Mum, Dad, Aunt and Uncle, for the courage they give me to move forward, for the hours of discussion and advice!

Contents

Nomenclature

A	Amplitude of the piezoelectric fan vibration	m
A_{XC}	Area of fan cross-section	m^2
Br	Brinkman number	[dimensionless]
C_s	LES model coefficient	[dimensionless]
$\mathrm{cond}(\mathbf{T})$	Condition number of $\mathbf{T}$	[dimensionless]
D_c	The magnitude coefficient	[dimensionless]
E	Young's modulus	Pa
f	Oscillating frequency	Hz
f_r	Resonant frequency of piezoelectric fan	Hz
G	Filter convolution kernel	[dimensionless]
$H(x)$	The amplitude envelope	m
$\mathrm{H}(y_m(t))$	Hilbert transform of $y_m(t)$	[dimensionless]
h	Sensible enthalpy of ideal gases	kJ/kg
h_c	Convective coefficient of heat transfer	[dimensionless]
I	Second moment of area	m^4
$\mathrm{imag}(\mathbf{w})$	Imaginary part of $\mathbf{w}$	[dimensionless]
$\vec{J_j}$	Diffusion flux of species j	$mol \cdot m^{-2} \cdot s^{-1}$
$\mathbf{K}$	Matrix of fan movements	[dimensionless]
k	Wave number	[dimensionless]
k_{eff}	Effective conductivity	W/(m·K)
k_t	Thermal conductivity of fluid	W/(m·K)
k	Wave number	[dimensionless]
L	Length of piezoelectric fan	m
L_{PZT}	The PZT length	m
$L_y(x,t)$	Flow-induced lateral force	N
$M(x,t)$	Actuation moment	N·s
$M_b(x,t)$	Bending moment	N·s
M_e	Resistance moment due to elasticity	N·s
M_v	Resistance moment due to viscosity	N·s

$m_a(x)$	Added mass	kg
Nu	Nusselt number	[dimensionless]
n	The value at the current time level, t	[dimensionless]
$n+1$	The value at the next time level, $t+\Delta t$	[dimensionless]
$n-1$	The value at the previous time level, $t-\Delta t$	[dimensionless]
p	Pressure	Pa
real($\mathbf{w}$)	Real part of $\mathbf{w}$	[dimensionless]
$S(x,t)$	Shear force	N
$(\mathbf{S}, \mathbf{y}_s)$	Sampled data sets in the vector space	[dimensionless]
S_h	Volumetric heat source	J/m^3
$\bar{S}_{ij}$	Resolved strain rate tensor	N/m^2
T	Temperature	°C
ΔT	Temperature difference	°C
t	Time	s
t_h	Thickness	m
t_n	Instant time during one oscillating period ($n = 1,2, \dots \dots N$)	s
U_{conv}	Convective velocity	m/s
u	Velocity defined in the x direction	m/s
u_b	Flow velocity u on the boundary	m/s
u_i	Velocity components in the corresponding directions	m/s
u_x^-	3-point backward difference	[dimensionless]
u_x^+	3-point forward difference	[dimensionless]
$V(t)$	Oscillating velocity at the inlet boundary	m/s
v	Velocity defined in the y direction	m/s
v_b	Normal velocity v on the boundary	m/s
W	Full width of piezoelectric fan	m
W_{PZT}	The PZT width	m
w	Velocity defined in the z direction	m/s
$\mathbf{w}_m$	Complex eigenvectors	[dimensionless]
x_m	Fan location along the axial direction ($m =$	m

	$1,2,\ldots\ldots M$)	
Δx	Local grid size in the x direction	m
x	Distance along the beam length	m
Y_j	Mass fraction of species j	[dimensionless]
$\hat{y}(\mathbf{x})$	Polynomial approximation	[dimensionless]
$y_m(t_n)$	Component of matrix **K** at the row m and the column n	[dimensionless]
$\mathrm{y}(x,t)$	Periodic movements of piezoelectric fan	m
Δy	Local grid size in the y direction	m
Δz	Local grid size in the z direction	m

Greek:

γ	The value of step size at each iteration	s
$\overline{\Delta}$	Filter size of LES model	[dimensionless]
δ_{ij}	Kronecker's delta	[dimensionless]
ε	Random error	[dimensionless]
ζ	Travelling index	[dimensionless]
λ_m	Real eigenvalues	[dimensionless]
ν_t	Turbulent eddy viscosity	Pa·s
ν	Viscosity	Pa·s
ρ	Density of fan material	kg/m^3
ρ_f	Density of fluid flow	kg/m^3
σ	Poisson's ratio of fan material	[dimensionless]
σ^2	Variance of sampled data	[dimensionless]
$\tau_{i,j}^d$	Deviatoric part of sub-grid scale stresses	[dimensionless]
φ	Phase of fan motions	rad
ω	Oscillating frequency	rad/s

List of Figures

List of Tables

List of Abbreviations

CFD	Computational Fluid Dynamics
CFL	Courant-Friedrichs-Lewy
CMOS	Complementary Metal Oxide Semiconductor
COD	Complex Orthogonal Decomposition
CP	Counter-phase
CPU	Central Processing Unit
DNS	Direct Numerical Simulation
GEK	Gradient-Enhanced Kriging
IP	In-phase
IT	Information Technology
LES	Large Eddy Simulation
LUD	Linear Upwind Differencing
N-S	Navier-Stokes
PC	Personal Computer
PE	Piezoelectric
PET	Polyethylene Terephthalate
PETSc	Portable, Extensible Toolkit for Scientific Computation library
PVC	Polyvinyl Chloride
PVF2	Polyvinyl Fluoride
PZT	Lead Zirconate Titanate
RK2	Second Order Runge-Kutta
RSM	Response Surface Methodology
3D	Three Dimensional

Chapter 1

Background

1.1 Introduction

Power electronics such as computers and servers use more and more energy. Taking the worldwide data centres as examples, the electricity consumption from 2000 to 2010 has increased from 71 billion kWh per year to 238 billion kWh per year (Koomey, 2008; Koomey, 2011). Compared with the electricity consumption of all sectors, the consumption growth of data centres is roughly 11% per year (labelled by symbol △), while 3% growth of all sectors (labelled by symbol □) as shown in Figure 1.1. Besides, the ratio between the electricity usage of data centres and the total electricity usage increased from 0.53% in 2000 to 1.31% in 2010 (Agency, 2010).

Nowadays, the growing demand of IT industry exceeds the technology development in energy management. During the year 2003 to 2008, the total energy consumption of computer servers has doubled, although there is a temporary slowdown (due to the global economic crisis) (Turner et al., 2009). IT equipment has made a great contribution to the global energy use, and such growth of energy consumption would continue in the future.

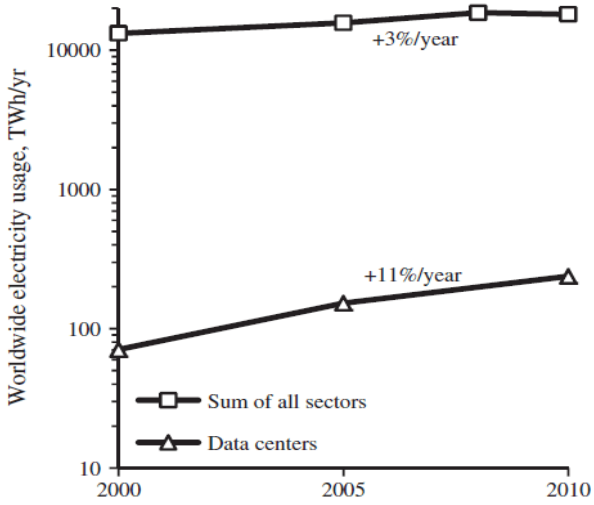

Figure 1.1: The growth rate of worldwide electricity usage from 2000 to 2010 (Koomey 2008; Koomey 2011; Agency,2010)

For current data centres, the available statistics demonstrate that 12% of the total operating cost is the energy cost, which is the fastest growing expenditure (Gartner, September 29, 2010). Even for the mobile and personal computing devices, their energy consumption also grows rapidly due to the rapidly growing market (Horvath and Masanet, 2007).

Although the energy consumption issue especially for cooling has been a rising concern, an effective approach is not yet available to deal with the thermodynamics problem of denser packaging. Figure 1.2 shows the distribution of power consumption in a data centre (Yole Développement, 2016). The cooling system consumes about 35% of the energy power, while the IT load consumes about 40% of power. The data in Figure 1.2 demonstrates that a more advanced cooling system is required. To design an excellent cooling system, a preferable solution is to design an individual cooling device with optimal performance of heat transfer. From a view of technological point, not only the heat transfer should be paid attention to, but the heat flux should also be controlled.

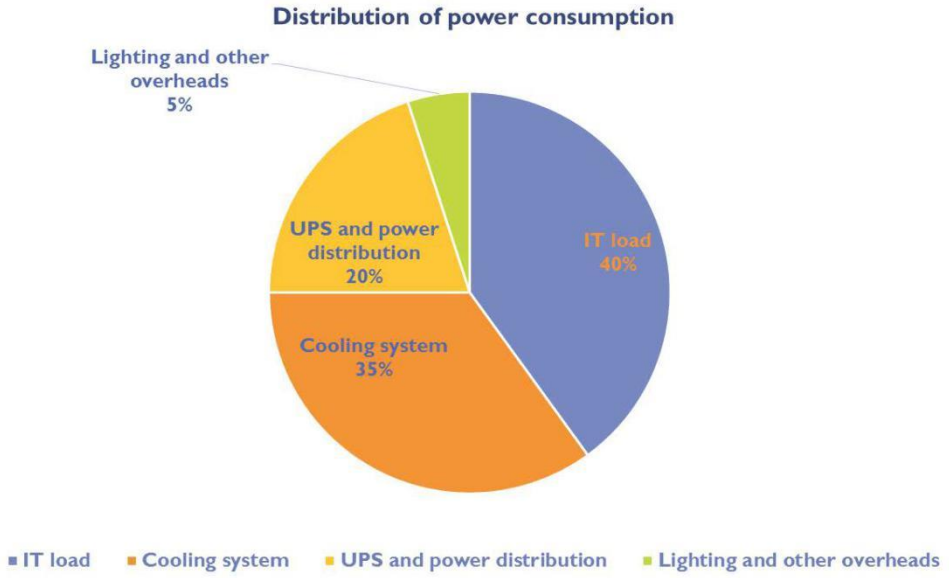

Figure 1.2: Distribution of the power consumption in the data centre (Yole Développement, 2016)

In the history of cooling technology, there are three development stages: (1) During the mid-1970s to 1980, the thermal management is inside the equipment; (2) The period 1980-1985, the representative work is the liquid cooling of bipolar transistor processors (Schmidt, 2005), in which the maximum power density is about 14 W/cm^2; (3) The period 1985–2000, the air cooling CMOS (Complementary Metal Oxide Semiconductor)

technology emerged and applied in the smaller scales and hot spots, which has replaced the bipolar cooling technology. Taking the hot spots as an example (Sri-Jayantha et al., 2008), a 40×40 mm^2 quad-core processor chip (the average heat flux 50 W/cm^2) can cause the local temperature with an increase of 30–40 ℃. By adopting the CMOS technology, the local heat transfer rate is high enough to maintain lower temperature, with heat flux of about 0.1 W/cm^2.

With the current trend of demand for highly sophisticated electronic equipment, there is an increasing power density on these devices. Heat flux increases exponentially as the power density of a component increases, and the problem related to the heat transfer is another important part of thermal management. The high-performance devices can only operate close to the allowable thermal limit. If the increase of heat flux is ignored, the component will be less reliable or even broken. Another complexity is associated with the packaging of electronic components, which is essential to their performance and system assembly. However, the thermal constraints in the electronics packaging are more complicated because of lacking conduction path. Therefore, improving cooling effectiveness can ultimately improve performance of the devices.

Although massive heat is generated from power electronics, the cooling solution to deal with the heat dissipation is lacking. For electronics cooling, thermal management solutions include forced air cooling, oil cooling and water cooling. The conventional methods of thermal management can be classified into passive and active methods. Passive methods include finned heat sink, heat pipes and phase change materials. They do not need power for operation and generate low noise. However, passive heat transfer methods are bulky and require more space, and hence have limited use in small size electronic devices. Heat sink is the most preferred method due to their simplicity of implementation (Ma et al., 2009; Ma et al., 2012c). On the other hand, active methods such as rotational fans, refrigeration cycles and liquid cooling systems offer a viable solution for heat removal from electronic devices. However, the PE fan has much lower energy consumption compared to those active methods.

In thermal management, the innovation that consumes the lowest power has become the preferred choice of heat management. Piezoelectric (PE) fan is emerging as the next big thing for the small size electronic devices cooling system. Their small size, low power consumption and low noise generation make them the best alternative for small electronic devices (Ma et al., 2012b; Zhang et al., 2011). A large number of studies have been

presented for heat dissipation of piezoelectric fan, e.g. (Ma et al., 2009; Ma et al., 2012c; Ma et al., 2012b; Zhang et al., 2011). In this thesis, the piezoelectric fan and its feasibility in cooling electronic components are investigated, where the characteristics of air flows generated by piezoelectric fan and the heat transfer characteristics will be studied.

1.2. The piezoelectric fan

1.2.1 Piezoelectricity

In certain crystalline materials, the piezoelectricity is the electric charge that resulted from the applied mechanical stress (Skoog et al., 2017). The piezoelectric effect is a reversible process, which is also defined as an interaction between mechanical state and electrical state (Gautschi, 2002). When piezoelectric material is squeezed, electrical charge collects on its surface. When the material is subject to electric field, it exhibits mechanical deformation. Piezoelectric effect is considered as transferring electrical energy to mechanical energy.

Piezoelectricity was first discovered in the 1880s in a single crystal of quarts by Jaques Curie and Pierri Curie (1880). Many researches on the piezoelectricity have been inspired by the discovery of ferroelectric ceramics, such as lead zirconate titanate (PZT), and polymer polyvinylidene fluoride. These materials have attracted engineers to design different types of piezoelectric devices, including transducers, actuators and sensors, etc., and they are widely used in the industrial and manufacturing market (Manbachi and Cobbold, 2011).

During the 1930s, the piezoelectric actuators were invented, which is much earlier than the idea of piezoelectric fan. Evolving from the piezoelectric actuators, the piezoelectric fan was made of piezoelectric layers, and actuated by a square wave signal (Kim et al., 2005). Air-flow is then generated with a certain velocity, with a very small consumption of power. Toda and Osaka found that the cooling effect of piezoelectric fan was 50%, which is much higher than the conventional radial fan (Toda and Osaka, 1979).

For any actuator, it can be defined as a device with the ability to transform energy into a controllable motion. These motions can be described by the displacement, frequency, force and electrical power input, etc. By contrast, the piezoelectric actuator can operate at

an excellent bandwidth and generate considerable force (Kimber and Garimella, 2007). The performance of piezoelectric actuators is usually determined by free deflection and blocking force. Specifically, the free deflection is the maximum deflection obtained at the maximum rated voltage when the actuator vibrates freely; the blocking force is the maximum force that an actuator can exert when the maximum recommended voltage is applied, and the actuator is completely blocked with zero deflection (Gilson et al., 2013; Challa et al., 2008; Petroski et al., 2010).

In general, there are four different available types of piezoelectric actuators, and they are listed as follows:

(1) Unimorph actuator: this actuator is formed by attaching a composite beam with one active layer and one inactive substrate.

(2) Stack actuator: a large number of piezo layers are stacked up linearly to form this type of actuator. It improves deflection abilities with a low voltage requirement.

(3) Bimorph actuator: this actuator is formed by bonding two thin ceramic plates together with opposite electric field. The lateral deflection of actuator results from the alternate contraction and expansion of the plates. Figure 1.3 shows both series and parallel connections can be used to fabricate the piezoelectric bimorph. Two piezoelectric plates with serial connection have opposite polarisation directions, while two piezoelectric plates have similar polarisation directions when the connection is parallel.

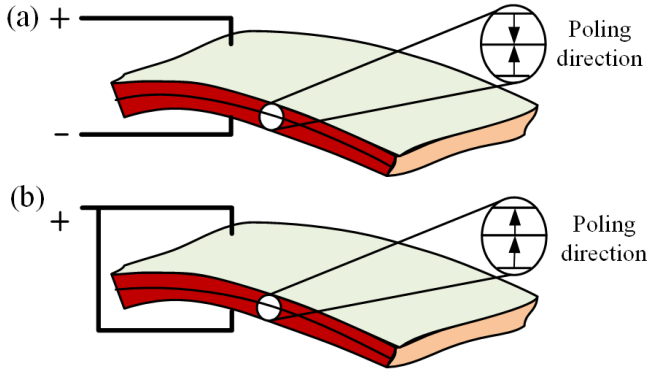

Figure 1.3: Bimorph Piezoelectric patches (a) bimorph in series and (b) bimorph in parallel connections

(4) Shear actuator: it is very difficult for the actuation mechanism of shear actuator to produce a transverse shear strain. This type is hard to make and not popular.

For all these piezoelectric actuators, one of the unique characteristics is their ability to expand and contract when an alternating voltage is applied to their electrodes. This is

the basic operating principle of piezoelectric fan, whereby the application of alternating current makes the PZT patch expand and contract alternately at the same frequency.

1.2.2 Piezoelectric fan

In essence, the piezoelectric fan is an air mover with ultra-low power consumption. It is made up of an elastic plate, the piezoceramic patches and electrodes, which as shown in Figure 1.4. During the operation, the alternating electrical current is applied to the electrodes of piezoelectric fan, and the expansion and contraction forces are produced to generate the reciprocating oscillation. When it is actuated at its resonance frequencies, a larger oscillation amplitude of fan is obtained to disturb the surrounding air-flow sufficiently. Vorticity is then generated, and heat transfer is realised through the interactions between air-flow and the piezoelectric fan.

The concept of piezoelectricity applies to realise deflection on a flexible plate, enough to cause air flow. The stress of the actuator is perpendicular to the direction of the electric field. When a positive electric field is implemented to the PZT actuator, the actuator contracts; when a negative electric field is applied, the PZT actuator expands. Since the steel plate is attached to the side of a piezoelectric actuator, the steel contacts, and the PZT expands. When an alternating current is applied, the elongated flexible plate will operate like a flapping fan to generate air flow.

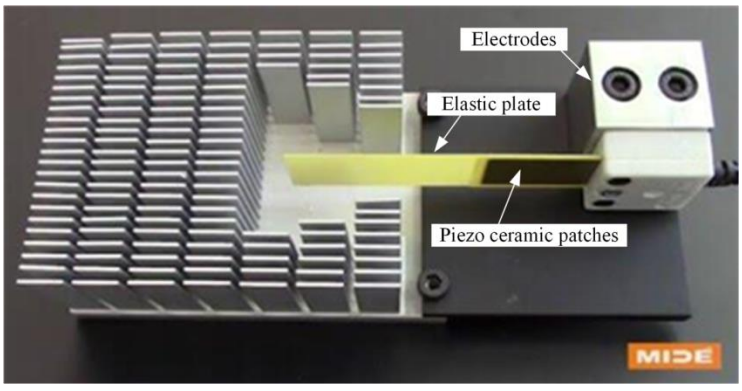

Figure 1.4: The operation condition of piezoelectric fan (MIDE Technology, 2016)

Piezoelectric fan is manufactured by bonding one or several PZT patches to a sheet, which is elastic and can be deformed easily. The patch can be placed on any side of the

elastic sheet if only one plate is in use. In a two-patch configuration, the elastic sheet is sandwiched between the two patches, such that when one expands, the other contracts. The elastic sheet could be either plastic or copper which acts as a cantilever beam. When an alternating current actuates the patch, there is a slight deformation of the patch, which results to the patch of expanding and contracting alternately. Consequently, the attached ultra-thin sheet flaps back and forth. The flapping motion generates air flow for cooling electronic devices.

Besides, researchers are now also focusing on using multiple piezoelectric fans to work together with finned heat sinks. The idea of two PZT fans was firstly proposed by Petroski et al. (2010). Multiple piezoelectric fan system is an array of several PZT fans, which have a high potential for electronic cooling, as shown in the right-hand side of Figure 1.5. However, the drawback of multiple piezoelectric system is that all piezoelectric fans are powered separately (Ma et al., 2014b). Hence, the compounding power usage becomes the primary concern of the power consumption, which is distinct from the conventional rotary fans.

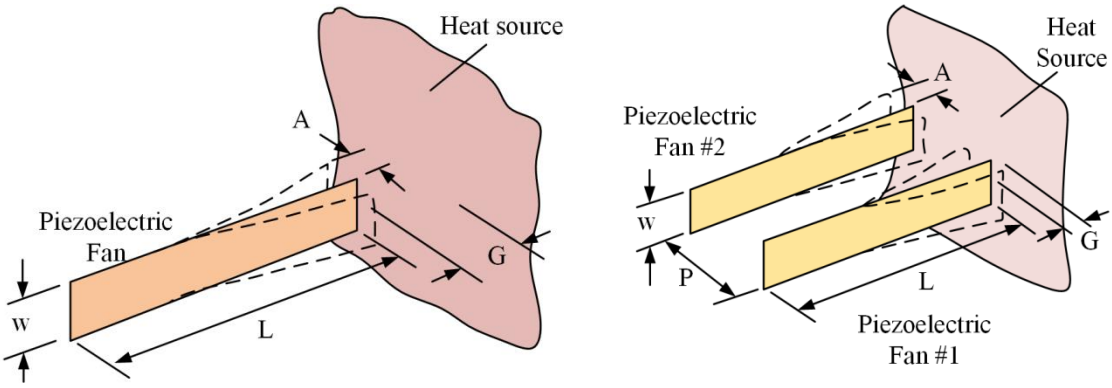

Figure 1.5: Multiple piezoelectric fan system

1.3 The development of piezoelectric fan

Piezoelectric fans have many advantages over the traditional cooling devices, such as the small size, long life, low noise generation, and low power consumption, etc. In the 1980s, the piezoelectric fan is firstly used in cooling application by Toda (1978; 1981). Eight layers of PVF2 (Polyvinyl fluoride) were used to fabricate the piezoelectric fan with a voltage of 140V at a frequency of 13 Hz. The experimental results show that the temperature of the panel surface decreased by 17°C.

In 2000, Yoo et al. (2000) tested several piezoelectric fans with different metal plates at 60 Hz with an application of 110V and 220V. The results showed that when the geometry parameters of the PZT plate were kept constant, the resonant frequency decreased with the plate length. Additionally, Acikalin et al. (2007) tested several parameters of piezoelectric fan to assess the cooling ability, and these parameters includes fan orientation, fan amplitude, length, frequency, and the distance between piezoelectric fan and heat source. The results demonstrated that the most crucial parameters for fan design were blade oscillation frequency and amplitude.

Recently, multiple piezoelectric fans have been used in the cooling system to increase heat transfer capabilities. In 2010, Petroski et al. (2010) proposed piezoelectric fan with two PZT fans, and the results showed that this system could transfer heat five times greater than a finned heat sink with natural conventions. Schmidt (1994) did the experiments of a vertical surface cooled by two piezoelectric fans and found that the characteristics of heat transfer can be significantly changed by varying the distance between the two fans as well as the distance between the fans and the heat source. Besides, Choi et al. (2012) use a discrete vortex method to develop a CFD model of piezoelectric fan, in which the flow field around the fan tips is simulated through a numerical approach.

Multiple PZT fan system is another direction of research, in which a vibrating multiple fan is preferred. The system takes advantage of both piezoelectric and magnetic force, and the power consumption requirement is relatively low. For a multiple fan that is made up of four passive magnetic fans and excited by a single PZT fan, Ma et al. (2013) investigated the effects of vibrating frequency, the position between fan and sink, power consumption, applied voltage and geometries of the fan. It was found that a combination of piezoelectric fan and magnetic fan produced a total amplitude of more than 400% compared with that of a single piezoelectric fan consuming the same power. Besides, Su et al. (2013) also investigated a system of miniature multiple fans that uses the piezoelectric and magnetic forces, and their results demonstrated that with the operational frequency of 36.4 Hz, the power consumption was only 0.08W. The temperature of the heat sink drops to 17°C when the fans operate 10 minutes.

1.4 The characteristics of piezoelectric fan

In general, piezoelectric fan can be regarded as a vibrating beam, which is actuated by

an alternating input signal. It consists of a flexible fan blade with the piezoelectric element bonding on it. The actuation of the piezoelectric material generates forces in the piezoelectric element, leading to the blade vibrations and the particular fan motions. Moreover, the interactions between the vibrating fan blade and the surrounding fluid flow enhance the heat transfer characteristics. It is vital that the vibrating frequency of piezoelectric fan is close to its resonance frequency (i.e. the first modal frequency), because a larger vibration amplitude can be easily obtained under this condition, even with small input power.

The devices of piezoelectric fan have a vast potential in the cooling applications, due to their unique advantages, such as the low power consumption, low noise, and long life. For now, the vibrations of piezoelectric fan coupled with heat transfer have triggered wide discussions in the literature (Maaspuro, 2016; Hales and Jiang, 2018b). In the following section, the fluid field, the shape optimisation and heat transfer characteristics and the movements of piezoelectric fan have been summarised, and some limitations of these studies are also presented.

1.4.1 Flow field

The vibration model of multi-layered piezoelectric polymers was proposed in 1980s (Toda, 1978; Toda, 1981), which is used to analyse the fluid field around vibrating cantilevers. Ihara and Watanabe (1994) studied the flow velocity at three different positions downstream of piezoelectric fan by adopting the flow visualisation and numerical techniques. Their results predicted that the fan tip speed approximately equals to the time-averaged flow velocity at a distance 3mm away from the free end of piezoelectric fan. For the flow field, Kim et al. (2004) found that the counter-rotating vortices appeared with a high velocity, which was shedding from the tip of piezoelectric fan. Further, Acikalin (2007) conducted the two-dimensional flow visualisation experiments, and the results demonstrated that the piezoelectric fan had the best performance when it was operated at the first resonance modes. However, when the piezoelectric fan was operated at other higher resonance modes, the consumed power would increase significantly, and the velocity of air around it would also drop dramatically.

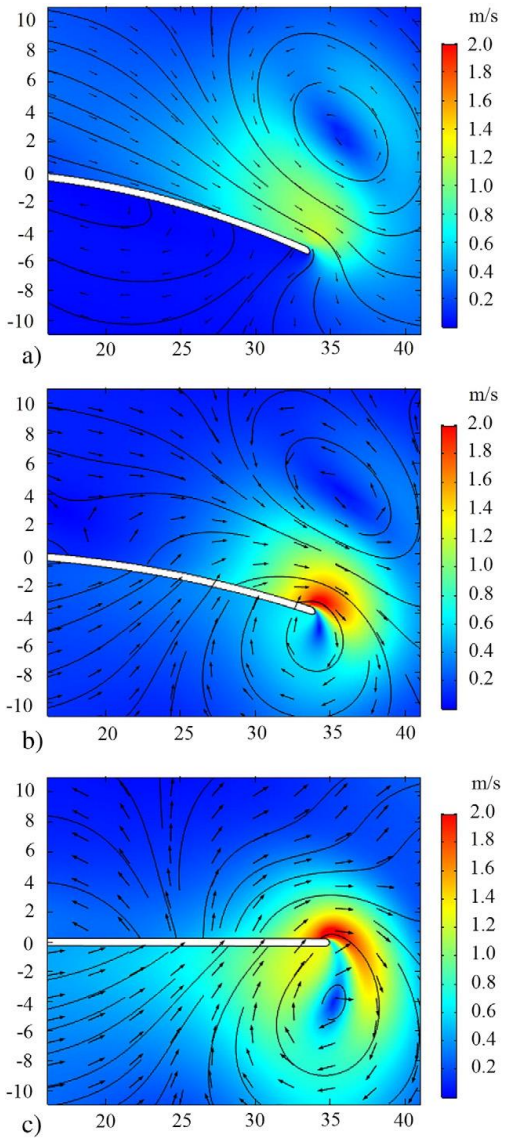

Figure 1.6: 2D CFD simulations of the piezoelectric fan (Maaspuro, 2016).

Computational fluid dynamics (CFD) can be used to study the flow field induced by piezoelectric fan oscillation. In Figure 1.6, there are two vortices that are generated with opposite rotating directions. One at the upper side of the PE fan referred as the pressure side, and the other at the down side of the PE fan referred as the suction side, which is shown in Figure 1.6 (Maaspuro, 2016). In Figure 1.6 (a), the oscillating amplitude of the PE fan is at its maximum. At the moment of maximum amplitude, the direction of the beam movement changes. In Figure 1.6 (b), the PE fan starts to move upwards, which is from its current suction side to the current pressure side. The vortex on the pressure side becomes smaller until it disappears, while the other one gets larger. Finally, in Figure 1.6 (c), the PE fan reaches the middle position, at that moment, the amplitude is 0 and the pressure side

becomes the suction side, and the cycle repeat itself. After that, the movements of piezoelectric fan change in an opposite direction, and the pressure side turns into the suction side. The characteristics of the flow field repeat with the fan oscillation period.

1.4.2 Shape optimisation of piezoelectric fan

The optimisation of fan shape, as well as the physical model of piezoelectric fan, has been studied widely in the literature. For instance, Burmann et al. (2002) used the lumped parameter method to develop a symmetric piezoelectric fan model, in which the design guidelines and the optimisation of fan tip deflection were presented. Different from that, Sheu et al. (2008) studied the model of an asymmetric piezoelectric fan, and the resonance frequencies of fan were analysed by solving a transcendental equation. Moreover, Basak and Raman (2007) adopted the composite beam theory and Hamilton's principle to analyse the dynamic profile of piezoelectric fans, which have either symmetric or asymmetric configurations.

Similar to the vibrations of the beam, the resonance frequencies of piezoelectric fan decrease within the fan length, which is always restricted by the space of the cooling device. However, the influence of fan width is much more complicated. The piezoelectric fan can be designed with variable blade width to improve the characteristics of heat transfer, which would change the flow field directly, such as the flow velocity, the streamlines and the vortices generated. For example, Lin et al. (2016) developed different types of piezoelectric fans, which have non-uniform width and the same oscillation frequencies and amplitudes. The results are analysed in terms of air propulsion and vortex generation. In Figure 1.7, a noticeable difference is shown in the vortex generation of Fan E. The cases of Fan A, Fan B, Fan C, and Fan D have similar results, because the streamlines that is close to the fan tip have been dragged back, which made a significant contribution to the vortices generation. This phenomenon disappears for the case of Fan E.

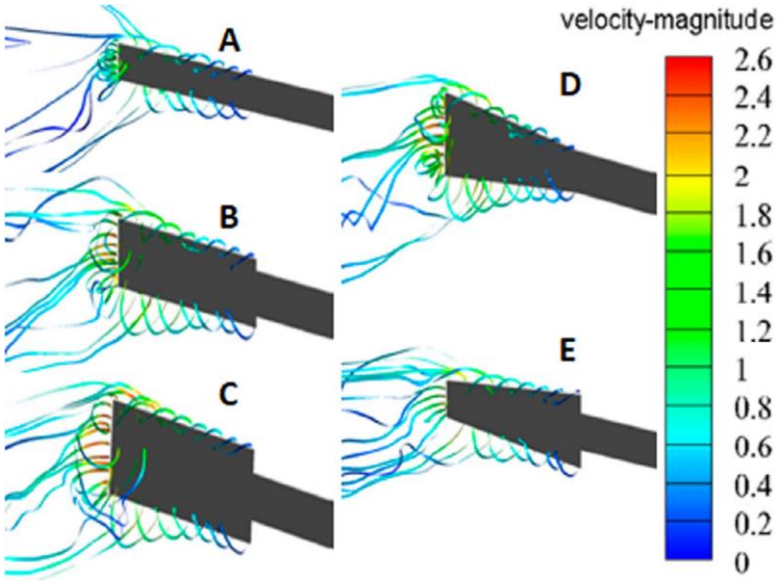

Figure 1.7: The streamlines of piezoelectric fan vary with shape geometry (Lin et al., 2016).

1.4.3 Heat transfer

The technology of piezoelectric fan offers massive opportunity to save energy in different kinds of industrial sectors, in which the airflow cooling system is widely used to control the temperature or to manage the thermal system effectively. In specific, the energy usage of data centre provides an excellent example to demonstrate the advantages of piezoelectric fan cooling the power electronics.

Acikalin (2007) studied the heat transfer of piezoelectric fans and found that the heat transfer coefficient has a 375% increase when it was compared with the traditional natural convection. Several experiments of piezoelectric fan were conducted for impinging on a heat source (Kimber and Garimella, 2009a; Kimber and Garimella, 2009b; Kimber et al., 2009b), in which the fan amplitudes and the distances change from the fan tip to the heat source. Both the local convective heat transfer coefficients and the Nusselt number were used to measure the air flow induced from a piezoelectric fan. Moreover, Liu et al. (2013) tested the influences of fan location relative to the heat source, i.e. the horizontal arrangement and the vertical arrangement, and found that these two different cases have a similar effect on the characteristics of heat transfer.

1.4.4 Design of piezoelectric fan

For engineers, designing and implementing the movements of piezoelectric fan

should be optimal. There are several types of piezoelectric fan made of different materials, such as plastics, metals and other materials like carbon fibre. In detail, the plastic materials include polyvinyl chloride (PVC), polyethylene terephthalate (PET) and Mylar, and the metal materials consist of the phosphor copper, bronze, stainless steel, brass, and aluminium.

The piezoelectric fan should be flexible enough to get a large oscillation amplitude. Its light and flexible characteristics are determined by the fan materials, which should have a suiting density, the viscosity, and the elasticity. The movements of piezoelectric fan should be tested through experimental work, in which the fan material and the geometric parameters (such as the length, the thickness, and the different shapes) should match properly.

Yoo et al. (2000) have studied the influence of fan materials on the velocity of air flow. In their experiments, the materials of piezoelectric fan included aluminium, brass and phosphor bronze, . Although the heat transfer of fans had a similar result, some differences among these piezoelectric fans did exist. The brass fan can produce an air flow with the velocity of 1–1.4 m/s, while the aluminium fan produced the air flow with similar velocity, 1–1.9 m/s. However, when the piezoelectric fan is made of phosphor bronze, the air flow had a highest velocity 2–2.3 m/s. Liu et al. (2013) made two piezoelectric fans with different materials: PET (polyethylene terephthalate) plastics and stainless steel, and the results demonstrated that a thinner piezoelectric fan has larger amplitude and can generate the air flow with a higher speed.

Besides, the glue is used to bond the flexible fan on a piezoceramic patch, and the thickness of glue layer also has a significant influence on the movements of piezoelectric fan. Sheu et al. (2008) have pointed out that the thickness of glue layer affected the fan bending stiffness, and the experiment results showed that when the glue thickness increased, the vibration amplitude of fan decreased due to the large bending stiffness.

Further, the resonance frequency of piezoelectric fans should also be solved analytically or tested by the vibration experiments. For example, Kimber et al. (Kimber and Garimella, 2009a; Kimber and Garimella, 2009b; Kimber et al., 2009b) have made two different piezoelectric fans: Mylar fan and stainless-steel fan. The Mylar fan with the resonance frequency of 60Hz was actuated with 10–30 mW power, while the stainless-steel fan was driven at the resonance frequency of 113 Hz, with the consumed power of 20–45mW. The results showed that there were no clear differences between these two fans

with different materials. It is notable that the length of these two fans were also different, therefore, it is unreasonable to judge the influences of fan materials.

1.5 Research motivation

1.5.1 Potential use

In the electronics industry, the microelectronic products with high functionality are developed rapidly with the growth of modern technology. The multi-function of electronic products results in high power consumption. The massive heat and surface heat flux can be generated in the limited size and weight of electronic components. Therefore, it is urgent to put forward an efficient approach to control the temperature of electronic products. The innovative design concepts, such as piezoelectric fan, should be realised to cool such devices efficiently.

Most commonly used cooling systems with heat sinks dissipate heat by natural convection or a conventional fan. Different from that, the piezoelectric fan that uses PZT piezoelectric material and an elastic cantilever beam has been used for cooling electronic devices. Besides, the heat generation of the low-cost CPU is about 20~30W lower than the normal PC. The demand for a cooling module thus drops. A compact and low power consuming fan that can integrate with a heat sink is necessary. Therefore, the low cost and mini-PC are considered as a potential market.

Although the piezoelectric fan is capable of transferring heat from electronic devices while operating at low power and producing low noise, the optimal design of piezoelectric fan system is still difficult to achieve. One of the reasons is a lack of understanding of the effects of various parameters of PE fans on the cooling effectiveness. Previous researches have not fully identified the mechanisms of PE fan cooling, including the unsteady motion of the PE fan and the associated fluid flow and heat transfer.

To take advantage of piezoelectric fan, the research in this thesis is now concerned with the optimisations of piezoelectric fan system. The CFD simulations investigate the cooling effectiveness of vibrating fan. For the piezoelectric fan, the problem is that the optimal motions of piezoelectric fan are still not apparent. Additionally, the dynamic characteristics of piezoelectric fan are not well understood they interact with the surrounding fluid complicatedly. Now the optimal performance of vibrating fan focuses on bringing down the power consumption.

1.5.2 Motivation and objectives

The piezoelectric fan has many advantages, such as the low-power consumption, low noise, and long life. With its massive potential in cooling power electronics, the mechanisms involved have not been fully understood, such as the deformation of piezoelectric fan, the interactions between the fan and the surrounding air flow, et.al. Although many studies towards the development of piezoelectric fans are available, there is no ready-made product available in the market for the cooling of electronic devices of compact size. The reason for this is mainly the lack of in-depth understanding of the mechanisms of fluid flow and heat transfer involved. With the ever-increasing energy consumption of power electronics, it is urgent to come up with a better thermal management system that can remove the heat effectively and save more energy. Further investigations on the movements of piezoelectric fan, the interactions with fluid flow as well as the characteristics of heat transfer associated with fan motions are essential.

It is known that the movements of piezoelectric fan disturb the surrounding air to format vortex and create downstream convection. The presence of eddies in internal turbulent flow is closely related to the characteristics of heat transfer. The basis of this research is the design and optimisation of piezoelectric fan, to maximise the airflow generation or maximise mixing of the fluid flow.

Figure 1.8 shows the research outline, and the chapter contents are described as follows:

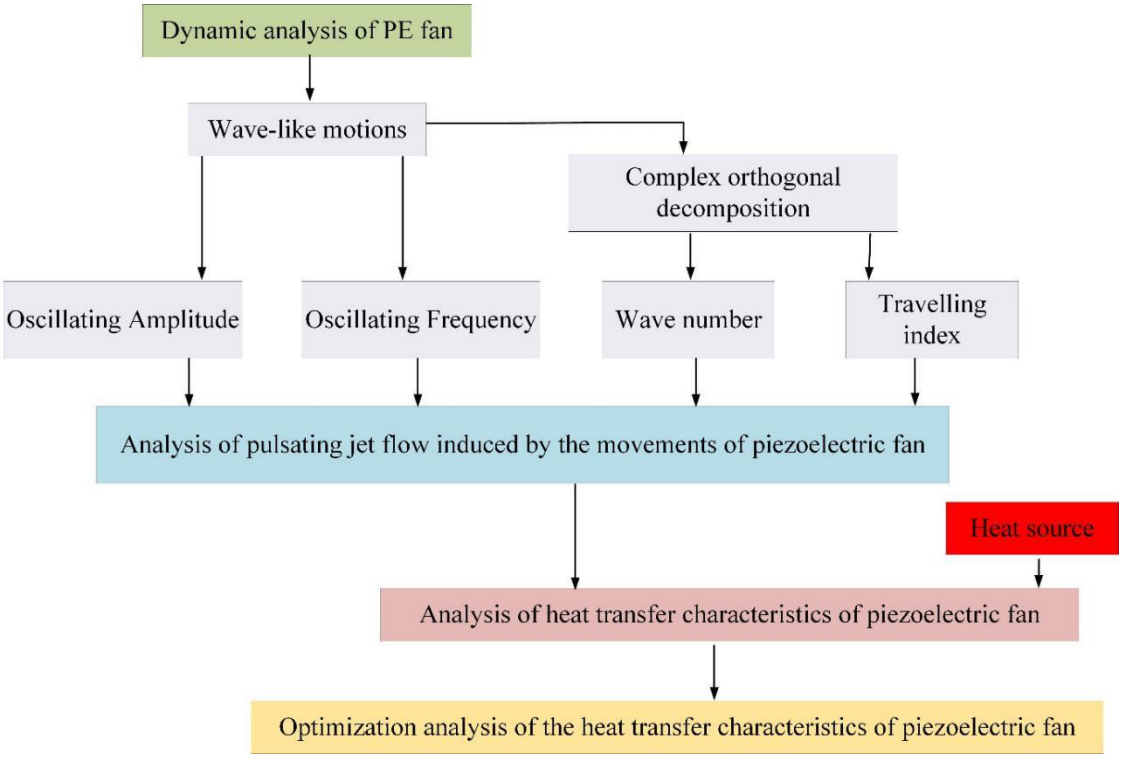

Figure 1.8: The research content of the PhD thesis.

Chapter 2: Dynamic analysis of piezoelectric fan. A simplified beam model analyses the dynamic property of piezoelectric fan with the analytical solution given in detail. The method of complex orthogonal decomposition helps analyse the complex modal characteristics of piezoelectric motions. The travelling index is proposed to evaluate the dynamic properties of piezoelectric fan.

Chapter 3: Flow characteristics of piezoelectric model. Using the large-eddy simulation (LES) based CFD approach, a numerical model is built to explore the interactions between its vibrating piezoelectric fan and the surrounding air flow. Its velocity profile replaces the fan displacement, and the influence of piezoelectric vibrating motions on fluid flow is investigated in terms of the maximum amplitude, the vibrating frequency and the travelling index.

Chapter 4: Heat analysis of piezoelectric model with a heat source. In this chapter, heat transfer of piezoelectric fan is examined. The characteristics of heat dissipation are analysed by the Nusselt number and the surface heat coefficient. The characteristics of air flow are used to study the heat transfer when considering the details of piezoelectric movements.

Chapter 5: Optimisation of heat transfer characteristics. The quadratic response surface method (RSM) is used to optimise the heat transfer characteristics of piezoelectric

fan. Optimising the factors of fan motions can help to obtain the best performance, which is also validated again the numerical model.

Chapter 6: Conclusion and future work.

Chapter 2

Dynamic Analysis of Piezoelectric Fan

2.1 Introduction

Piezoelectric fans generate air flow via an intrinsic oscillation of the blades. Accordingly, the power consumption is much lower compared with the currently used air movers such as axial fans. The heat transfer characteristics are closely related to the movements of piezoelectric fan. PE fan motion is too complex to be thoroughly analysed using theoretical or mathematical approaches. This has motivated the dynamic analysis in this Chapter. Because PE fan blades vibrate as a wave-like motion, this chapter studies and analyses the PE fan motion theoretically from this perspective.

From the aspect of dynamic analysis, the movements of piezoelectric fan are in essence the forced vibrations of viscoelastic beam immersed into the air flow. In this chapter, the bending fan can be simplified as a viscoelastic beam with a uniform cross-section. According to the Lighthill's elongated body theory (Lighthill, 1971), the interactions between piezoelectric fan and surrounding air flow can be described by the inertia force, which is modelled by the added mass. Further, the modal characteristics of both the free vibration and the forced vibration are analysed by the method of variable separation, and the qualitative relations between the viscoelastic parameters and the motions of piezoelectric fan are analysed in detail.

For the unique motions of piezoelectric fan, the method of complex orthogonal decomposition (COD) is adopted to analyse their complex characteristics, which cannot be thoroughly analysed by other theoretical/mathematical approaches. Traditionally, the representation of piezoelectric fan are simple formulas, which uses the vibrating frequency and amplitude. However, these simple formulas are not able to reveal the mechanisms of fan movements. In this chapter, the theoretical approach is based on analysing the motions of the midline of the blade. The motions of piezoelectric fan are decomposed into a travelling part, and a standing part, and the travelling index is proposed to describe the curviness of fan motions.

2.2 Description of piezoelectric fan motion

2.2.1 Physical model of piezoelectric fan

The sophisticated electronic equipment calls for new cooling technologies, which have low power consumption and high cooling effectiveness. In Figure 2.1, a piezoelectric fan is regarded as an ultra-low power air mover (Maaspuro, 2016). It is made up of a flexible beam, a piezo actuator and a clamp. The piezoelectric fan can be regarded as an oscillating cantilever, which is operated by a signal generator. When the electric signal is applied over the piezoelectric material, the expansion and contraction of piezoelectric fan are generated with a particular deforming pattern (Meirovitch, 1967; Liu et al., 2013). The characteristics of piezoelectric fan depend on various parameters influencing the blade motion, which is closely related to the airflow generation.

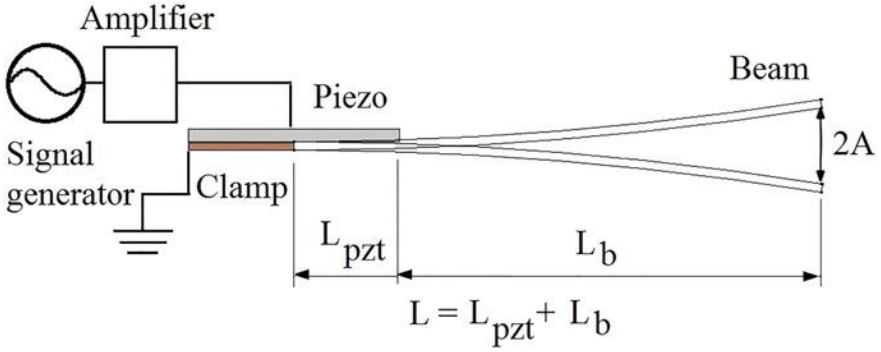

Figure 2.1: The operation model of piezoelectric fan (Maaspuro, 2016)

In Figure 2.1, a thin beam made of flexible material will be attached to the piezoelectric patch. In fact, the bending of piezoelectric fan is measured in some micrometres, and it cannot generate a significant air flow to transfer the heat. Similar to the oscillation of flexible beam, the piezoelectric fan is oscillating with a specific frequency. A previous study demonstrated that when the signal frequency is close to the resonance frequency of piezoelectric fan, a significant oscillation amplitude takes place (Maaspuro, 2016).

For most piezoelectric fans, the first fundamental resonance frequency is the best for the operation. If the driving frequency of signal is far away from the resonance frequency, the oscillation of piezoelectric fan attenuates quickly (Li et al., 2017). In the oscillation, the electrical energy will be transformed into mechanical energy. This process actualises with the maximum effectiveness when the fan is actuated at the resonance conditions (Yoo

et al., 1997).

In general, a jet-like air stream is produced at the fan tip, and the rotating airflows are also formed on both sides of piezoelectric fan (Ma et al., 2014a). All these air flows have the same magnitude, aiming at cooling the electronic equipment. According to the direction of the produced airflow, there are two configurations of piezoelectric fan, and they are shown in Figure 2.2 (Meirovitch, 1967). One configuration is that the fan is vertically oriented, and the other one is that the fan is horizontally oriented. The parameters of piezoelectric fan for both face-to-face and edge-to-edge orientation are also shown in Figure 2.2. The fan can be located above the surface of the hot plate or in front of it, which also affects the cooling effectiveness significantly (Liu et al., 2009). Besides, the cooling effectiveness can also be improved by the fan's deformed pattern, the optimal geometry of fan shape, and the arrangement of piezoelectric fan.

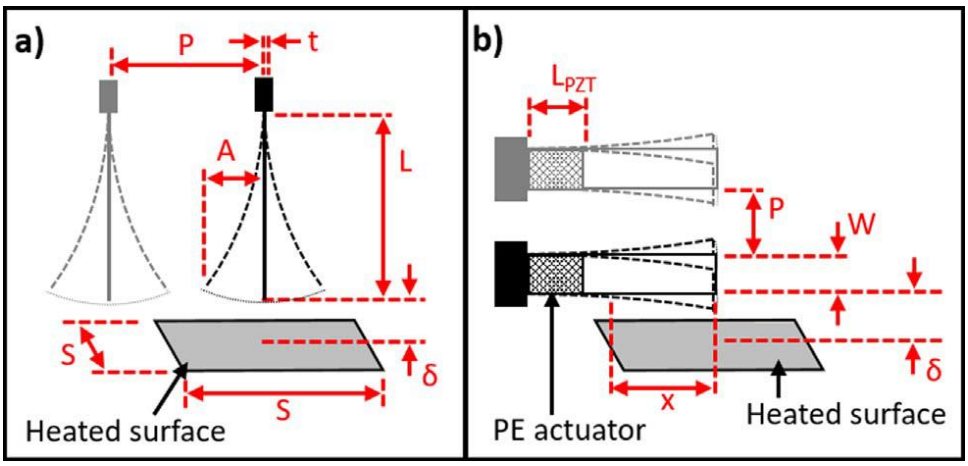

Figure 2.2: Two configurations of piezoelectric fan: (a) face-to-face (b) edge-to-edge (Hales and Jiang, 2018b).

2.2.2 Movements description of piezoelectric fan

In Figure 2.3, when the piezoelectric fan is deformed, its mode shape can be theoretically defined by the following equation (Maaspuro, 2016):

$$\begin{aligned} Y(x) = A_{XC}[&((\sin(\beta L) - \sinh(\beta L)) \cdot (\sin(\beta x) - \sinh(\beta x)) \\ &+ (\cos(\beta L) - \cosh(\beta L)) \cdot (\cos(\beta x) - \cosh(\beta x))] \end{aligned} \tag{2-1}$$

where $Y(x)$ is the amplitude of piezoelectric fan;

x is the distance along the beam length;

L is the fan length;

A_{XC} is the area of fan cross-section.

The coefficient β is defined as (Maaspuro, 2016):

$$\beta = \pm\sqrt{\frac{2\pi f_r m}{LIE}} \tag{2-2}$$

where m is the fan mass;

I is the second moment of area;

E is Young's modulus;

f_r is the first resonant frequency of piezoelectric fan.

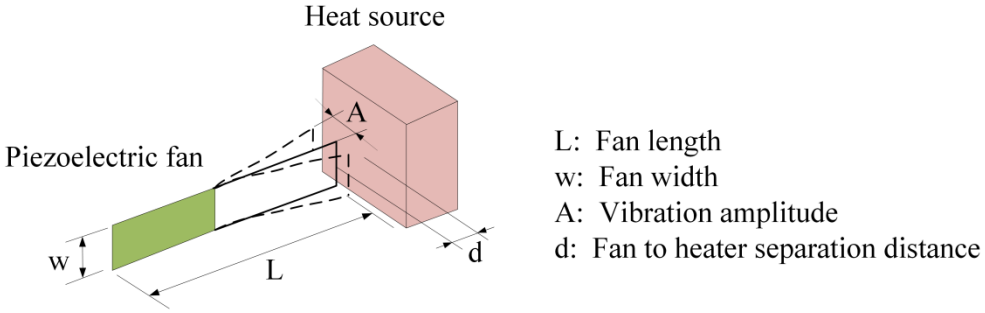

Figure 2.3: Illustration of geometry parameters of piezoelectric fan

Besides, an empirical function (Meirovitch, 1967) has been defined to describe the amplitude of piezoelectric fan deflection, $Y(x)$, which can also be used in the numerical simulations of heat transfer induced by the movements of piezoelectric fan. Here the displacement from the centre of oscillation $\mathrm{y}(x,t)$, at any given time, t, along the piezoelectric fan is defined as:

$$\mathrm{y}(x,t) = D_c Y(x) sin(2\pi f t) \tag{2-3}$$

where D_c is the magnitude coefficient;

f is the oscillating frequency.

A simple formula to describe the movements of piezoelectric fan, it is described as:

$$y(x,t) = A\left(\frac{x}{L}\right)^2 sin(2\pi f t) \tag{2-4}$$

where $\mathrm{y}(x,t)$ is the periodic movements of piezoelectric fan;

A is the oscillating amplitude.

In Eq. (2-4), the amplitude envelope is shown in Figure 2.4, and the motions during half of the oscillating period are shown in Figure 2.5. Here FL stands for the length of piezoelectric fan.

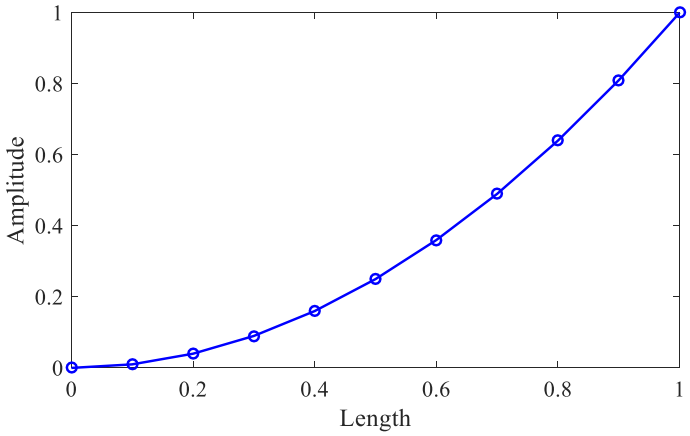

Figure 2.4: The amplitude envelope of piezoelectric movements described by Eq. (2-4)

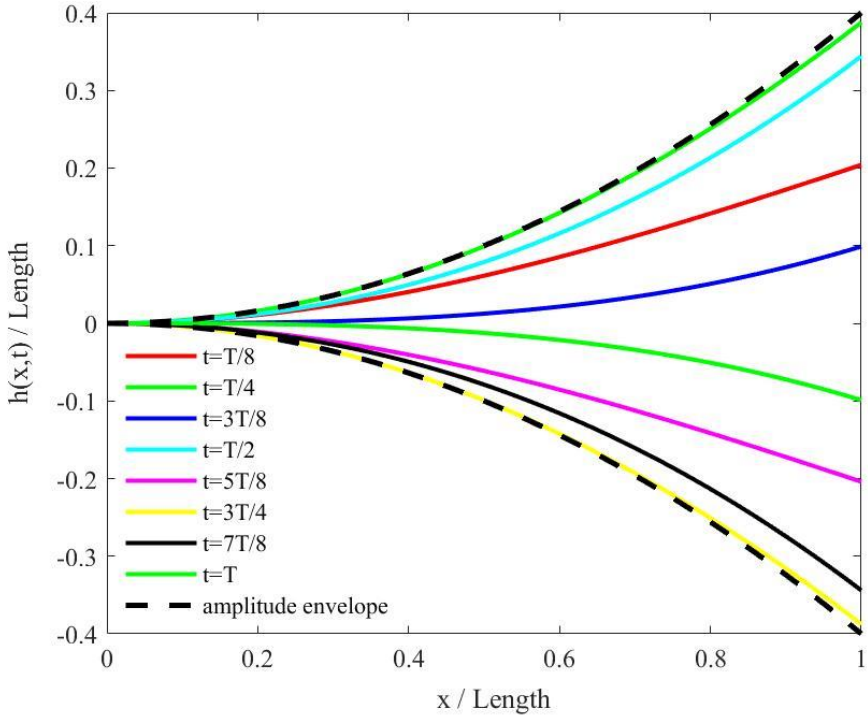

Figure 2.5: The movements of piezoelectric fan described during one oscillating period

Summarising the previous studies (Park and Kim, 2011; Maaspuro, 2016; Bidakhvidi et al., 2012; Acikalin et al., 2003; Ma et al., 2012a), the motions of PE fan can be described by different mathematical formulae. Some of them are summarised in Table 2-1, and the basic format is expressed as:

$$y(x,t) = A(x)^2 sin(2\pi f_{osc} t + \varphi) \quad (2\text{-}5)$$

In Eq. (2-5), the oscillating amplitude varies with the length of piezoelectric fan, and the oscillating frequency is an independent factor. Therefore, the amplitude envelope and the oscillating frequency are selected as two independent factors, which are used to analyse the influence of the effect of piezoelectric fan movements. It is noticed that the phase $\varphi =$

kx is not considered in previous studies, and k is the wave number. Different from the frequency, the wave number is related to spatial variations.

The movement of piezoelectric fan is reduced to a set of trajectories in space and time. The small differences of such motions are difficult to observe, and their mathematic descriptions are often not unique. For example, this type of motion can be described as:

$$\mathrm{h(x,t)} = H(x)\sin(\omega t + kx) \tag{2-6}$$

where $\omega = 2\pi f$ is the oscillating frequency;

k is the wave number;

$H(x)$ is the amplitude envelope.

Table 2-1 The different formats of piezoelectric fan movements

References	Functions	Amplitude	Frequency
Park and Kim, 2011	$\mathrm{G}(x) = \left(\frac{x}{L}\right)^2 \times \frac{1}{2}Amp$ $\mathrm{Y}(t) = G(x) \times sin(2P\pi t)$	2 mm	115 Hz
Maaspuro, 2016	$\mathrm{y}(x,t) = A\left(\frac{x}{L}\right)^2 sin(2\pi f_{osc} t)$	$\mathrm{A} = \frac{FL^3}{3EI}$	$f_{osc} = \frac{\alpha_n^2}{2\pi}\sqrt{\frac{EI}{mL^4}}$ $= \frac{\alpha_n^2}{2\pi}\sqrt{\frac{K}{m_{eff}}}$
Bidakhvidi et al., 2012	$\mathrm{y}(x,t) = H(x)sin(2\pi f t)$ $H(x) = -212334.25x^6$ $+ 54750.2x^5$ $- 4496.08x^4$ $+ 137.62x^3$ $+ 0.71x^2$ $- 0.0086x + 9.61$ $\cdot 10^{-6}$	10.3 mm	84.84 Hz
Acikalin et al., 2003	$\dot{y}(x,t) = \mathrm{Re}\left[A\omega \cdot sin\left(\frac{\pi \cdot x}{L}\right) \cdot e^{i\omega t}\right]$	0.8 mm	60 Hz
Ma et al., 2012a	$\mathrm{y}(x,t) = \frac{\alpha_n}{2}\left(\frac{x}{L}\right)^2 sin(2\pi\omega t)$	18 mm	30 Hz

In Table 2-1, α_n are the unitless coefficients. The first natural frequency α_1 is 1.875, second and third natural frequency are 4.694 and 7.885 respectively (Maaspuro, 2016). The motions of piezoelectric fan are in a complicated format (Acikalin et al., 2003), and it

can be rewritten as:

$$\dot{y}(x,t) = Re\left[A\omega \cdot sin\left(\frac{\pi \cdot x}{L}\right) \cdot [cos(\omega t) + isin(\omega t)]\right] \quad (2\text{-}7)$$

$$\dot{y}(x,t) = A\omega \cdot sin\left(\frac{\pi \cdot x}{L}\right) \cdot cos(\omega t) \quad (2\text{-}8)$$

For movements of piezoelectric fan, the effects of spatial variations have not been thoroughly understood, *i.e.* the differences between Eq. (2-4) and Eq. (2-6) are not clarified concerning practical applications of piezoelectric fans. The dynamic differences between them, and the influences of these differences on the induced air flow and heat transfer have not become an active research topic so far. In this thesis, the dynamic analysis of piezoelectric model can help explain these differences. CFD numerical simulations then investigate the influences of these differences. Besides, a variable of travelling index is used to evaluate the differences in the dynamic properties of piezoelectric fan.

2.3 Dynamic Model of piezoelectric fan

2.3.1 Viscoelastic beam model

In practical applications, the actuation frequency of piezoelectric fan is set as its first resonant frequency, and the maximum flow disturbances is achievable with minimal power consumption. In this study, the piezoelectric fan is simplified as a cantilever beam, which is shown in Figure 2.6. The fan's cross-section is a rectangle with constant width and height. One end of piezoelectric fan is fixed, and the other one is free. Therefore, the piezoelectric fan can be termed as a cantilever beam.

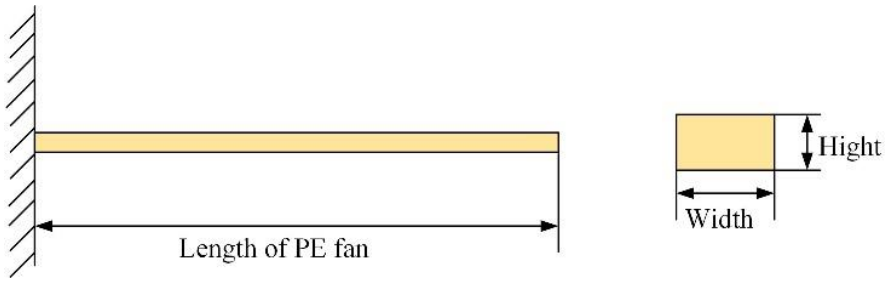

Figure 2.6: Cantilever beam model of piezoelectric fan

In Figure 2.7(a), the piezoelectric fan is regarded as a thin beam, which vibrates in the direction normal to its longitudinal axis. The transverse displacement of piezoelectric fan is in the y-direction, and x is the longitudinal dimension of the fan. The dynamic characteristics of the oscillating cantilever beam can be analysed by the Bernoulli-Euler

theory (Dimarogonas, 1996), in which the resonance frequencies and mode shapes can be obtained. Such a vibration actuated by a bending moment can be called as the transverse or lateral vibration (Timoshenko et al., 1974). In Figure 2.7, a small element of piezoelectric fan is selected to analyse its dynamic characteristics.

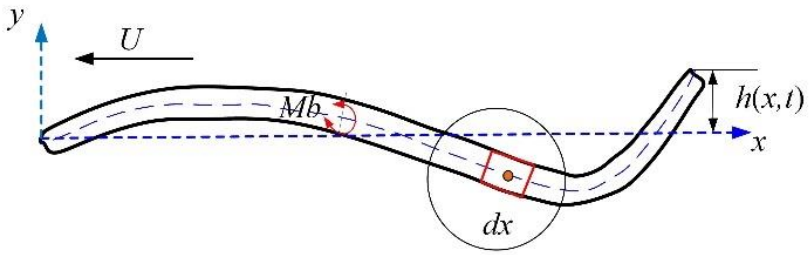

(a) Flexible PE fan actuated by a concentrated moment

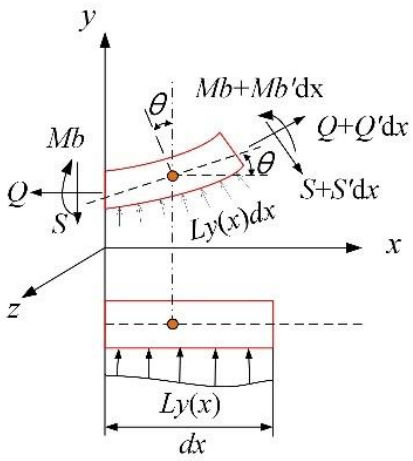

(b) Force analysis

Figure 2.7: Dynamic analysis of piezoelectric fan immersed into the air flow

The Lighthill's large-amplitude elongated body theory (Lighthill, 1971) is used to simulate the interactive force between piezoelectric fan and its surrounding air flow. In this theory, the lateral force $L_y(x)$ exerted on the piezoelectric fan is estimated by the local kinematics, and it is expressed as:

$$L_y\,(x) \approx m_a(x)\frac{\partial^2 h(x,t)}{\partial t^2} \tag{2-9}$$

where $m_a(x) \approx \pi\rho_f W(x)^2$ is the added mass of the cross section, $W(x)$ is the width of piezoelectric fan, and ρ_f is the density of fluid flow.

In Figure 2.7(b), the piezoelectric fan has a small deflection, and the cross sections remain plane and perpendicular to the fan centreline after deformation. The forces acting on fan element $\mathrm{d}x$ include the shear force $S(x,t)$, the bending moment $M_b(x,t)$, and the flow-induced lateral force $L_y(x,t)$. The bending moment M_b is a combination of the

actuation moment $M(x,t)$, the resistance moment $M_e = EI\frac{\partial^2 h}{\partial x^2}$ due to elasticity, and the resistance moment $M_v = \mu I\frac{\partial}{\partial t}\left(\frac{\partial^2 h}{\partial x^2}\right)$ due to viscosity. Here the viscosity can also be regarded as a characteristic of solid in a plastic regime. The solid materials of piezoelectric fans, such as many polymers, can be regarded as simply liquids with a very high viscosity (larger than 10^{12} Pa·s), which also deformed with the shear stress.

In present studies, the materials of piezoelectric fan have the properties of both elasticity (reaction to deformation) and viscosity (reaction to the rate of deformation). Therefore, the bending moment is expressed as $M_b \approx M - M_e - M_v$. Application of the force balance in y-direction yields:

$$-\rho A\mathrm{d}x\frac{\partial^2 h}{\partial t^2} + S - \left(S + \frac{\partial S}{\partial x}\mathrm{d}x\right) - L_y(x)\mathrm{d}x = 0 \tag{2-10}$$

while the equilibrium of moments yields:

$$-\left(M_b + \frac{\partial M_b}{\partial x}\mathrm{d}x\right) + M_b - L_y(x)\mathrm{d}x\frac{\mathrm{d}x}{2} + S\mathrm{d}x = 0 \tag{2-11}$$

The element $L_y(x)\mathrm{d}x\frac{\mathrm{d}x}{2}$ is neglectable due to the small term dx. Combining Eq. (2-9) with Eq. (2-10) and Eq. (2-11), the dynamic equation of the piezoelectric fan can be expressed as:

$$\frac{\partial^2}{\partial x^2}\left(M - EI\frac{\partial^2 h}{\partial x^2} - \mu I\frac{\partial}{\partial t}\left(\frac{\partial^2 h}{\partial x^2}\right)\right) = \rho A\frac{\partial^2 h}{\partial t^2} + m_a\frac{\partial^2 h}{\partial t^2} \tag{2-12}$$

Equation (2-12) models the dynamic behaviours of piezoelectric fan undulating in air flow in terms of the elastic property, the geometry parameters and the actuation conditions. However, this equation is too difficult to be solved by analytical methods, because of the nonlinear changes of mechanical property.

2.3.2 Free vibration characteristics of piezoelectric fan

2.3.2.1 Proportional/Zero damping system

For the piezoelectric fan, if the viscosity is zero or a proportional damping, the dynamic equation of piezoelectric fan with free vibration is simplified as:

$$EI\frac{\partial^4 h}{\partial x^4} + (\rho A + m_a)\frac{\partial^2 h}{\partial t^2} = 0 \tag{2-13}$$

The solution of this equation is assumed as $\mathrm{h}(x,t) = \varphi(x)q(t)$, which is independent of the derivative of space and time. Therefore, the variable separation method is adopted

to solve the Eq. (2-13), and then:

$$\begin{cases} q(t)'' + \omega^2 q(t) = 0 \\ \varphi(x)'''' - \frac{\rho A(x)+m_a(x)}{EI}\omega^2\varphi(x) = 0 \end{cases} \quad (2\text{-}14)$$

where ω is the oscillating frequency (rad/s).

In Eq. (2-14), the solution of time derivative is $\mathrm{q}(t) = asin(\omega t + \theta)$, and the solution about the derivative of space is $\varphi(x) = e^{\lambda x}$. Therefore, the characteristic equation is expressed in the following equation, and the corresponding eigenvalues are $\lambda = \pm\beta, \pm i\beta$.

$$\lambda^4 - \frac{m_0}{EI}\omega^2 = \lambda^4 - \beta^4 = 0 \quad (2\text{-}15)$$

where m_0 is the mass per length of piezoelectric fan, $m_0 = \rho A(x) + m_a(x)$.

According to the fixed-free boundary conditions of piezoelectric fan, the corresponding equations are expressed as:

(1) Fixed boundary condition:

$$h(x=0) = 0;\ \frac{\partial h}{\partial x}(x=0) = 0 \quad (2\text{-}16)$$

(2) Free boundary condition:

$$\frac{\partial^2 h}{\partial x^2}(x=l) = 0\ ,\ \frac{\partial^4 h}{\partial x^4}(x=l) = 0 \quad (2\text{-}17)$$

Here $\varphi(x)$ can be rewritten into:

$$\varphi(x) = C_1 cos\beta x + C_2 sin\beta x + C_3 cosh\beta x + C_4 sinh\beta x \quad (2\text{-}18)$$

Therefore, the equations of boundary condition are written into a matrix form:

$$\begin{vmatrix} -(cos\beta l + cosh\beta l) & -(sin\beta l + sinh\beta l) \\ -(-sin\beta l + sinh\beta l) & -(cos\beta l + cosh\beta l) \end{vmatrix} = 0 \quad (2\text{-}19)$$

The resonance frequency of piezoelectric fan can be solved by:

$$\omega_n = (\beta_n l)^2 \sqrt{\frac{EI}{\rho A l^4}},\ \mathrm{n} = 1,2,3\ldots \quad (2\text{-}20)$$

where $\beta_1 l = 1.875$, $\beta_2 l = 4.694$, $\beta_3 l = 7.854$ and $\beta_4 l = 10.9955$.

$$\varphi(x) = (cos\beta_n x - cosh\beta_n x) - \frac{cos\beta_n l + cosh\beta_n l}{sin\beta_n l + sinh\beta_n l}(sin\beta_n x - sinh\beta_n x) \quad (2\text{-}21)$$

As demonstrated, when the dynamic system of piezoelectric fan is a proportional damping system or undamped system (the viscosity of fan dynamic system is zero), the motions can be divided into two independent parts: the temporal part $q(t)$ and the spatial part $\varphi_n(x)$, and they are the pure standing waves.

2.3.2.2 General damping system

In general, if the viscosity of fan materials is non-zero, the dynamic system of piezoelectric fan is a general damping system. Therefore, when the actuation moment is zero, the corresponding equation for free vibration is expressed as:

$$\frac{\partial^4 h}{\partial x^4} + \eta \frac{\partial}{\partial t}\left(\frac{\partial^4 h}{\partial x^4}\right) = -\frac{(\rho A + m_a)}{EI}\frac{\partial^2 h}{\partial t^2} \tag{2-22}$$

The damping part $\eta \frac{\partial}{\partial t}\left(\frac{\partial^4 h}{\partial x^4}\right)$ in Eq. (2-22) is a coupling term for time and space variables. Similarly, this equation can also be solved by the variable separation method, and its solution is expressed as $\mathrm{h}(x,t) = \varphi_n(x)q_n(t)$. Therefore, the Eq. (2-22) can be further simplified as:

$$\varphi_n'''' q_n + \eta \varphi_n'''' \dot{q_n} = -\frac{(\rho A + m_a)}{EI}\varphi_n \ddot{q_n} \tag{2-23}$$

In Eq. (2-23), the expression of the time derivative is $\mathrm{q}_n(t) = e^{i\lambda_n t}$, and the amplitude term of the solution is shown as:

$$\varphi_n'''' - \gamma^4 \varphi_n = \varphi_n'''' - \frac{(\rho A + m_a)\lambda_n^2}{EI(1+i\lambda\eta)}\varphi_n = 0 \tag{2-24}$$

According to the boundary conditions of piezoelectric fan (one fixed end and one free end), the corresponding eigenvalues are calculated as:

$$\frac{(\rho A + m_a)}{EI(1+i\lambda\eta)}\lambda_n^2 = \left(n + \frac{1}{2}\right)^4 \frac{\pi^4}{L^4},\ n = 1,2,3,\ldots \tag{2-25}$$

Further, the Eq. (2-25) can be simplified as:

$$\lambda_n = \frac{iA_n\eta \pm \sqrt{4A_n - (A_n\eta)^2}}{2},\ A_n = \frac{EI}{\rho A + m_a}\left(n + \frac{1}{2}\right)^4 \frac{\pi^4}{L^4} \tag{2-26}$$

Therefore, the motions of piezoelectric fan are expressed as:

$$h(x,t) = \varphi_n(x)e^{i\lambda_n t} \tag{2-27}$$

$$\varphi_n(x) = (cos\gamma_n x + cosh\gamma_n x) - \frac{sin\gamma_n l + sinh\gamma_n l}{cos\gamma_n l + cosh\gamma_n l}(sin\gamma_n x + sinh\gamma_n x) \tag{2-28}$$

2.3.3 Forced vibration characteristics of piezoelectric fan

When the actuation torque is non-zero, the piezoelectric fan is forced to vibrate under the external concentrated moment, and the deformed pattern of the fan is closely related to the actuation conditions, the elasticity and viscosity of fan materials. The midline motions of the piezoelectric fan can also be solved by the variable separation method. In the present study, the piezoelectric fan with general damping is actuated by a concentrated actuation

torque, and the forced vibration characteristics are analysed in detail.

A simple harmonic force is applied at one end of piezoelectric fan, and it is expressed as $f(x) = f_0 cos(w_0 t)$, w_0 is the oscillating frequency. The movement format of piezoelectric fan is assumed as $h(x,t) = H(x)e^{iw_0 t}$, in which the real part is the amplitude of fan motions, and the imaginary part represents the phase of fan motions. Therefore, the Eq. (2-12) can be further replaced by:

$$H(x)'''' - k^4 H(x) = \frac{f(x)}{EI + iw_0 \mu I}, \quad k^4 = \frac{\omega_0^2 m_0}{EI + iw_0 \mu I} \tag{2-29}$$

The solution of Eq. (2-29) can be written into:

$$H(x) = C_1 sin(kx) + C_2 cos(kx) + C_3 ch(kx) + C_4 sh(kx) \tag{2-30}$$

The coefficients C_1, C_2, C_2 and C_4 can be solved by the fixed-free boundary conditions, and the detailed equations are shown as:

$$h(x=0) = 0; \frac{\partial h}{\partial x}(x=0) = 0 \tag{2-31}$$

$$\frac{\partial}{\partial \mathrm{x}}\left(M - EI\frac{\partial^2 h}{\partial x^2} - \mu I \frac{\partial}{\partial t}\left(\frac{\partial^2 h}{\partial x^2}\right)\right)_{x=L} = 0; \left(M - EI\frac{\partial^2 h}{\partial x^2} - \mu I \frac{\partial}{\partial t}\left(\frac{\partial^2 h}{\partial x^2}\right)\right)_{x=L} = 0 \tag{2-32}$$

The midline motions of piezoelectric fan then can be solved as:

$$h(x,t) = Re\left\{\frac{M_0 e^{i\omega_0 t}}{k^3(EI + i\mu I\omega_0)}[k\phi_3(x-a)u(x-a) + \phi_4(x-a)\delta(x-a) - Q_1(a)\phi_3(x) - Q_2(a)\phi_4(x)]\right\} \tag{2-33}$$

where $\phi_1(x) = \frac{\cosh(kx)+\cos(kx)}{2}$;

$\phi_2(x) = \frac{\sinh(kx)+\sin(kx)}{2}$;

$\phi_3(x) = \frac{\cosh(kx)-\cos(kx)}{2}$;

$\phi_4(x) = \frac{\sinh(kx)-\sin(kx)}{2}$;

$Q_1 = -\frac{k(\phi_1(l-a)\phi_1(l) - \phi_4(l-a)\phi_2(l))}{\phi_4(l)\phi_2(l) - \phi_1(x)\phi_1(l)}$;

$Q_2 = -\frac{k(\phi_4(l-a)\phi_1(l) - \phi_1(l-a)\phi_4(l))}{\phi_4(l)\phi_2(l) - \phi_1(x)\phi_1(l)}$.

Under the actuation of an external moment, one piezoelectric fan is taken as an example to demonstrate the deforming patterns of piezoelectric fan. The fan length is assumed as 0.3m, the density is 1000 kg/m^3, the elastic modulus of fan material is 5000 N/m^2, and the viscosity coefficient is 90 Ns/m^2. When the actuation frequency varies, the motions of the piezoelectric fan change accordingly, calculated by the formula (2-33). At different actuation frequencies, 3.6 Hz and 4.0 Hz, the deformed patterns of the

piezoelectric fan are shown in Figure 2.8. The horizontal x-axis is the distance along the fan length, and the vertical y-axis is the lateral movements of piezoelectric fan, which stands for the deformed pattern at different times. In Figure 2.8, FL is the full length of piezoelectric fan. These results are obtained from the dynamic analysis of complex modal vibrations, and the motions of piezoelectric fan are unique waves.

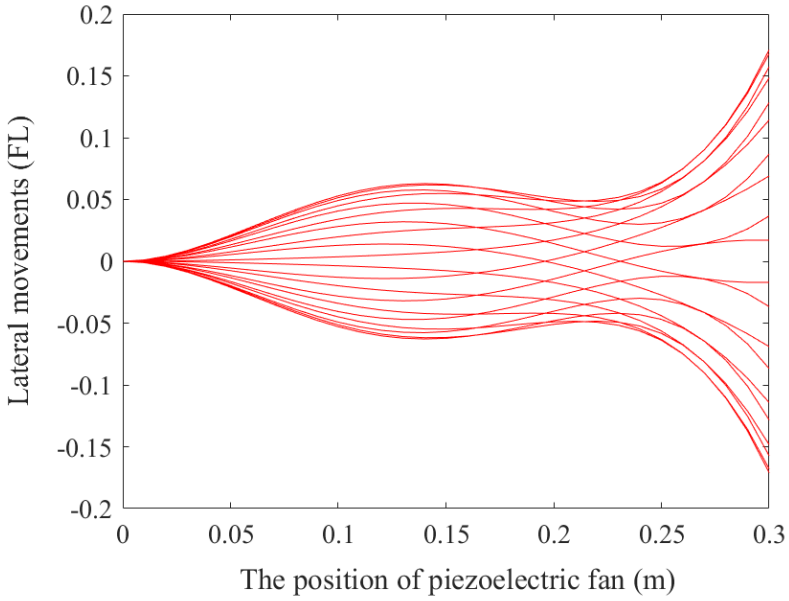

(a) Actuation frequency 3.6 Hz

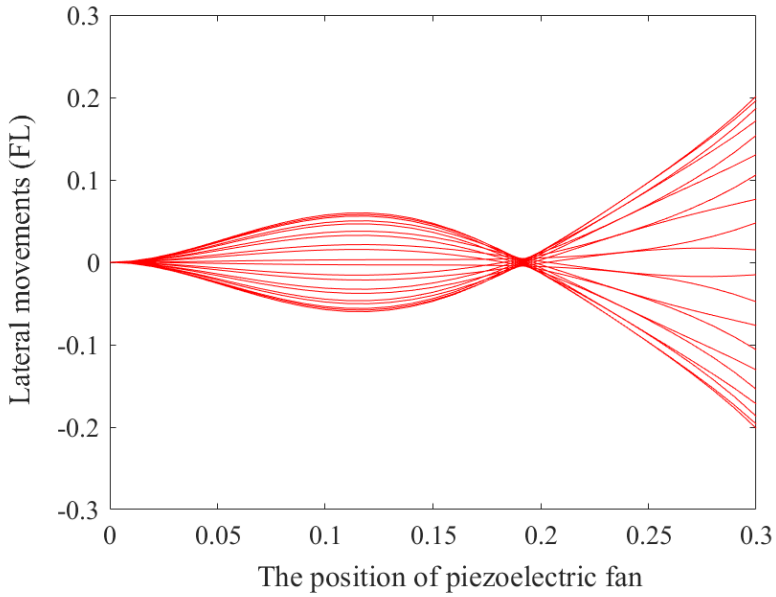

(b) Actuation frequency 4.0 Hz

Figure 2.8: The motions of piezoelectric fan when actuated at different driving frequencies

2.4 Complex modal analysis of piezoelectric fan movements

2.4.1 Complex orthogonal decomposition (COD) method

In the present study, the unique motions of the piezoelectric fan are analysed by the method of complex orthogonal decomposition (COD) (Feeny, 2008). This method was also used to study the waves in flexible beams, the movements of worms, and the motions of whiting fish (Feeny, 2013). The reason for choosing COD method is that the complex modal characteristics of fan motions, which are analysed from the dynamic analysis of fan vibration. Based on the COD method, the motions of piezoelectric fan are decomposed into two components. One part is a standing wave, and the other part is a travelling wave. Further, the travelling index is adopted to evaluate the ratio between these two components.

In this study, the motions of piezoelectric fan can be quantified by the parameter of travelling index, which is analysed by the COD method. To analyse the complex characteristics of fan motions, the matrix **K** of fan movements is generated at first:

$$\mathbf{K}_{M\times N} = [\mathbf{k}_1, \mathbf{k}_2, \dots\dots, \mathbf{k}_M]^{\mathrm{T}}, \tag{2-34}$$

$$\mathbf{k}_j = [y_j(t_1), y_j(t_2), \dots\dots, y_j(t_N)]^T. \tag{2-35}$$

Here, $y_m(t_n)$ in Eq. (2-35) is the component of matrix **K** at the row m and the column n, and it also represents the motions $h(x_m, t_n)$ of piezoelectric fan at the location x_m and the time t_n. In present study, $x_m = mL/M$ is the fan location along the axial direction, and $m = 1,2, \dots\dots M$; $t_n = nT/N$ is the instant time during one oscillating period, and $n = 1,2, \dots\dots N$.

Based on the matrix **K**, a complex matrix is generated as:

$$\mathbf{Z}_{M\times N} = [\mathbf{z}_1, \mathbf{z}_2, \dots\dots, \mathbf{z}_M]^{\mathrm{T}} \tag{2-36}$$

$$\boldsymbol{z_m}(t) = y_m(t) + \mathrm{i}\mathrm{H}(y_m(t)) \tag{2-37}$$

where i is the imaginary unit, and $\mathrm{H}(y_m(t))$ is the Hilbert transform of $y_m(t)$. A complex Hermitian matrix $\mathbf{R}_{M\times M} = \mathbf{Z}\bar{\mathbf{Z}}^{\mathrm{T}}/N$ is then conducted, and it has the real eigenvalues λ_m and the complex eigenvectors $\mathbf{w}_m$. Here the overbar indicates the conjugate of a complex number.

Further, the travelling index ζ is calculated as:

$$\zeta = 1/\mathrm{cond}(\mathbf{T}), \tag{2-38}$$

where $\mathbf{T} = [\mathrm{real}(\mathbf{w}), \mathrm{imag}(\mathbf{w})]$ is a matrix, $\mathrm{real}(\mathbf{w})$ is the column of the real part of $\mathbf{w}$, $\mathrm{imag}(\mathbf{w})$ is the column of the imaginary part of $\mathbf{w}$, and $\mathrm{cond}(\mathbf{T})$ stands for the condition

number of **T**. In particular, if the value of travelling index is 0, the motions of piezoelectric fan can be represented by a pure standing wave. If the travelling index is 1.0, the motions of piezoelectric fan are in the form of pure travelling wave.

2.4.2 COD analysis of piezoelectric fan movements

For any fan motions, these particular motions can be decomposed into a pure standing wave and a pure travelling wave. The fan motions are described by Eq. (2-6), the frequency is 2 Hz, and the wave number is 7. The motions in one vibrating period are shown in Figure 2.9. Due to the boundary conditions of the piezoelectric fan, it is noticeable that one end of these motions is fixed, and the other one is free.

According to the COD method, the motions of the piezoelectric fan are decomposed into two parts in Figure 2.10. The calculated travelling index is 0.63. The parts of the pure standing wave and pure travelling wave are displayed in Figure 2.10 (a) and Figure 2.10 (b) respectively. The lines represent the motions at different time in one period.

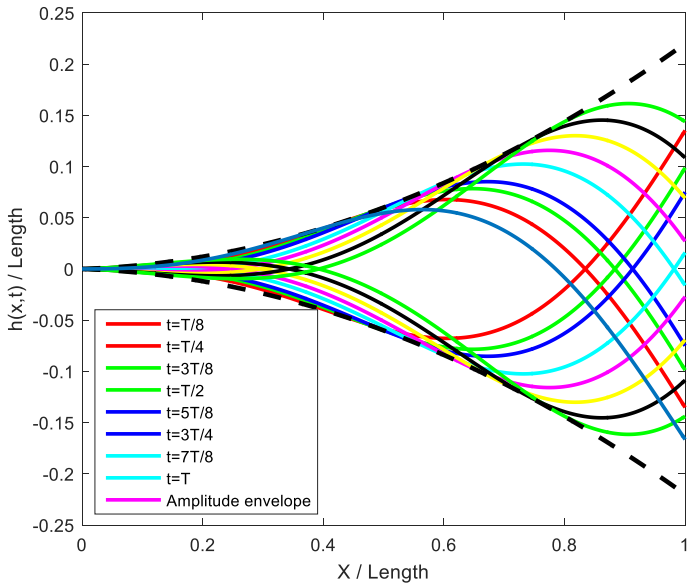

Figure 2.9: The motions of piezoelectric fan in one vibrating period

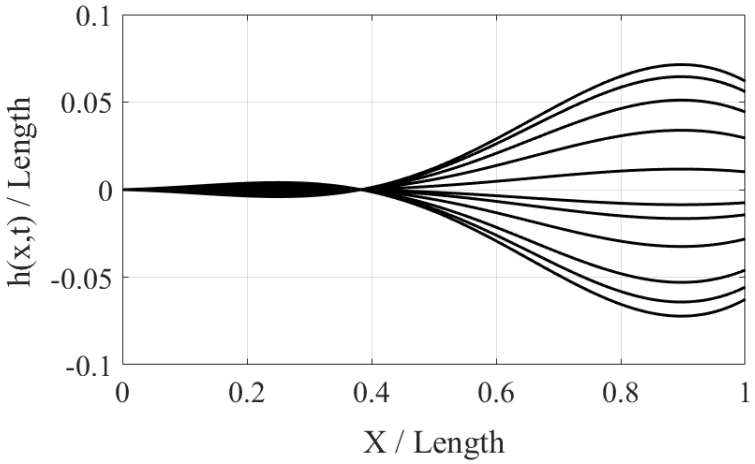

(a) The part of standing wave

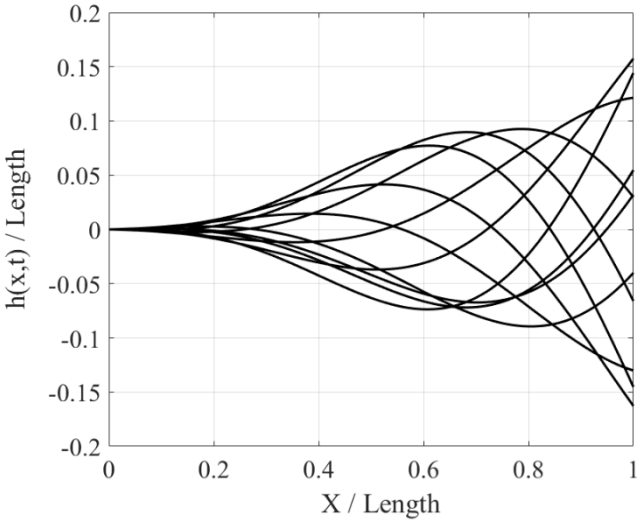

(b) The part of travelling wave

Figure 2.10: The decomposition of piezoelectric fan motions by the COD method

2.4.3 Dynamic property of piezoelectric fan motions

From the perspective of dynamic analysis, a standing wave of the piezoelectric fan can be obtained when the dynamic system is a proportional damping system (or the zero-damping system). However, when the viscosity is non-zero, the piezoelectric fan is deformed differently, and the unique wave-like motions would be obtained. Similar to the undulatory plate in the water flow, the characteristics of the dynamic system determine the deforming pattern. For example, Ramananarivo et al. (2013) conducted several experiments of rectangular Mylar plate, which was hanged vertically and vibrated in the air and water respectively. Different bending patterns of Mylar plate are developed when the plate is controlled with different frequency and amplitude. In the experiments, a

standing wave and travelling wave form when it is immersed into the air flow and water respectively. The results showed that the propagating wave could naturally emerge in a forced elastic plate, and the dynamical response passes from standing waves to travelling waves. The deformed patterns of the Mylar plate are shown in Figure 2.11. Later, a mathematical model aims at analysing the mechanism of the transition from a standing wave to a travelling wave (Ramananarivo et al., 2014). The motions in Figure 2.11(b) are observable when the damping is non-zero, and the standing waves in Figure 2.11(a) is observable when the damping is zero.

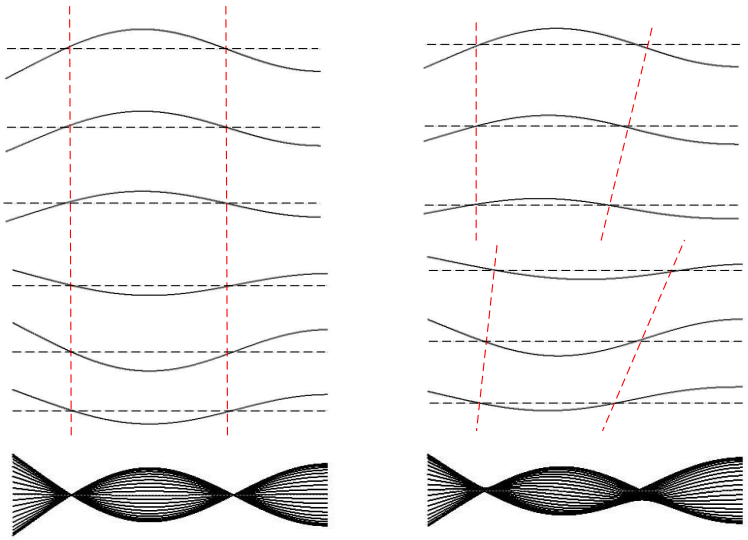

a) The standing wave b) The travelling wave

Figure 2.11: Undulatory movements of the rectangular Mylar plate with different viscosity (Ramananarivo et al., 2013; Ramananarivo et al., 2014)

In the present study, the piezoelectric fan can be regarded as a viscoelastic beam immersed into the air flow. The interactive force between the piezoelectric fan and surrounding flow can be described by the added mass, which is calculated by Lighthill's elongated-body theory (Lighthill, 1971). According to the Euler-Bernoulli beam theory, the deformed pattern of piezoelectric fan is determined by the inertial mass, the stiffness distribution and the viscous damping. It is notable that the viscosity of fan materials (or the viscous damping) contributes to the built-up of travelling waves.

From the point of dynamic analysis, the deforming pattern of piezoelectric fan is a pure standing wave when the dynamic system is a proportional damping system or a non-damping system. However, when the dynamic model is a general damping system, a particular motion with mixed standing and travelling parts would be generated. If the

damping is weak, the travelling index is close to zero. On the contrary, if the damping is active, the travelling index is close to one.

2.5 Summary

In this chapter, a theoretical model of the piezoelectric fan has been developed to analyse the dynamic characteristics of fan vibrations.

(1) The piezoelectric fan is simplified as a viscoelastic beam with a uniform cross-section. An inertia force models the interactions between piezoelectric fan and surrounding air flow. The modal characteristics of both the free vibration and the forced vibration are analysed by the variable separation method, and the qualitative relations between the viscoelastic parameters of fan materials and the fan motions are analysed in detail.

(2) When the dynamic model of piezoelectric fan is a proportional damping system or a non-damping system, the real mode of vibration modal generates a standing wave; when the dynamic model is a general damping system, the complex mode of vibration modal triggers. These results demonstrate that the deformed motions of piezoelectric fan are the complex modal shapes of vibrating fan, revealing the complex modal characteristics of its motions.

(3) The motions of piezoelectric fan are decomposed into the travelling and standing components by the method of complex orthogonal decomposition (COD). The matrix with its two columns being the real and imaginary parts of complex modal shape is used to define the travelling index. In the present study, the travelling index is used to evaluate the deformed pattern of piezoelectric fan. It is different from the traditional description of fan motions, using the vibrating frequency and amplitude.

Overall, these results demonstrate that the deformed patterns of piezoelectric fan are the complex modal shapes of fan vibration, revealing the complex modal characteristics of its motions. It also suggests that the viscoelastic properties of the piezoelectric fan have a crucial influence on the motions of the piezoelectric fan, which will, in turn, affect the airflow and the effectiveness of heat transfer in cooling applications.

Chapter 3

Numerical Investigation on the Flow Field Induced by the Movements of Piezoelectric Fan

3.1 Introduction

Compared to the traditional axial fans, piezoelectric fans have a huge advantage in reducing energy consumption through generating air flow. However, the motion of the PE fan is complicated and incomprehensible. In this chapter, the flow field of air flow generated will be simulated and analysed by CFD numerical simulations, the Large Eddy Simulation (LES) method will be applied. Also, the effects of three parameters, oscillating frequency, oscillating amplitude and wave number on the flow field will be particularly analysed.

When external energy is applied to the piezoelectric fan, the viscoelastic material is attached to the piezoelectric patch, transferring the electric energy into mechanical energy. The bending of the blade surface produces air flows on both sides of the fan. Besides, a jet-like air stream is produced at the tip of fan blade for cooling. The periodic vibrations of piezoelectric fan cause the flow of ambient air to realise convective heat transfer.

Typically, the motions of the piezoelectric fan can be described by the oscillating frequency, the oscillating amplitude and the wave number. To study the influences of these kinematic parameters on the characteristics of heat transfer, a CFD model of piezoelectric fan is developed to analyse the unsteady flow field associated with the motions of the PE fan. In this chapter, the numerical results can provide understandings of the air flow generated by the piezoelectric fan and used for the relations among the flow field and the fan movements. All these results can provide the theoretical guidelines to cool the system component of power electronics.

3.2 Numerical methods

3.2.1 Flow field governing equations

For viscous flow of a Newtonian fluid with constant density, the governing equations for the flow field in Cartesian coordinates are expressed as:

$$\frac{\partial u_i}{\partial t} + \frac{\partial (u_i u_j)}{\partial x_j} = -\frac{1}{\rho}\frac{\partial p}{\partial x_i} + \nu \frac{\partial^2 u_i}{\partial x_j \partial x_j} \ , \tag{3-1}$$

$$\frac{\partial u_i}{\partial x_i} = 0, \tag{3-2}$$

where $x_i (i = 1, 2, 3)$ is the Cartesian coordinates (x, y, z);

u_i is the velocity components in the corresponding directions (u, v and w);

t is the time;

p is the pressure;

ν is the kinematic viscosity of the fluid.

In Eq. (3-1), the Navier-Stokes (N-S) momentum equation is shown, and the effect of body force such as buoyancy has been neglected. In this study, due to the fact that the flow is relatively low speed, the compressible form of the governing equations was not considered.

For laminar flows, Eq. (3-1) and Eq. (3-2) are integrated in space and time without introducing any model. For turbulent flows, the approach of large eddy simulation (LES) is used to separate the energy carrying large eddies from the small scales. LES model is a mathematical model for modelling turbulence in CFD. It was initially proposed to simulate atmospheric air currents in 1963 (Smagorinsky, 1963), and was explored by Deardorff (1970). The simulation of turbulent flows requires resolving a very wide range of time and length scales, which affect the flow field. This kind of resolution can be achieved with direct numerical simulation (DNS), but DNS is costly, which prohibits the simulations of practical engineering systems.

The principal idea of LES is to reduce the computational cost by not resolving the smallest length scales via low-pass filtering of the Navier–Stokes equations. These smallest length scales are the most computationally expensive to resolve. With the low-pass filtering, it can be regarded as a time- and spatial-averaging, effectively removing small-scale information from the numerical solution. However, this information on small scales is not

irrelevant, and their effect on the flow field must be modelled. This task is an active area of research for turbulent flows, and small-scales can play an important role in high-speed flows (Pope, 2001).

The LES filter can be applied to a spatial and temporal field $\phi(x,t)$ and perform a spatial filtering operation, a temporal filtering operation, or both. The filtered field, denoted with a bar, is defined as follows (Meneveau, 2010):

$$\overline{\phi(x,t)} = \int_{-\infty}^{\infty}\int_{-\infty}^{\infty}\phi(r,t')G(x-r,t-t')dt'dr, \tag{3-3}$$

where G is the filter convolution kernel. This can also be written as:

$$\bar{\phi} = G * \phi \tag{3-4}$$

The filter kernel G has an associated cutoff length scale Δ and cutoff time scale τ_c. Scales smaller than these are eliminated from $\bar{\phi}$. Using the above filter definition, any field ϕ may be split up into a filtered and sub-filtered (denoted with a prime) portion, as:

$$\phi = \bar{\phi} + \phi' \tag{3-5}$$

It is important that the large eddy simulation filtering operation does not satisfy the properties of a Reynolds operator. A spatial filtering operation on the Navier-Stokes equations is applied, and the Smagorinsky eddy viscosity model (Germano et al., 1991) is used to model the sub-grid scale stresses. The resulting equations governing the evolution of large scales have the following form:

$$\frac{\partial\bar{u}_i}{\partial t} + \frac{\partial(\bar{u}_i\bar{u}_j)}{\partial x_j} = -\frac{1}{\rho}\frac{\partial\bar{p}}{\partial x_i} + \nu\frac{\partial^2\bar{u}_i}{\partial x_j\partial x_j} - \frac{\partial\tau_{ij}^d}{\partial x_j}\ , \tag{3-6}$$

$$\frac{\partial\bar{u}_i}{\partial x_i} = 0, \tag{3-7}$$

where the overbar denotes a filtered variable; $\tau_{i,j}^d$ is the deviatoric part of sub-grid scale (SGS) stresses, modelled as:

$$\tau_{i,j}^d = \tau_{ij} - \frac{1}{3}\delta_{ij}\tau_{kk} = -2\nu_t\bar{S}_{ij} = -2C_s\bar{\Delta}^2|\bar{S}|\bar{S}_{ij}. \tag{3-8}$$

where δ_{ij} is Kronecker's delta;

$\bar{S}_{ij} = \frac{1}{2}\left(\frac{\partial\bar{u}_i}{\partial x_j} + \frac{\partial\bar{u}_j}{\partial x_i}\right)$ is the resolved strain rate tensor with magnitude $|\bar{S}| = \sqrt{2\bar{S}_{ij}\bar{S}_{ij}}$;

ν_t is the turbulent eddy viscosity;

$\bar{\Delta}$ is the filter size, defined as $(\Delta x\Delta y\Delta z)^{1/3}$ with Δx, Δy and Δz as the local grid size in the x , y and z directions respectively.

C_s is model coefficient, determined using the dynamic procedure of the Germano subgrid-scale closure method (Lilly, 1992).

3.2.2 Space discretization

In the current study, the primary variables are defined on a staggered grid, which is shown in Figure 3.1. The velocity components are defined at the centre of cell surfaces, and the velocity u, v, and w are defined in the x, y, and z directions respectively. All other variables are defined at the centre of the grid cell, such as the pressure p, the density ρ and the viscosity ν.

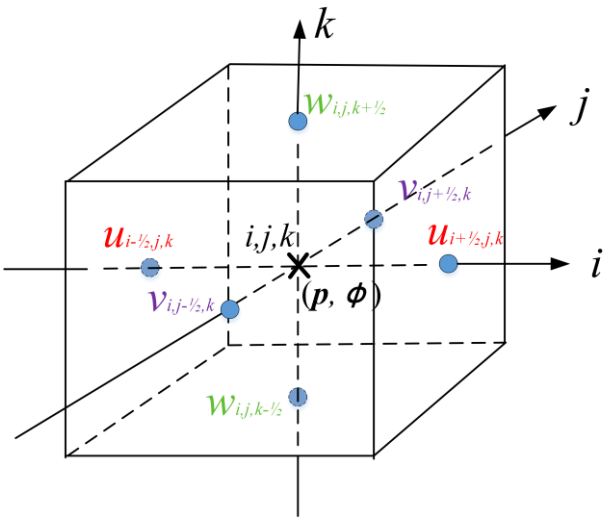

Figure 3.1: The sketch of 3D staggered Cartesian grid cell with different variables

The Navier–Stokes equations are discretized on the staggered Cartesian grid by a finite difference method. For the time integration, the second order Runge-Kutta (RK2) method is used, and a fractional-step method (Kim and Moin, 1985) is used in each sub-step of RK2 method. The N-S equation is solved by the fractional step method, and the divergence-free requirement is ensured by the projection method. In particular, the pressure Poisson equation is solved using a Krylov-based multigrid solver from the Portable, Extensible Toolkit for Scientific Computation library (PETSc) (Balay et al., 1997).

The N-S equation is discrete on the cartesian coordinate system. The spatial discretization methods include the central difference scheme and the upwind scheme. All these schemes have the second order accurate.

(1) Upwind scheme

To illustrate the method of upwind scheme, a linear advection equation is presented, and it is expressed as:

$$\frac{\partial u}{\partial t} + a\frac{\partial u}{\partial x} = 0 \tag{3-9}$$

Equation (3-9) describes a wave propagating along the x axis with a velocity a. In Figure 3.2, a grid point i in one-dimensional domain is selected to demonstrate the upwind scheme. For Eq. (3-9) if the velocity a is positive, the solution is a travelling wave propagating towards the right, the left side of i is upwind side. On the contrary, if a is negative, the solution is a wave propagates towards the left, the left side is downwind side.

If the finite difference scheme for the spatial derivative, $\partial u/\partial x$ contains more points in the upwind side, and it is called an upwind scheme. For the second-order upwind scheme, u_x^- becomes the 3-point backward difference, and is defined as:

$$u_x^- = \frac{3u_i^n - 4u_{i-1}^n + u_{i-2}^n}{2\Delta x} \tag{3-10}$$

and u_x^+ is the 3-point forward difference, which is defined as:

$$u_x^+ = \frac{-u_{i+2}^n + 4u_{i+1}^n - 3u_i^n}{2\Delta x} \tag{3-11}$$

Compared to the first-order scheme, this scheme is less diffusive, and it is also named as linear upwind differencing (LUD) scheme.

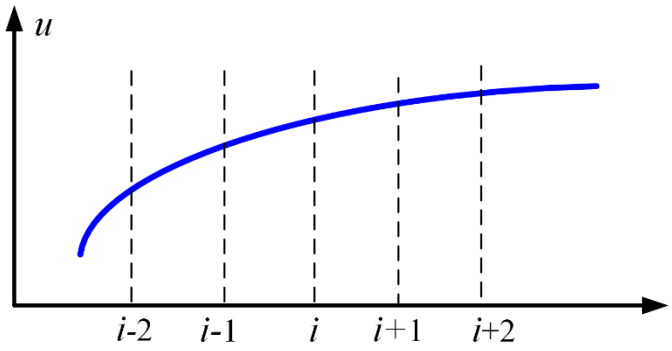

Figure 3.2: The scheme of unwind method

(2) Centre difference scheme

Taking two dimensional grids as an example, the centre difference scheme is used to demonstrate the spatial derivatives. In Figure 3.3, the velocity and the pressure are defined on two-dimensional grid points. At first, for the right source term of Pressure Poisson equation, the velocity divergence term defined on (i,j) can be calculated directly by the central difference scheme. For the convection term u of point (i,j), i.e. $\frac{\partial uu}{\partial x}(i)$ and $\frac{\partial uv}{\partial x}(i,j)$, the corresponding discrete graphs are shown in Figure 3.4, and the schemes are shown as:

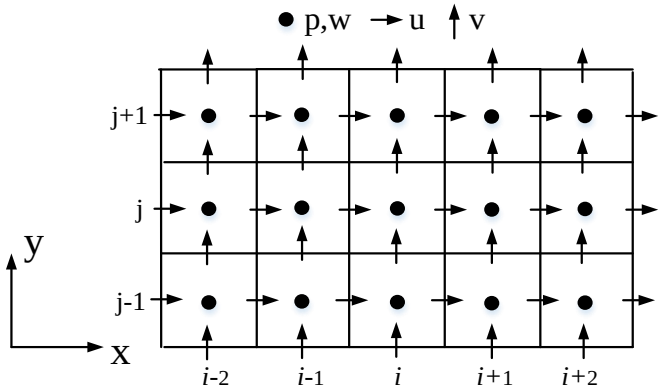

Figure 3.3: Variable on the staggered grid coordinates on the x-y plane

$$-\frac{\partial uu}{\partial x}(i) = -\frac{\left(u\left(i+\frac{1}{2}\right)\right)^2-\left(u\left(i-\frac{1}{2}\right)\right)^2}{\frac{dx(i-1)+dx(i)}{2}} = -\frac{\left(\frac{u(i+1)+u(i)}{2}\right)^2-\left(\frac{u(i)+u(i-1)}{2}\right)^2}{\frac{dx(i-1)+dx(i)}{2}} \tag{3-12}$$

$$-\frac{\partial uv}{\partial y}(i,j) = -\frac{uv(i,j+1)-uv(i,j)}{dy(j)} \tag{3-13}$$

$$uv(i,j+1) = \frac{dy(j)u(i,j+1)+dy(j+1)u(i,j)}{dy(j)+dy(j+1)} \cdot \frac{dx(i-1)v(i,j+1)+dx(i)v(i-1,j+1)}{dx(i)+dx(i+1)} \tag{3-14}$$

$$uv(i,j) = \frac{dy(j-1)u(i,j)+dy(j)u(i,j-1)}{dy(j-1)+dy(j)} \cdot \frac{dx(i-1)v(i,j)+dx(i)v(i-1,j)}{dx(i)+dx(i+1)} \tag{3-15}$$

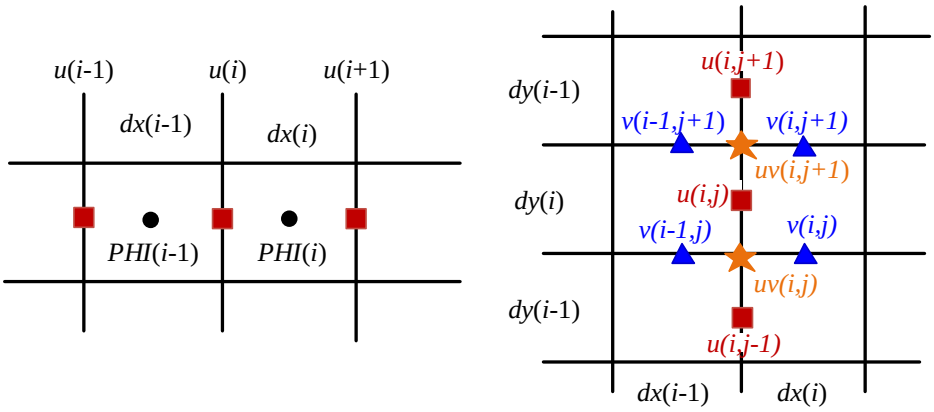

Figure 3.4: The schematic of convection in central difference scheme

3.2.3 Time integration

To conduct the numerical simulations, the Navier–Stokes governing equations should be discretized in both space and time. At first, a generic formula to demonstrate the process of time evolution is given by:

$$\frac{\partial f}{\partial t} = g(t,f) \tag{3-16}$$

When the method of backward difference is used to discretize the time derivative in Eq. (3-16), the first-order and second-order temporal discretization are given by:

$$\frac{f^{n+1}-f^{n}}{\Delta t} = g(f) \tag{3-17}$$

$$\frac{3f^{n+1}-4f^{n}+f^{n-1}}{2\Delta t} = g(f) \tag{3-18}$$

where f is a scalar quantity;

$n+1$ is the value at the future time $t+\Delta t$;

n is the value at the current time t;

$n-1$ is the value at the previous time $t-\Delta t$;

For implicit time integration, the expression to evaluate $g(f)$ at the future time $t+\Delta t$ is shown as:

$$\frac{f^{n+1}-f^{n}}{\Delta t} = g(f^{n+1}) \tag{3-19}$$

In the "implicit" integration, f^{n+1} in a given cell is related to f^{n+1} in neighbouring cells through $g(f^{n+1})$, and it is expressed as:

$$f^{n+1} = f^{n} + \Delta t g(f^{n+1}) \tag{3-20}$$

For the fully implicit scheme, it is unconditionally stable with respect to time step size. In general, the time step Δt is restricted by the stability limit of the underlying solver (or the Courant-Friedrichs-Lewy condition).

It would be more accurate when the same time step is used in the cells of the whole computational domain. To get a convergent result, the time step must be the minimum of all the local time steps in the domain, which is also referred to as "global time stepping". By comparison, the explicit time stepping is relative complicate, and it is used primarily to capture the transient behaviour of unsteady fluid flow. In such cases, it is more accurate and expensive than the method of implicit time stepping.

In the current study, the second order Runge-Kutta (RK2) scheme is used to deal with the time integration of the governing N-S equation. The partial differential equation $\frac{\partial f}{\partial t} = \mathrm{g}(t, f)$ is also used to demonstrate the discrete process as an example. Here f^{n} is the value of function $f(x)$ at the time of t^{n}, f^{n+1} and $f^{n+1/2}$ are the function values at the time t^{n+1} and $t^{n+1/2}$ respectively.

For the RK2 algorithm, the specific process is shown in Figure 3.5. The formulas are combined to solve the value of n+1 step in the middle step, expressed as:

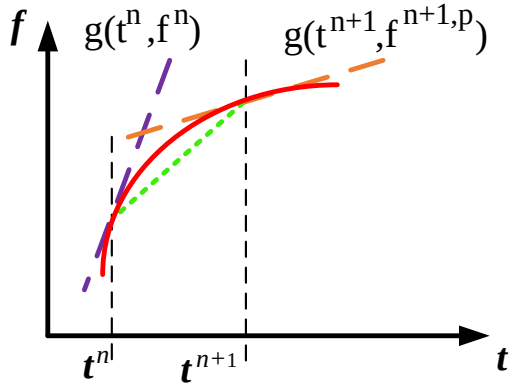

Figure 3.5: The time schematic of RK2 method

$$f^{n+1,p} = f^n + \Delta t \cdot g(t^n, f^n) \tag{3-21}$$

$$f^{n+1} = f^n + \Delta t \cdot \frac{1}{2}\left(g(t^{n+1}, f^{n+1,p}) + g(t^n, f^n)\right) \tag{3-22}$$

$$f^{n+1} = f^{n+1,p} + \Delta t \cdot \frac{1}{2}\left(g(t^{n+1}, f^{n+1,p}) - g(t^n, f^n)\right) \tag{3-23}$$

Combined with N-S governing equation, the mathematical expressions of RK2 method are shown as below:

$$(1):\ \frac{u_p^* - u^n}{\Delta t} = RHS^n \tag{3-24}$$

$$(2):\ \nabla \cdot \frac{\nabla p_p}{\rho} = \frac{\nabla \cdot (u_p^*)}{\Delta t},\ \frac{u_p - u_p^*}{\Delta t} = -\frac{\nabla p_p}{\rho} \tag{3-25}$$

$$(3):\ \frac{u_c^* - u_p}{0.5\Delta t} = (RHS^p - RHS^n) - \left(-\frac{\nabla p_p}{\rho}\right) \tag{3-26}$$

$$(4):\ \cdot \frac{\nabla p_c}{\rho} = \frac{\nabla \cdot u_c^*}{0.5\Delta t},\ \frac{u^{n+1} - u_c^*}{0.5\Delta t} = -\frac{\nabla p_c}{\rho} \tag{3-27}$$

To reduce the computational error, the CFL number is calculated as below, and its value is smaller than 0.5 in this study.

$$\mathrm{CFL} = \Delta t\left(\frac{|u|}{\Delta x} + \frac{[v]}{\Delta y} + \frac{[w]}{\Delta z} + 2v\left(\frac{1}{\Delta x^2} + \frac{1}{\Delta y^2} + \frac{1}{\Delta z^2}\right)\right) \tag{3-28}$$

3.2.4 The pressure Poisson equation

The N-S governing equations can be further written into:

$$\frac{\partial u}{\partial t} = -\frac{1}{\rho(\phi)}\nabla p - R.h.s \tag{3-29}$$

where $R.h.s = \nabla \cdot (\vec{u}\vec{u}) + \frac{1}{\rho}\frac{1}{Re}\nabla \cdot \left(2\mu(\phi)\overline{\overline{D}}\right)$.

Assume the velocity at the middle step is $\vec{u}^*$, then:

$$\frac{\vec{u}^* - \vec{u}^n}{\Delta t} = R.h.s \tag{3-30}$$

$$\frac{\vec{u}^{n+1} - \vec{u}^*}{\Delta t} = -\frac{1}{\rho(\phi)}\nabla p \tag{3-31}$$

The pressure Poisson equation can be solved by the projection method, which is shown below.

$$\nabla \cdot \left(\frac{\vec{u}^{n+1} - \vec{u}^*}{\Delta t}\right) = -\nabla \cdot \frac{1}{\rho(\phi)}\nabla p \tag{3-32}$$

According to the continuity equation $\nabla \cdot \vec{u}^{n+1} = 0$, so $\frac{\nabla \cdot \vec{u}^*}{\Delta t} = \nabla \cdot \frac{1}{\rho(\phi)}\nabla p$, and the velocity at the $n+1$ step is:

$$\vec{u}^{n+1} = \vec{u}^* - \nabla \cdot \frac{1}{\rho(\phi)}\nabla p \tag{3-33}$$

In Figure 3.6, the pressure Poisson equation is discretized with a seven-point stencil. The pressure located at the centre of gird is solved by Eq. (3-34), which is also based on the pressure values of surrounding points.

$$\nabla \cdot \frac{1}{\rho(\phi)}\nabla p = A_{i-1,j,k}p_{i-1,j,k} + A_{i,j,k}p_{i,j,k} + A_{i+1,j,k}p_{i+1,j,k} + A_{i,j-1,k}p_{i,j-1,k} +$$

$$A_{i,j+1,k}p_{i,j+1,k} + A_{i,j,k-1}p_{i,j,k-1} + A_{i,j,k+1}p_{i,j,k+1} = \frac{\nabla \cdot \vec{u}^*}{\Delta t} \tag{3-34}$$

To save the computational memory, the coefficient matrix is written into:

$$\mathrm{A} = \mathrm{D} + A_x^L + A_x^U + A_y^L + A_y^U + A_z^L + A_z^U \tag{3-35}$$

where$A_x^L(i,j,k) = A_{i-1,j,k}$, $A_x^U(i,j,k) = A_{i+1,j,k}$, $A_y^L(i,j,k) = A_{i,j-1,k}$, $A_y^U(i,j,k) = A_{i,j+1,k}$, $A_Z^L(i,j,k) = A_{i,j,k-1}$, $A_Z^U(i,j,k) = A_{i,j,k+1}$, $D(i,j,k) = A_{i,j,k}$.

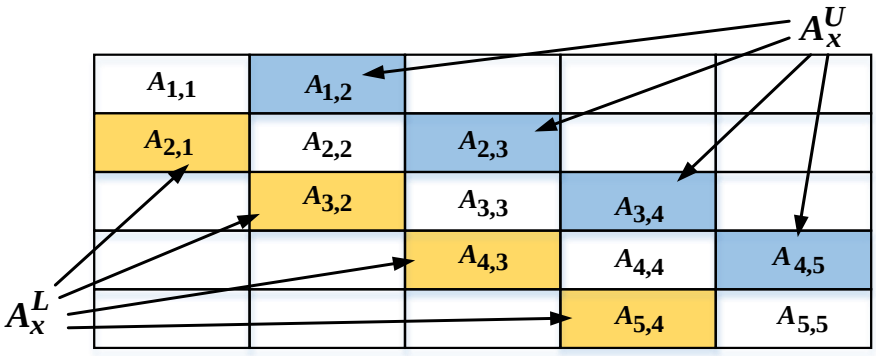

Figure 3.6: The matrix schematic of Poisson equation

3.2.5 Boundary condition

The boundary conditions are necessary to solve the Poisson equation. In this study, the ghost cells are used to expand the grid spacing near the boundary. It provides a generalized form for all grid points at which the N-S equations can be solved. Besides, this approach also provides a natural way to implement parallelization via domain decomposition technique.

(1) Neumann boundary condition and Dirichlet boundary condition

To demonstrate the Dirichlet and Neumann boundary conditions, the velocity and pressure distribution are shown in Figure 3.7.

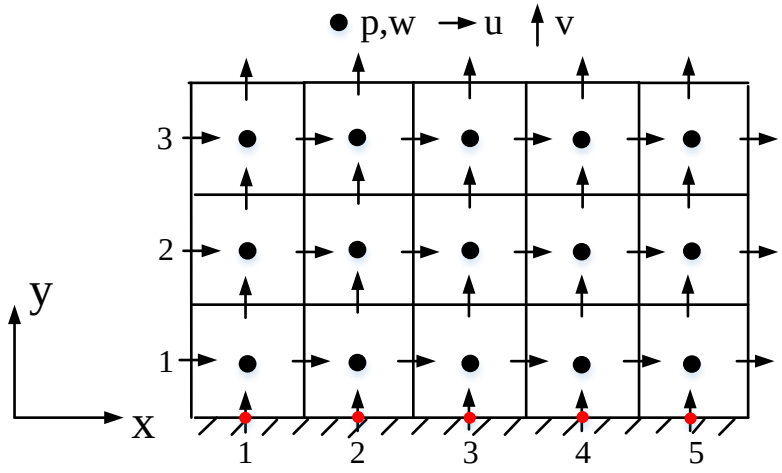

Figure 3.7: The schematic of Dirichlet and Neumann boundary condition

The Dirichlet boundary condition is directly enforced on the lower boundary condition by the following equation:

$$u_{i+\frac{1}{2},\frac{1}{2},k} = u_b \ , \ v_{i,\frac{1}{2},k} = v_b \tag{3-36}$$

where u_b and v_b are the flow velocity u and normal velocity v on the boundary respectively.

The Neumann boundary is enforced on the boundary condition, and its mathematical expression is $\frac{\partial p}{\partial y} = 0$, and its discrete expression is shown as:

$$\mathrm{p}\left(i, \frac{1}{2}, k\right) = p(i, 1, k) \tag{3-37}$$

(2) Inlet-outlet boundary condition

The inlet-outlet boundary condition is shown below, which is proposed by Orlanski (1976). The boundary velocity can be solved by the following equation:

$$\frac{\partial u_i}{\partial t} + U_{conv}\frac{\partial u_i}{\partial x} = 0 \tag{3-38}$$

where u_i is the velocity component at any direction;

U_{conv} is the convective velocity.

(4) Shear-free boundary condition

The tangential velocity of the upper and lower boundaries is zero, that is, no shear force. The corresponding boundary conditions are:

$$\mu\left(\frac{\partial u}{\partial y} + \frac{\partial v}{\partial x}\right) = \mu\left(\frac{\partial w}{\partial y} + \frac{\partial v}{\partial z}\right) = 0,\ \frac{\partial u}{\partial y} = \frac{\partial w}{\partial y} = 0 \tag{3-39}$$

(5) Wall boundary condition

The velocity at the boundary of solid wall is zero, i.e.,

$$u = v = w = 0 \tag{3-40}$$

3.3 Numerical modelling of oscillating jet flow

3.3.1 Physical model

For the piezoelectric fan, a three-dimensional (3D) CFD model is developed to study the influences of its movements on the fluid flow. In Figure 3.8, the computational domain is a cuboid with the size of 15L×15L×0.08L, L is the length of piezoelectric fan. The small distance chosen in the third direction is to ensure the simulation is 3D, which is essential to LES. The solution in the third direction is of no physical meaning as the problem under investigation is physically two-dimensional.

In this study, the velocity of piezoelectric fan is to replace the displacements of the fan, which avoids the process of remeshing. It reduces the compute largely and saves the

computational time seriously. The flow field of oscillating jet flow is then discussed concerning the blade vibrating amplitude, vibrating frequency and the wave number of fan motions.

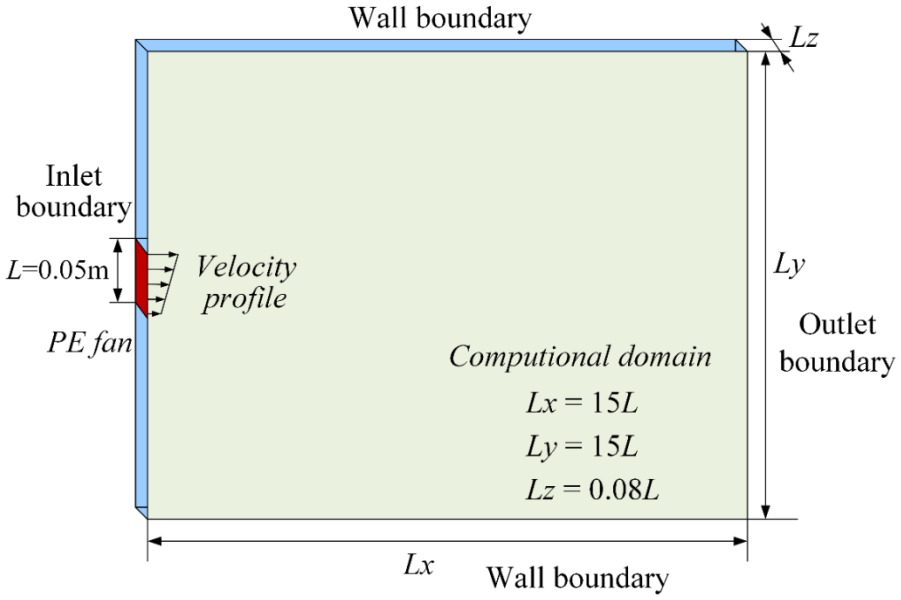

Figure 3.8: Computational domain of piezoelectric fan (3D with uniform z-direction)

In Table 3-1, a number of numerical cases are calculated with various kinematic parameters, and their parameters are listed as well. The formula for the oscillating velocity $V(t)$ at the inlet boundary can be given as:

$$V(t) = 2\pi f \times A\left(\frac{y}{L}\right)^2 \times \cos(2\pi f t + ky) \tag{3-41}$$

where f is the oscillating frequency in unit Hz;

L is the length of the piezoelectric fan in unit m;

A is the amplitude of the piezoelectric fan vibration in unit m;

t is the time in unit s;

k is the wave number.

For the motions of piezoelectric fan, it is notable that the wave number is related to spatial variations while the frequency is related to temporal variations.

The inlet velocity of piezoelectric fan is a general cosine function, which is parameterized with the fan length. All these kinematic parameters of fan motions have a significant impact on the flow field. Therefore, different oscillating frequencies, oscillating amplitudes and wave numbers are selected to examine their effects on the fluid flow. The parameter values of specific cases are shown in the following table (Table 3-1).

Table 3-1 The computational cases to study the fluid flow induced by the movements of piezoelectric fan

Case number (No.)	Frequency (Hz)	Amplitude (m)	Wave number
1	5	0.02	2
2	10	0.02	2
3	20	0.02	2
4	10	0.01	2
5	10	0.02	2
6	10	0.04	2
7	10	0.02	0
8	10	0.02	2
9	10	0.02	7

CFD numerical simulations can measure the influences of PE fan motions on the surrounding fluid flow. The LES method is applied, and the Smagorinsky-Lilly model can model the sub-grid scale turbulent viscosity. In order to make the simulation converge faster, the second order upwind discretization is used for the momentum equation with the pressure-velocity coupled scheme. The second order Runge-Kutta scheme is used for the temporal discretization.

The grid independency and the time-step independency are examined through different grid resolutions and different time step. Based on previous convergence studies, the time step is set as 0.0025s. The simulation will be run over 20000 steps (500 oscillating periods for the frequency is 10Hz), and it is judged by convergence when the difference of mass flow rate between inlet and outlet is very small, around 10^{-5}.

3.3.2 Effects of oscillating frequency

Three different oscillating frequencies of piezoelectric fan, 5 Hz, 10 Hz and 20 Hz, are selected to demonstrate the effect on the flow field. During the simulation, the time step is 0.0025s, which is 1/20 times of the oscillating period when the frequency is 20 Hz.

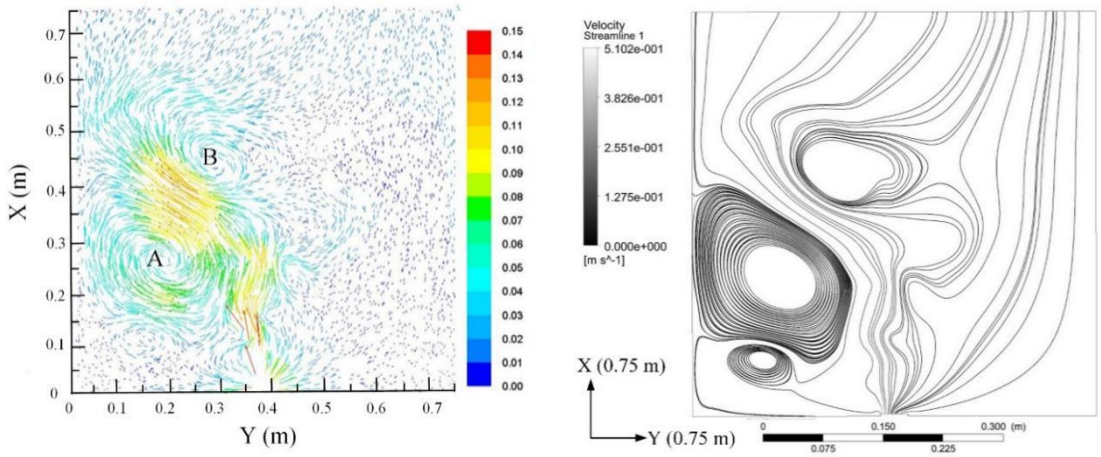

(a) f=5 Hz

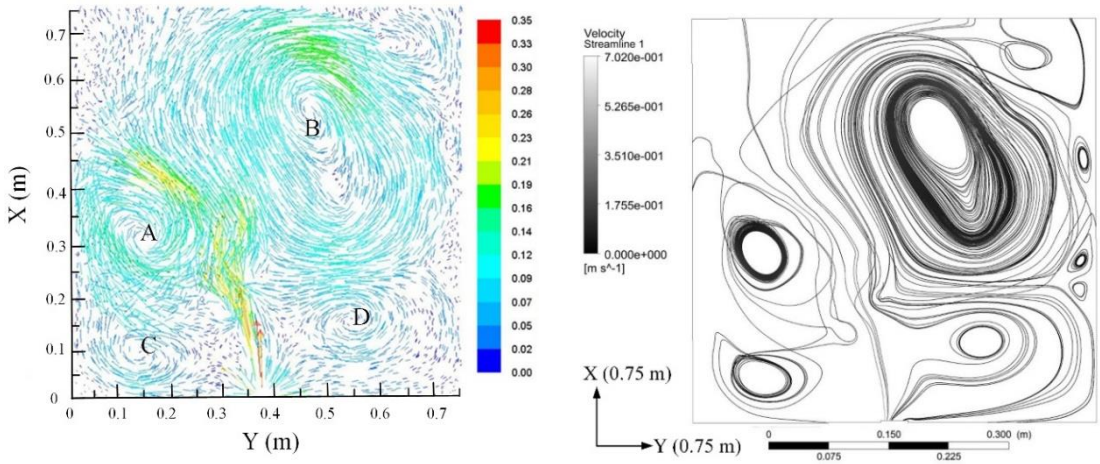

(b) f=10 Hz

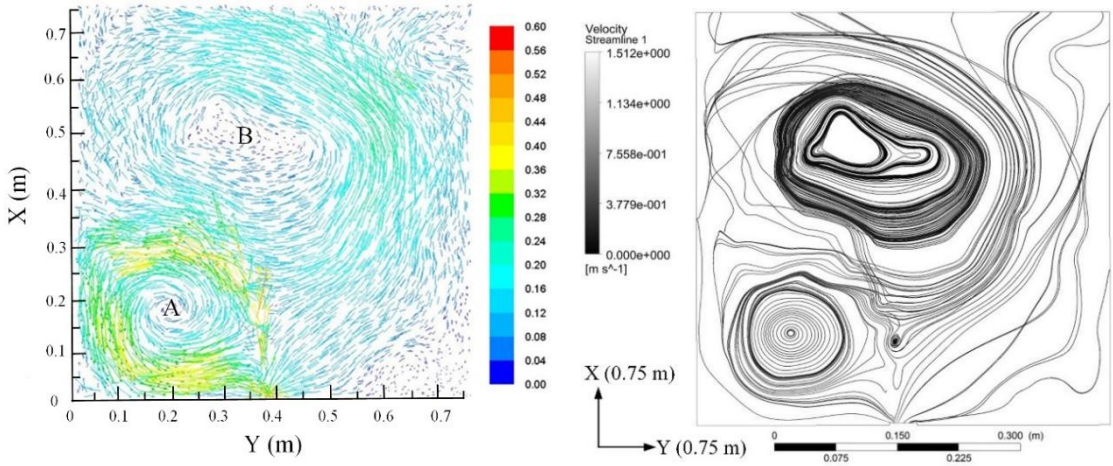

(c) f=20Hz

Figure 3.9: Velocity vectors coloured by velocity magnitude (m/s) with different frequencies when :A=0.02m and k=2 at 500T (T is the oscillating period) compared with the streamline diagrams

Figure 3.9 shows that under the same amplitude (0.02 m) and wave number (k=2),

different frequencies will lead to different numbers of circulation zones in the flow field. When the oscillating frequency is 5Hz, there are mainly three circulation zones located above the left side of inlet. For 10Hz and 20Hz, there are about eight and two circulation zones respectively. The large circulation zones control bulk mixing in the flow field, while the small circulation zones play a major part in local mixing.

The circulation zone has different sizes at different frequencies. At 5Hz, the circulation zones are mainly located left. The circulation zone “A” is the largest, “B” is smaller than “A”, and there is also one small circulation zone under “A”. At 10Hz, there are two circulation zones located on the left side of the fan, which are indicated as “A” and “C” in Figure 3.9 (b). The circulation zones “B” and “D” are located on the right side of the PE fan with circulation zone “D” emerging below “B”, which is larger than the others. At 20Hz, two large circulation zones can be observed, where the circulation zone “B” is very large and located above the PE fan in the middle of the computational domain.

Due to the complex interactions between the inlet oscillatory velocity of piezoelectric fan and wall boundary, these circulation zones have observable trends, where the wall confinement affects the flow development while the oscillatory velocity may lead to formation of vortical structures. All these results suggest that the oscillating frequency has a strong influence on the circulation zone distributions and the velocity of flow field.

For 5 Hz, 10 Hz and 20 Hz, the velocity vectors within one oscillation cycle are shown in Figure 3.10, Figure 3.11 and Figure 3.12 respectively. After 500 oscillation periods, the velocity vectors are coloured by the velocity magnitude (m/s). Within one oscillating period, the flow exhibits a quasi-steady behaviour with sizes and locations of the main circulation zones remain largely stable. There are still variations in the flow field during one period. The two large circulation zones “A” and “B” are largely stable. However, other circulation zones are more dynamic, which evolve with time with an instantaneous presence. They are located near the piezoelectric fan and have the characteristics of flow vortical structures.

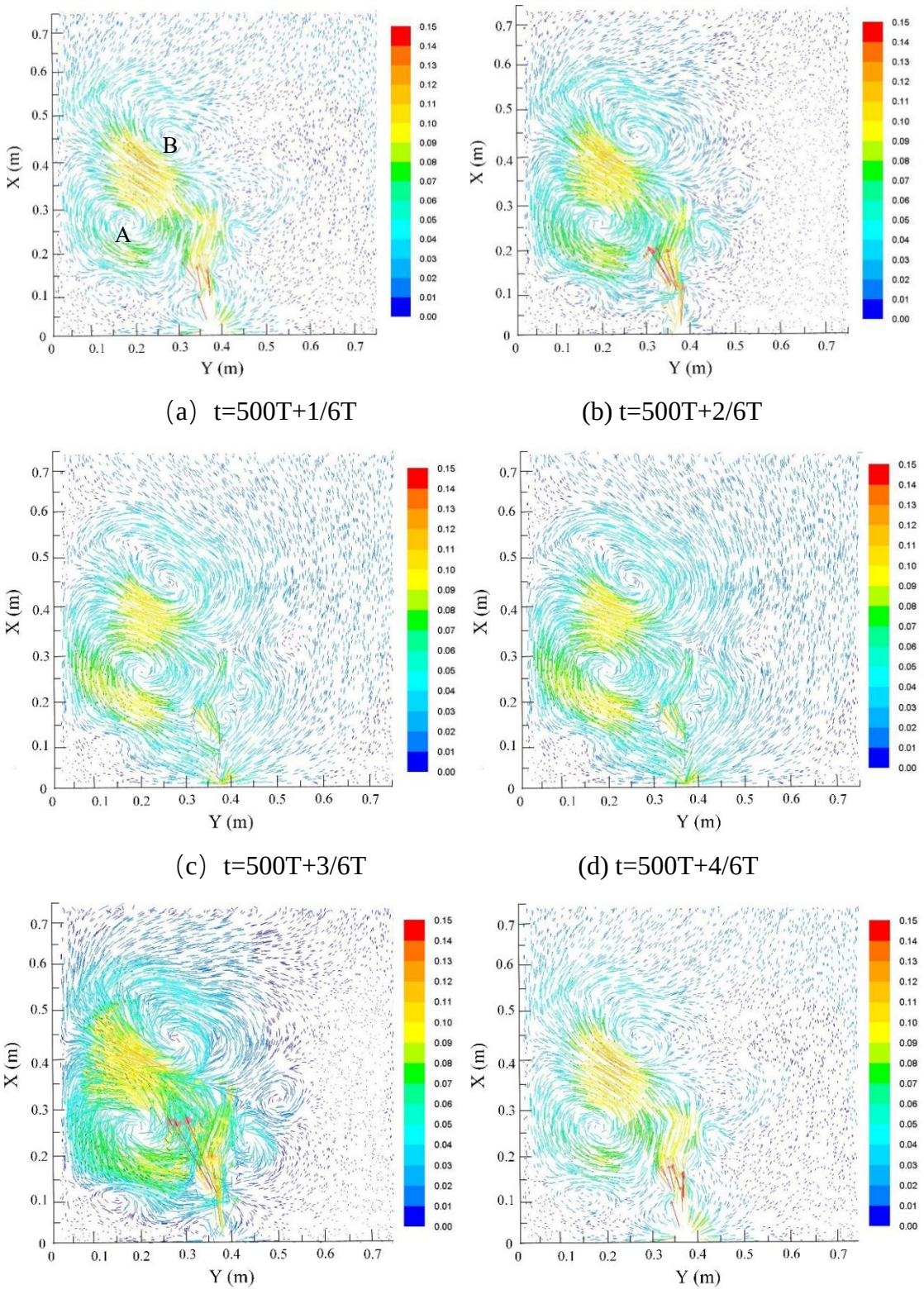

(a) t=500T+1/6T (b) t=500T+2/6T

(c) t=500T+3/6T (d) t=500T+4/6T

(e) t=500T+5/6T (f) t=500T+6/6T

Figure 3.10: Velocity vectors coloured by velocity magnitude (m/s) within one oscillation cycle (f=5 Hz, A=0.02 m, k = 2)

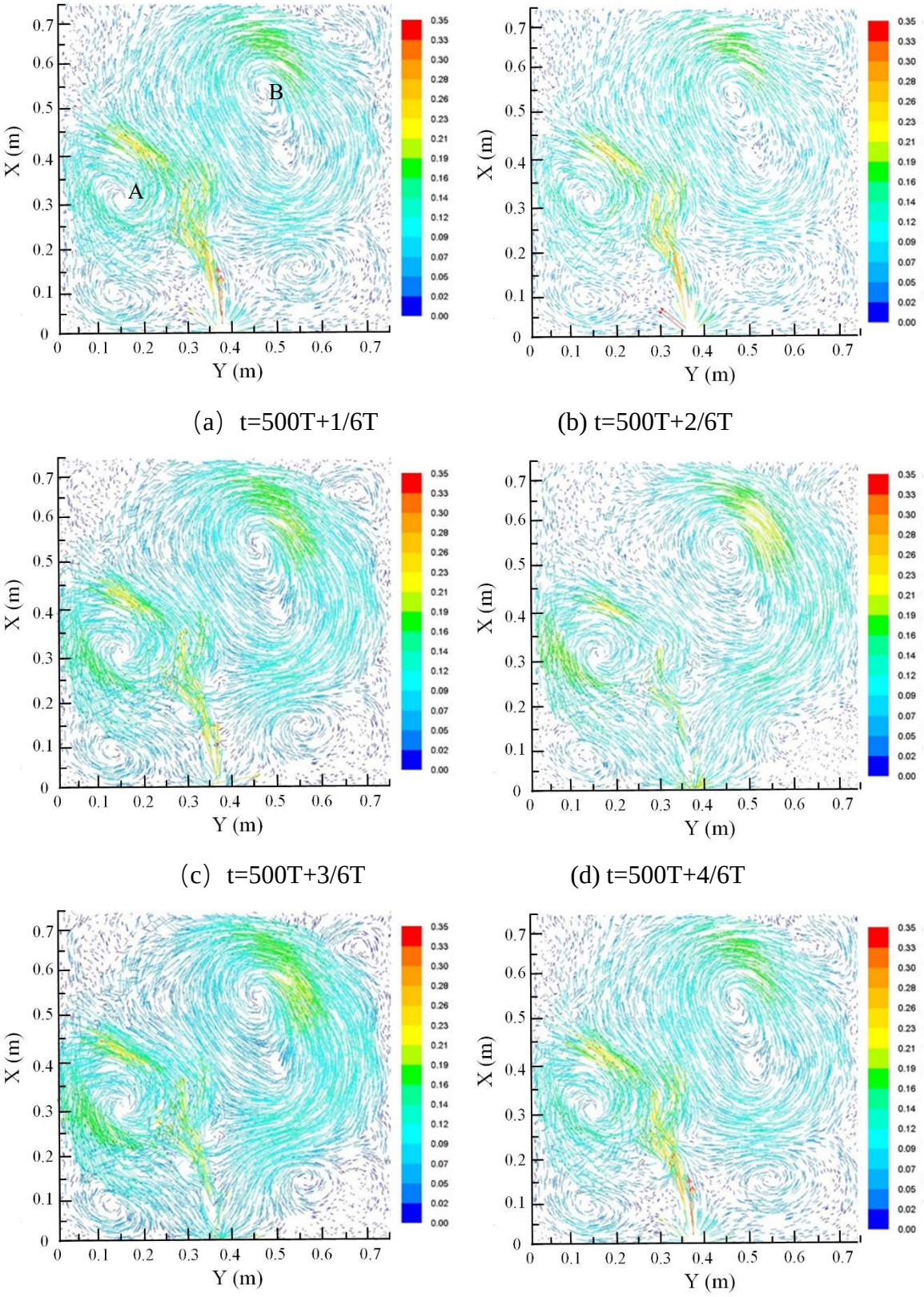

(a) t=500T+1/6T (b) t=500T+2/6T

(c) t=500T+3/6T (d) t=500T+4/6T

(e) t=500T+5/6T (f) t=500T+6/6T

Figure 3.11: Velocity vectors coloured by velocity magnitude (m/s) within one oscillation cycle (f=10 Hz, A=0.02 m, k = 2)

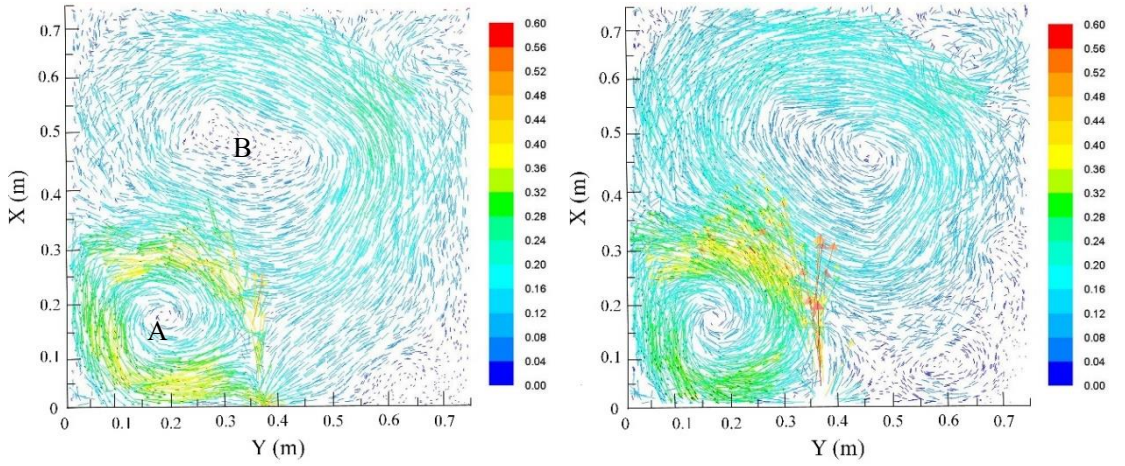

（a） t=500T+1/6T　　(b) t=500T+2/6T

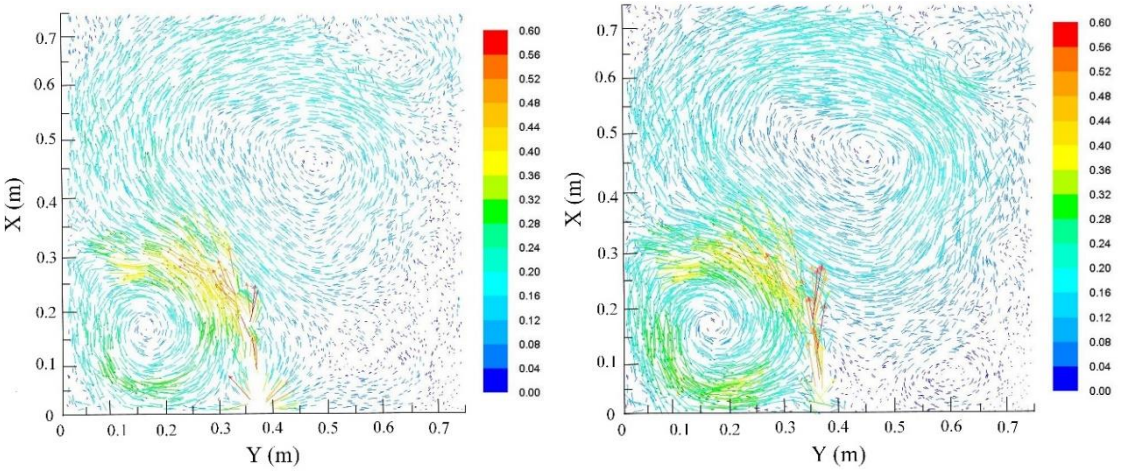

（c） t=500T+3/6T　　(d) t=500T+4/6T

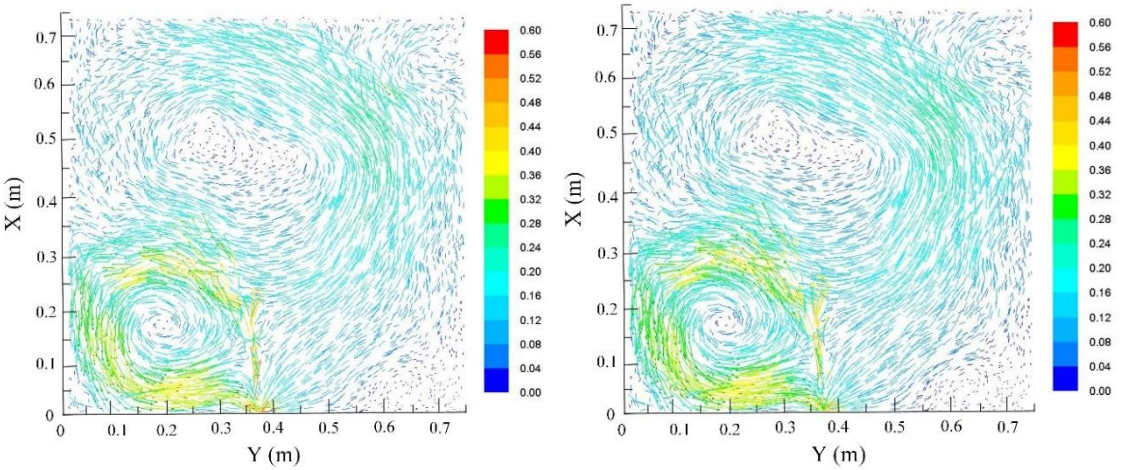

(e) t=500T+5/6T　　(f) t=500T+6/6T

Figure 3.12: Velocity vectors coloured by velocity magnitude (m/s) within one oscillation cycle (f=20 Hz, A=0.02 m, k = 2)

The frequency variation of piezoelectric fan seems to have a major impact on the flow circulation zones. Although the flow does not experience significant changes within one

oscillation period with a fixed frequency. This is evident from the comparisons between Figure 3.10, Figure 3.11 and Figure 3.12. As a whole, the results in these figures show that the oscillating frequency has a significant influence on the circulation patterns in the flow field, which, in turn, has a major impact on the mixing. The flow circulation seems the strongest for the 10 Hz case with the biggest number of circulation zones compared with the other two cases with the frequencies of 5 Hz and 20 Hz. This indicates that there may be an optimal frequency that can maximise the mixing. Overall, the oscillating frequency has an important effect on the number, sizes and locations of the circulation zones in the flow field.

3.3.3 Effects of oscillating amplitude

To examine the influences of oscillating amplitude on the flow field, three amplitudes, 0.01m, 0.02m and 0.04m, have been simulated in this study. They represent three different cases: the small amplitude, the middle amplitude and the large amplitude respectively.

Under the same frequency (f=10 Hz) and wave number (k=2), the numerical results show that the number of circulation zones varies with different amplitudes. And they are shown in Figure 3.13. In Figure 3.13(a), when the amplitude is 0.01 m, the velocity at the inlet boundary is relatively low, there are mainly six circulation zones formed and distributed in the flow field. In Figure 3.13(b) and Figure 3.13(c), when the amplitudes are 0.02m and 0.04m, the number of circulation zones are about eight and four respectively.

Moreover, the locations and sizes of the circulation zones vary with the amplitudes of fan motions. The locations and sizes of circulation zones at the high amplitude (such as the case: A=0.04m, f=10 Hz and k=2) are similar to those at high frequency under medium amplitude (such as the case: A=0.02 m, f=20 Hz and k=2). The results indicate that there may be an optimal amplitude that can maximise the mixing in the flow field because the circulation zones are greatly affected by the pulsating amplitude of the PE fan.

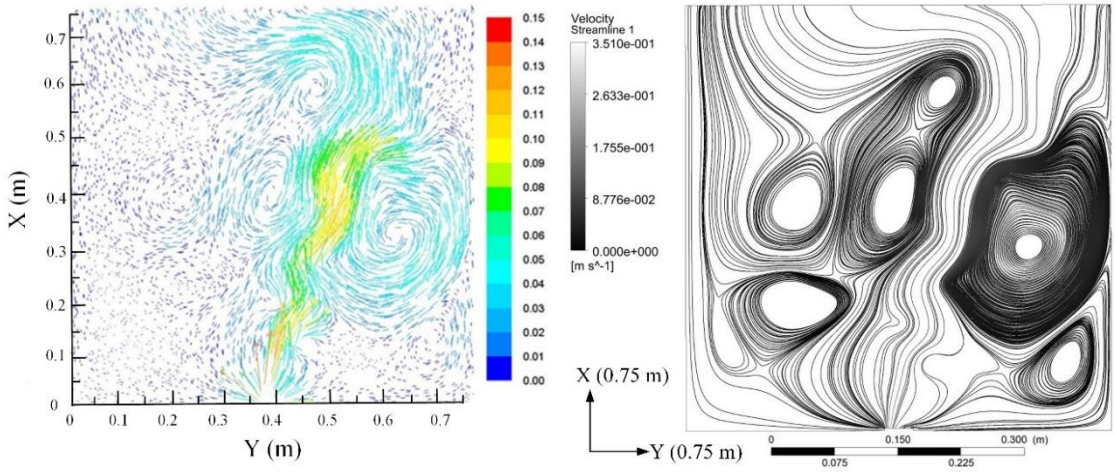

(a) A=0.01m

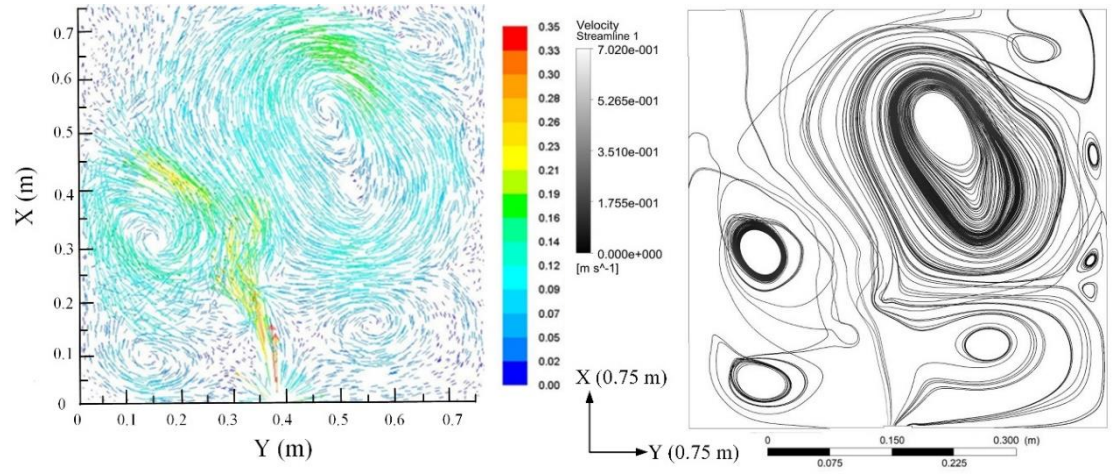

(b) A=0.02m

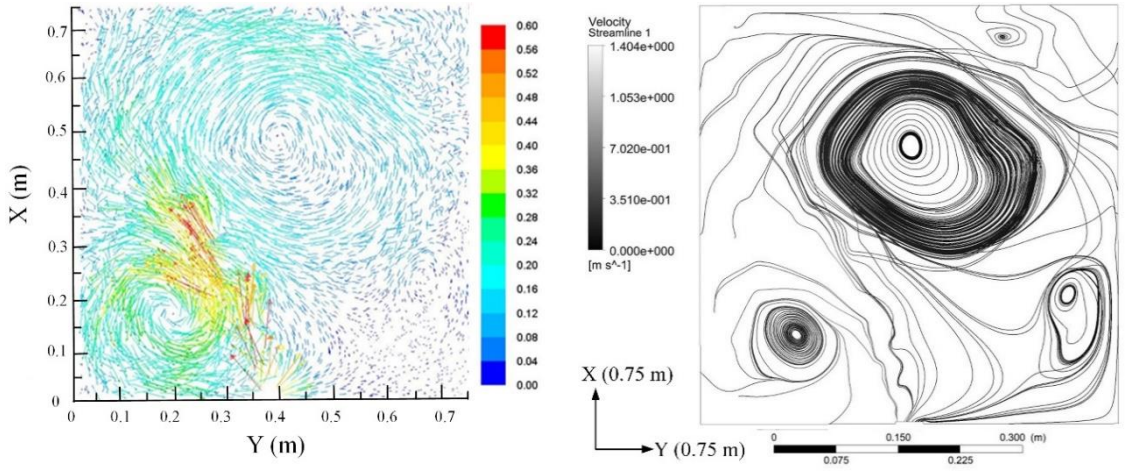

(c) A=0.04m

Figure 3.13: Velocity vectors coloured by velocity magnitude (m/s) when f=10 Hz, k = 2 with different amplitudes at 500T compared with the streamline diagrams

With a fixed pulsating amplitude, after the oscillation cycle 500T, the distributions of

large circulation zones within one period are largely stable, which are shown in Figure 3.14 and Figure 3.15 respectively. These results indicate that the flow exhibits a quasi-steady behaviour within the whole oscillation cycle.

Comparing these cases, when the amplitudes are 0.01 m and 0.04 m, the velocity of fluid flow increases with the amplitude, and the maximum velocities are 0.1 m/s and 0.6 m/s respectively. There are small variations between circulation zones within one period, especially at locations near the domain inlet and outlet boundaries. In conclusion, the oscillating amplitude has a significant influence on the number, sizes and locations of circulation zones, and the velocity of fluid flow increases with the amplitude.

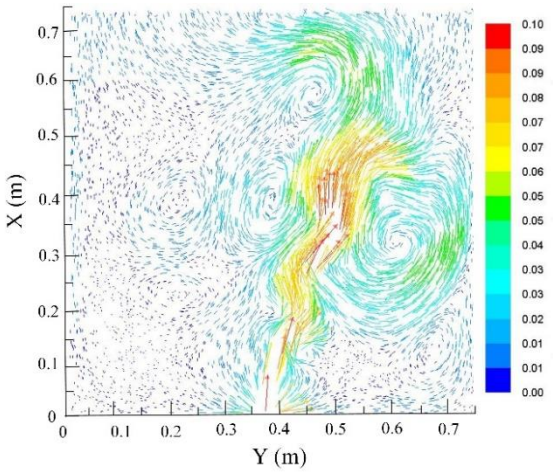

（a） t=500T+1/6T

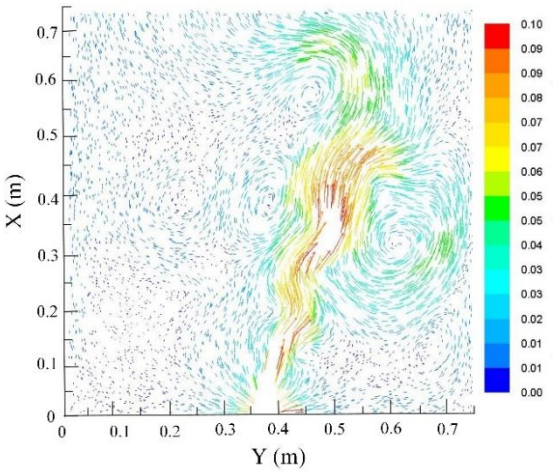

(b) t=500T+2/6T

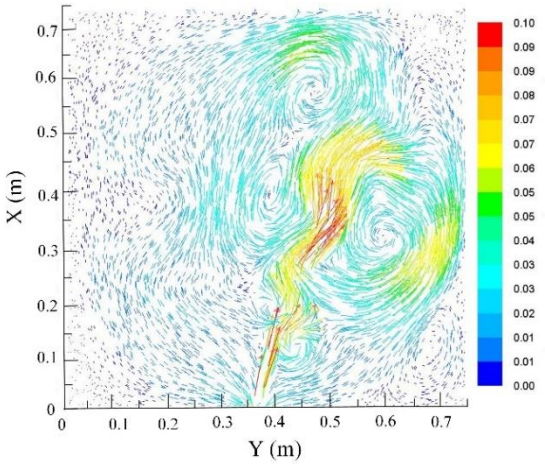

（c） t=500T+3/6T

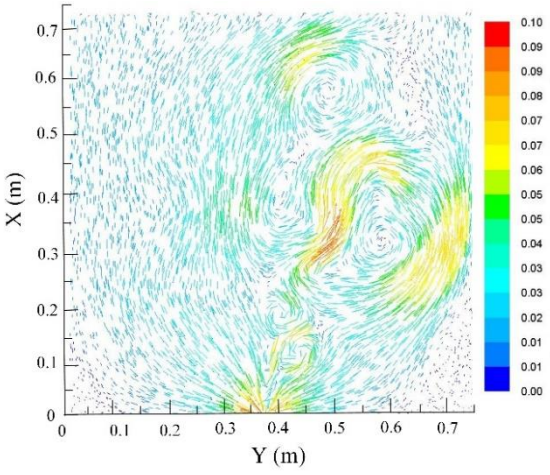

(d) t=500T+4/6T

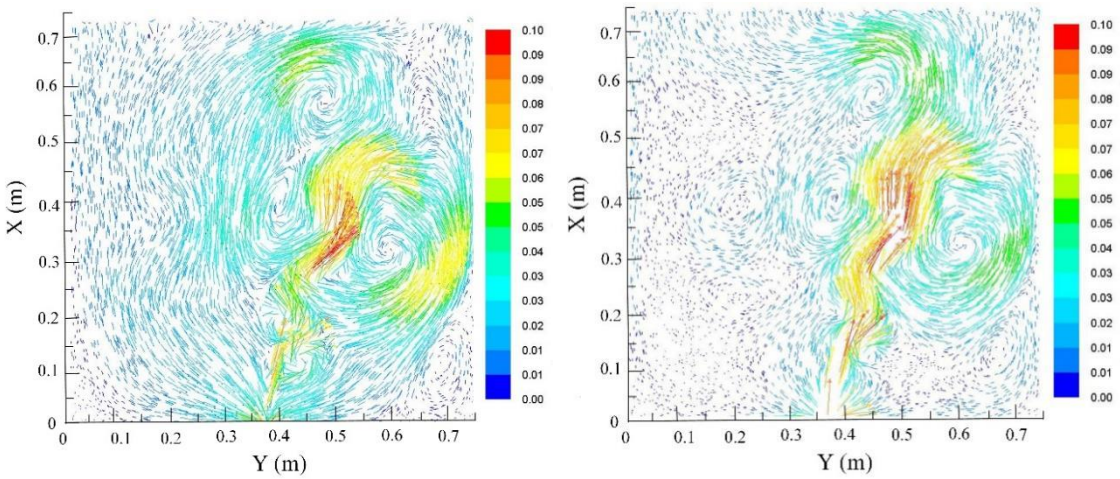

(e) t=500T+5/6T (f) t=500T+6/6T

Figure 3.14: Velocity vectors coloured by velocity magnitude (m/s) within one oscillation cycle (f=10Hz, A=0.01m, k = 2)

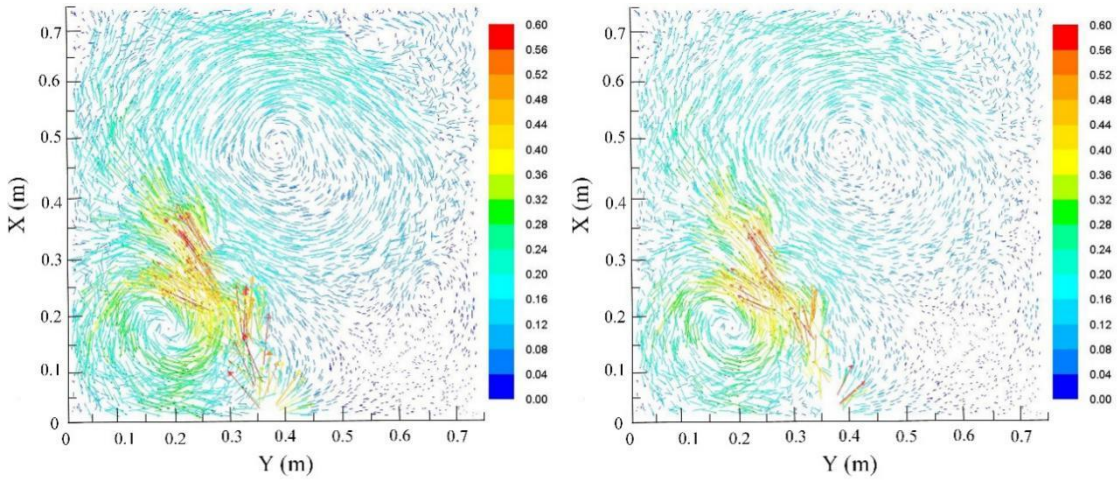

（a） t=500T+1/6T (b) t=500T+2/6T

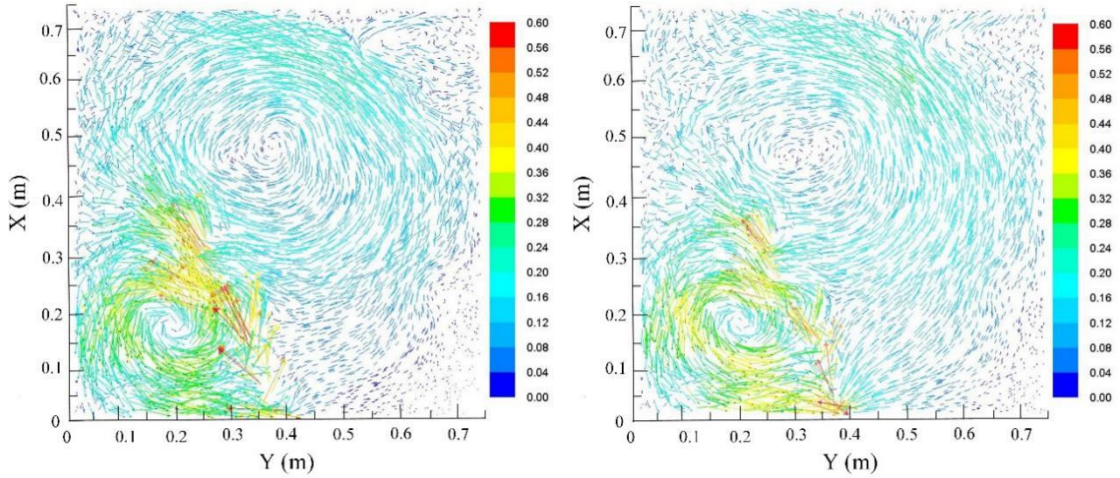

（c） t=500T+3/6T (d) t=500T+4/6T

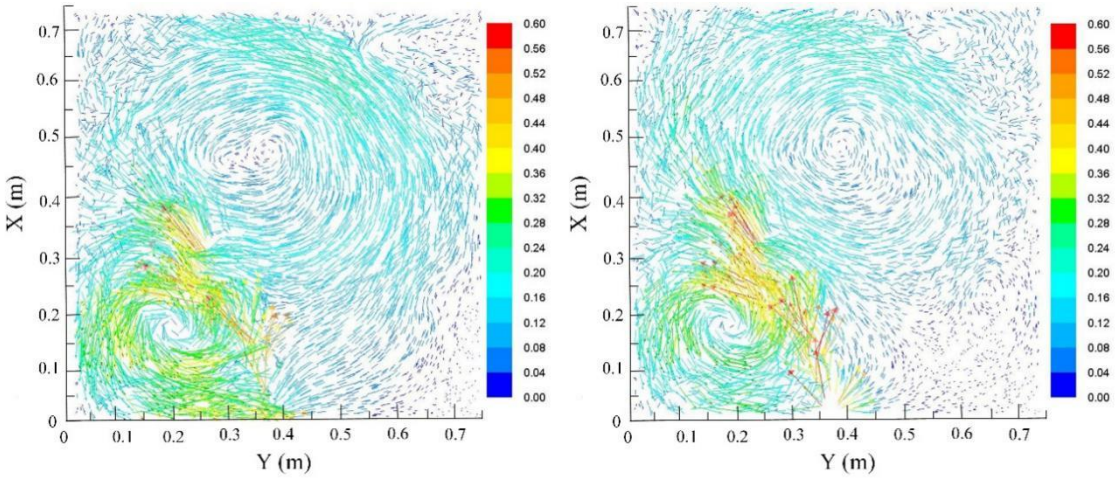

(e) t=500T+5/6T (f) t=500T+6/6T

Figure 3.15: Velocity vectors coloured by velocity magnitude (m/s) within one oscillation cycle (f=10Hz, A=0.04m, k = 2)

3.3.4 Effects of wave number

Three different wave numbers, k=0, k=2 and k=7, can measure the influences of wave number on the flow field. When k=0, the motions of piezoelectric fan are pure standing wave. For k=2 and k=7, the motions are inclined to the mixed waves, which are composed of pure standing wave and pure travelling wave. The component of pure travelling wave, i.e. the travelling index, increases with the wave number.

In Figure 3.16, the numerical results show that the velocity of fluid flow does not change radically when the wave number varies between 0, 2 and 7. The maximum velocity is between 0.35 m/s and 0.4 m/s. The distributions of circulation zones change slightly with the wave number under the same amplitude (A=0.02m) and frequency (f=10 Hz). Meanwhile, the number of large circulation zones also change slightly with the wave number of fan motions.

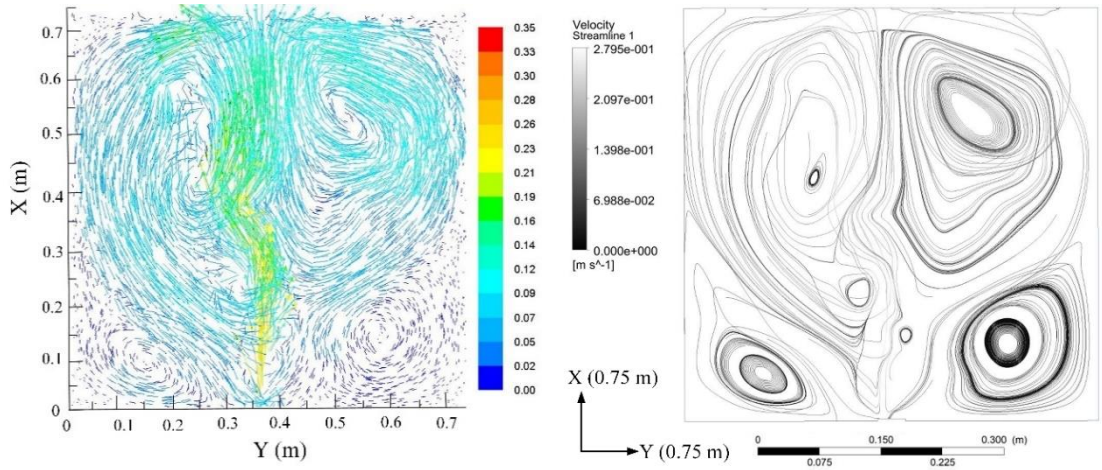

(a) k=0

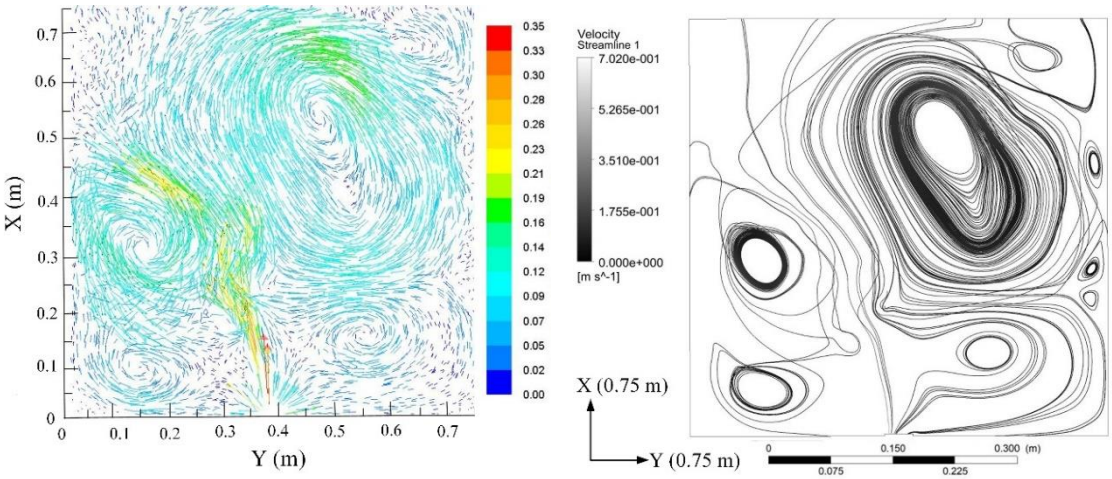

(b) k=2

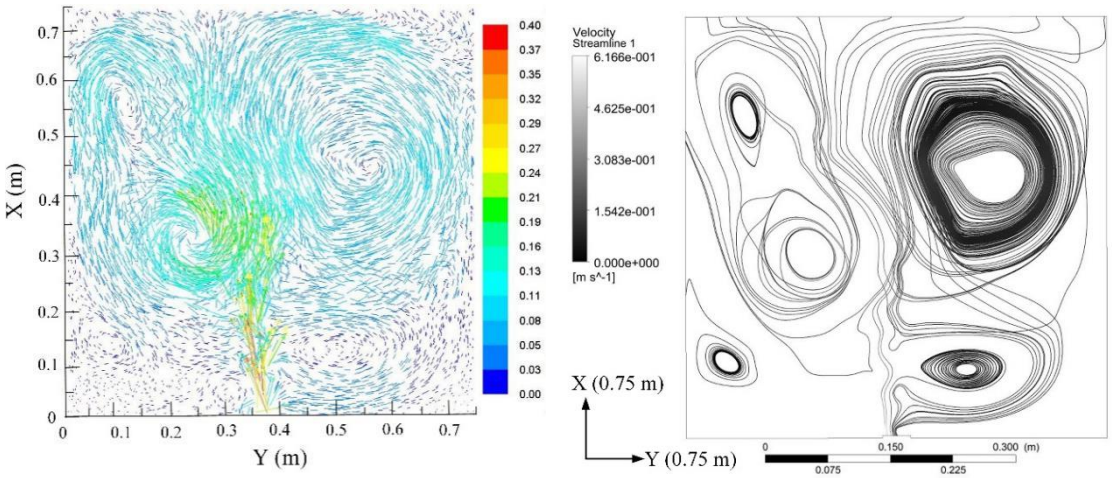

(c) k=7

Figure 3.16: Velocity vectors coloured by velocity magnitude (m/s) when f=10Hz, A=0.02m with different wave numbers at 500T compared with the streamline diagrams

Within one oscillation cycle, when the wave number is zero (f=10 Hz, A=0.02 m),

the location of circulation zones is nearly symmetrically distributed in the whole fluid domain. However, the symmetrical distribution of circulation zone is broken when the wave number turn to 2 or 7, and the size of circulation zones at the upper right corner also increases.

The main difference between Figure 3.17 and Figure 3.18 is the velocity distribution of fluid flow. When the flow symmetry is broken, the tendency of flow transition to turbulence is enhanced, which can, in turn, enhance the mixing in the flow field. Therefore, it provides a new approach to enhance the mixing in the fluid domain, i.e., the characteristics of heat transfer.

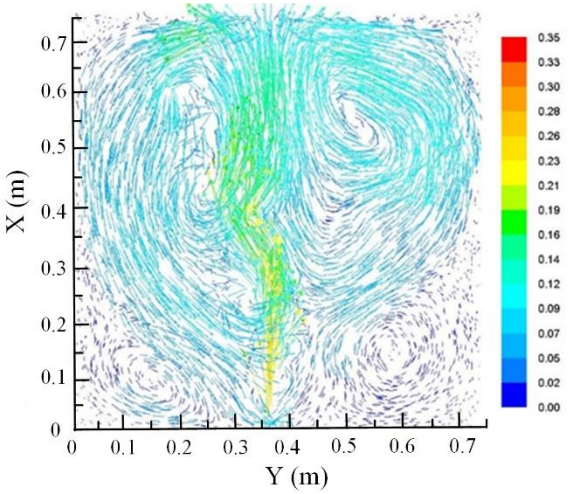

(a) t=500T+1/6T

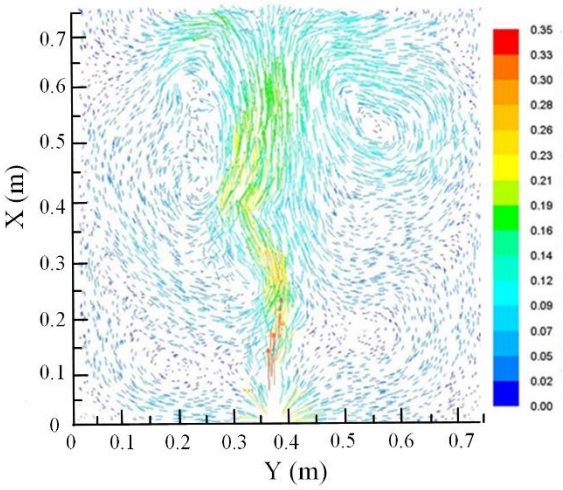

(b) t=500T+2/6T

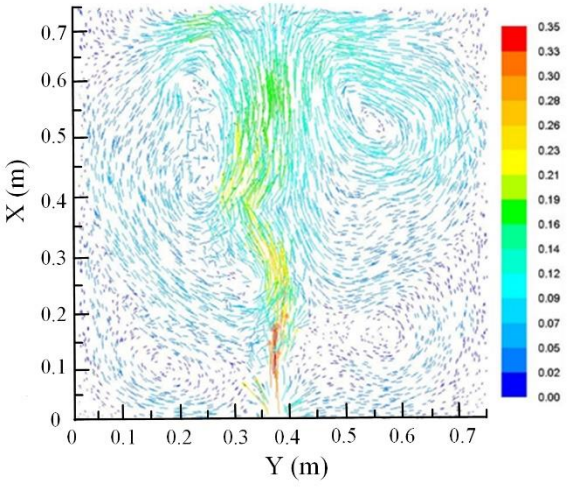

（c） t=500T+3/6T

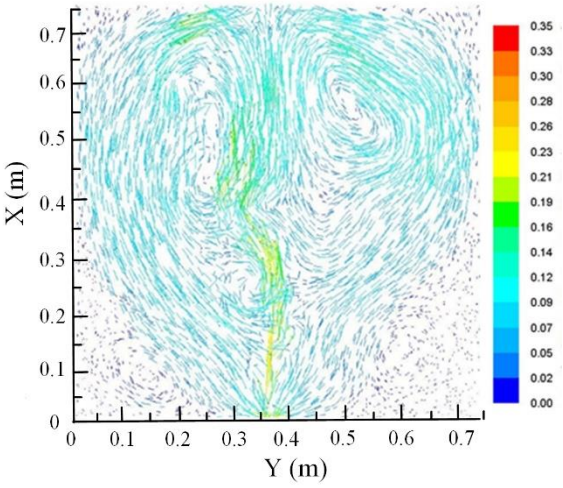

(d) t=500T+4/6T

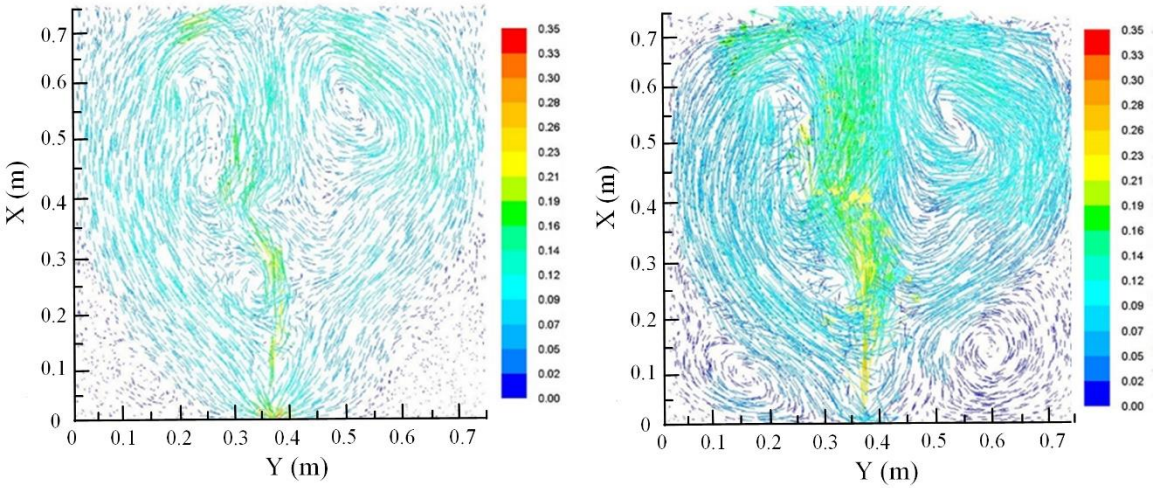

(e) t=500T+5/6T (f) t=500T+6/6T

Figure 3.17: Velocity vectors coloured by velocity magnitude (m/s) of the flow field of piezoelectric fan with a motion of standing wave (f=10Hz, A=0.02m, k = 0) within one oscillation cycle .

In summary, the effects of wave number on the flow field are the topology of the circulation zones, which is closely related to the wave number. The symmetrical distribution can be broken down by a non-zero wave number.

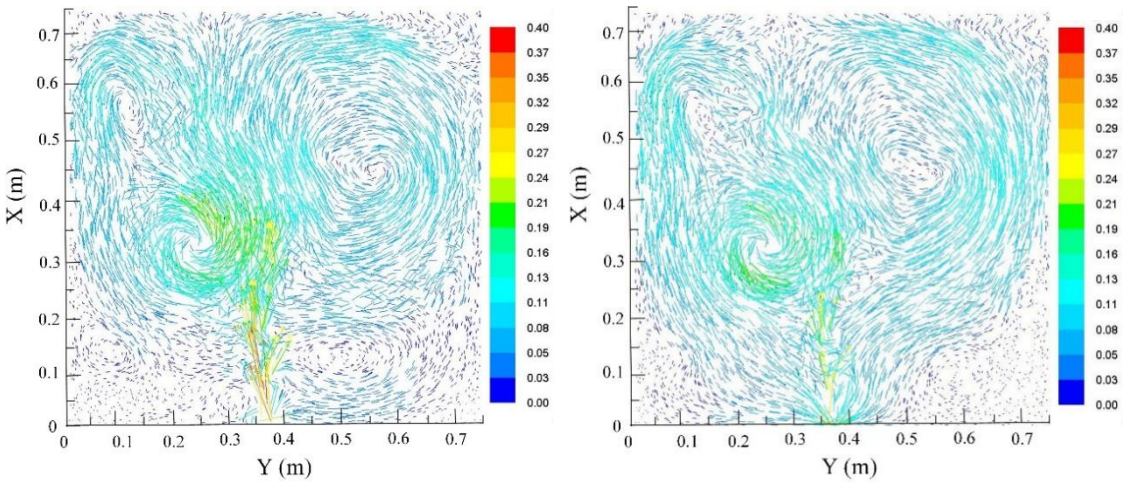

（a） t=500T+1/6T (b) t=500T+2/6T

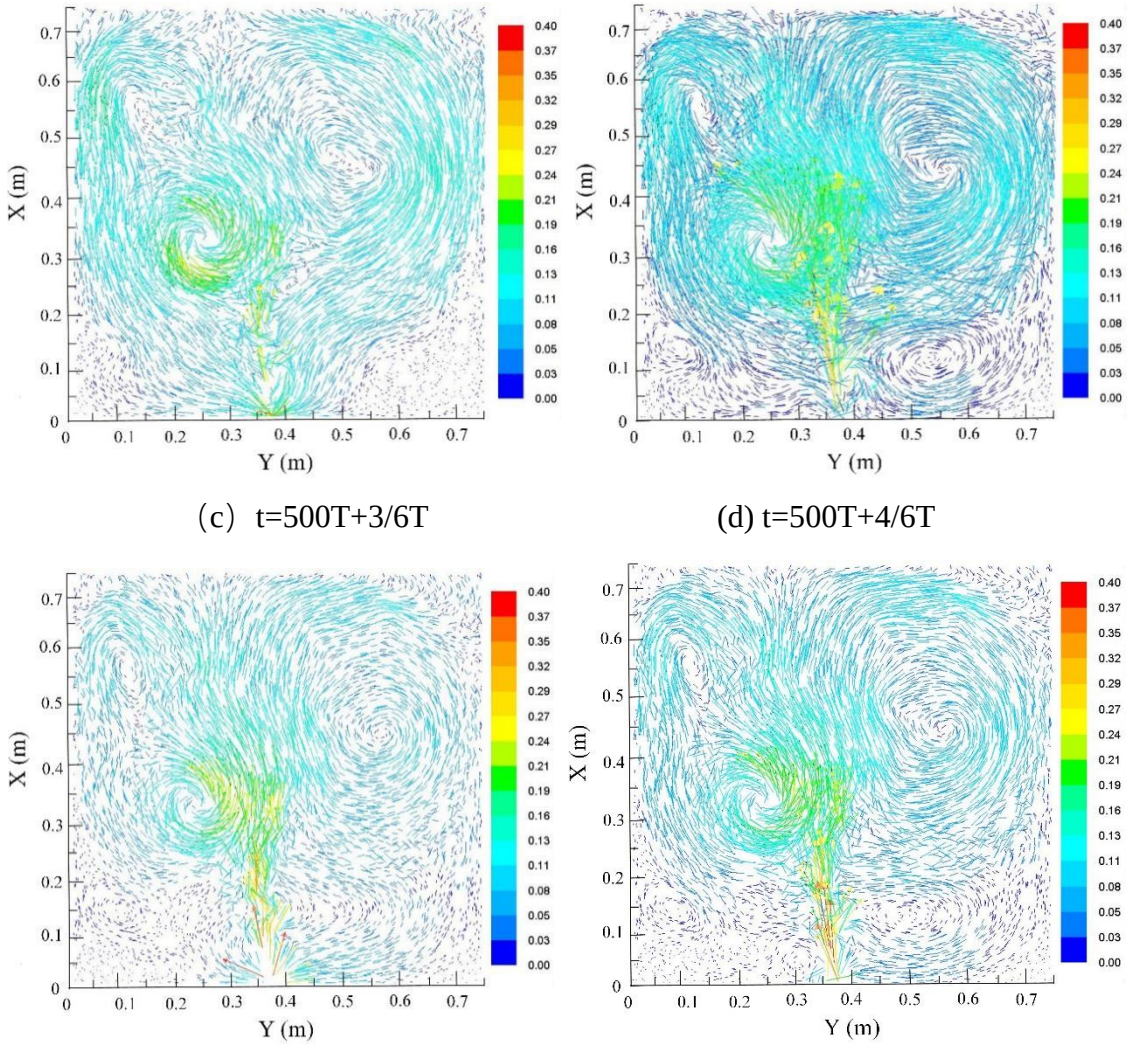

(c) t=500T+3/6T (d) t=500T+4/6T

(e) t=500T+5/6T (f) t=500T+6/6T

Figure 3.18: Velocity vectors coloured by velocity magnitude (m/s) of the flow field of piezoelectric fan with a motion of travelling wave (f=10 Hz, A=0.02 m, k = 7) within one oscillation cycle.

All the above results suggest that there may be an optimal frequency and amplitude of PE fan pulsation that can maximise the mixing of fluid flow by developing favourable circulation zones. Meanwhile, an optimised wave number may also exist, leading to the formation of flow structures that can evolve into turbulence in the flow field.

3.4 Summary

In this chapter, the LES method is adopted to develop a three-dimensional CFD model of piezoelectric fan. A method of upwind scheme is used to discretize the N-S equations,

and the Runge-Kutta method is used for time integration. For the motions of piezoelectric fan, CFD numerical simulations can measure the influences of three kinematic parameters (including the frequency, the amplitude and the wave number) on fluid flow, in which the LES method is applied.

The numerical results show that:

(1) Different frequencies will lead to different numbers, sizes and locations of circulation zones in the flow field. The large circulation zones control bulk mixing in the flow field, while the small circulation zones play a major part in local mixing. The oscillating frequency has a strong influence on the circulation zone distributions and the velocity of flow field. The frequency variations seem to have a major impact on the flow circulation zones, which, in turn, have a major impact on the mixing in the flow field.

(2) The oscillating amplitude has a significant influence on the number, sizes and locations of circulation zones, and the velocity of fluid flow increases with the amplitude. The locations and sizes of the circulation zones at the high amplitude are similar to those at high frequency under medium amplitude. The results indicate that there may be an optimal amplitude that can maximise the mixing of fluid flow.

(3) The velocity of the fluid flow, the distributions and the number of large circulation zones change slightly with the wave number. When the wave number is zero, the location of circulation zones is nearly symmetrically distributed, but the symmetrical distribution of circulation zone is broken when the wave number turn to 2 or 7. When the flow symmetry is broken, the tendency of flow transition to turbulence is enhanced, which can in turn, enhance the mixing in the flow field. Therefore, it provides a new approach to enhancing the mixing in the fluid domain.

In summary, the oscillating frequency, the oscillating amplitude have a significant influence on the formation of the circulation zones, however, the wave number has a rather weak influence on that. All these numerical results suggest that the large circulation zones and small vortices in the flow field are significantly affected by the motions of the PE fan, which are also closely related to the mixing in the flow field that determines the heat transfer effectiveness of the cooling system.

Chapter 4

Numerical Analysis of Heat Transfer of Piezoelectric Fan

4.1 Introduction

Increasing the fluid mixing near the heat source plays an important role in the performance of piezoelectric fan cooling. When the oscillating piezoelectric fan generates airflow in the ambient environment, the fan movements affect the flow field, including the velocity magnitudes, streamlines and vorticities, which have a significant impact on the cooling effectiveness. Understanding these influences is crucial for designing the cooling system or improving the cooling effectiveness.

In this chapter, a heat source represented by a high temperature wall is added to develop the CFD model of the piezoelectric fan. A parametric study can investigate the fluid flow and heat transfer, in which the motions of the PE fan vary with the oscillating frequency, the oscillating amplitude, and the wave number. The flow field is disturbed by the movements of the PE fan, and the flow structures near the hot wall including the circulation zones dominate the heat transfer process. The temperature and the surface Nusselt number of the hot wall can be used to evaluate the performance of heat transfer. The numerical results are expected to reveal the effects of the piezoelectric fan location as well as the frequency, the amplitude and the wave number on the heat transfer process. These results will lay the foundation for designing cooling systems using PE fans.

4.2 Piezoelectric fan model with a heat source

4.2.1 Heat transfer analysis

Heat transfer can be classified into three types: conduction, convection and radiation. Convection is the dominant mode of heat transfer for cooling applications using PE fans

(Lienhard IV and Lienhard, 2008). The energy equation should be taken into consideration for CFD studies of heat transfer. It can be solved in the following form:

$$\frac{\partial}{\partial t}(\rho E) + \nabla \cdot \left(\vec{v}(\rho E + p)\right) = \nabla \cdot \left(k_{eff}\nabla T - \sum_j h_j \overrightarrow{J_j} + \left(\bar{\bar{\tau}}_{eff} \cdot \vec{v}\right)\right) + S_h \quad (4\text{-}1)$$

where k_{eff} is the effective conductivity, $\overrightarrow{J_j}$ is the diffusion flux of species j, and S_h is the volumetric heat source. The first three terms on the right-hand side of Eq. (4-1) represent energy transfer due to conduction, species diffusion and viscous dissipation respectively. E is expressed as:

$$E = h - \frac{p}{\rho} + \frac{v^2}{2} \quad (4\text{-}2)$$

where sensible enthalpy h of ideal gases is defined as:

$$h = \sum_j Y_j h_j \quad (4\text{-}3)$$

and for incompressible flows as:

$$h = \sum_j Y_j h_j + \frac{p}{\rho} \quad (4\text{-}4)$$

In Equations (4-3) and (4-4), Y_j is the mass fraction of species j and

$$h_j = \int_{T_{ref}}^{T} c_{p,j}\, dT \quad (4\text{-}5)$$

In the sensible enthalpy calculation, the value of T_{ref} depends on the solver and models. For the pressure-based solver, the energy equation (4-1) does not include h due to the viscous heating (Cengel and Pérez, 2004). On the other hand, the viscous heating can be ignored when the Brinkman number, Br, is larger than unity, where

$$Br = \frac{\mu U_e^2}{k\Delta T} \quad (4\text{-}6)$$

and ΔT represents the temperature difference in the thermal system.

For piezoelectric fans, the performance of heat transfer is evaluated by Nusselt number, which is expressed as:

$$Nu_L = \frac{h_c L}{k_t} \quad (4\text{-}7)$$

where h_c is the convective coefficient of heat transfer; L is the characteristic length, and k_t is the thermal conductivity of the fluid. In the heat transfer, the Nusselt number is the ratio of convective to conductive energy across the boundary (Bergman et al., 2011). Both the convective and conductive components are measured under the same conditions. It is notable that when Nusselt number is close to one, the flow exhibits typical characteristic

of laminar flow; when Nusselt number is large, typically in the range of 100~1000, the flow is prone to turbulent flow with active convection.

4.2.2 Numerical model of piezoelectric fan

A heat source is added into the CFD model to investigate the heat transfer of the PE fan. In the present study, the heat source is a hot wall with constant temperature 400K. The PE fan is located at the inlet boundary of the computational domain, and the hot wall is perpendicular to the inlet boundary. The computational model of piezoelectric fan is shown in Figure 4.1, in which the length of the PE fan is L= 0.05m. The size of computational domain is $15L \times 15L \times 0.08L$, and the velocity profile is also used to demonstrate the movements of PE fan. The ambient air is at the atmospheric pressure and temperature is 300K which is similar to room temperature.

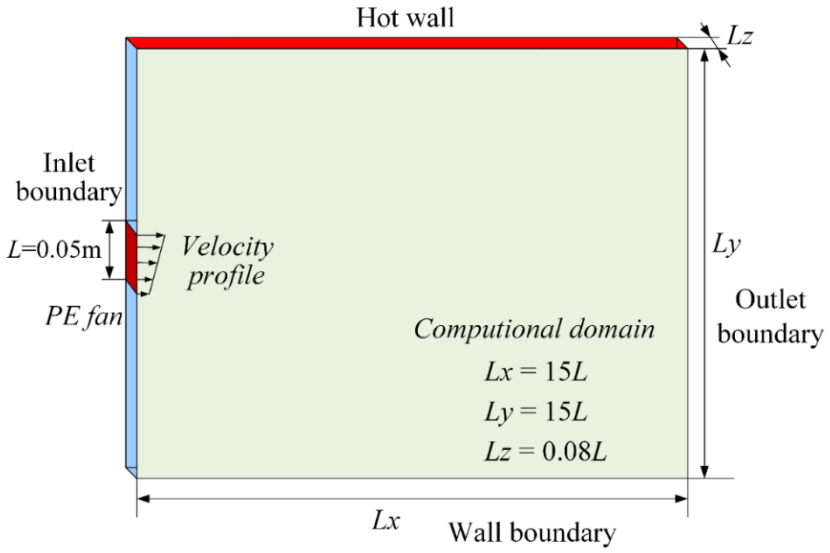

Figure 4.1: The computational model of piezoelectric fan with an added heat source

In Figure 4.1, the computational domain is bounded by sidewalls, which has inlet and outlet boundaries in the stream direction. In the present study, the inlet conditions are governed by the PE fan blade oscillation, describing by the oscillating frequency, the oscillating amplitude and the wave number. In the computational domain, the fan oscillation at the inlet boundary generates airflow. When the inlet air touches the sidewalls, the velocity decreases while pressure increases. The nearby airflow will carry away the thermal energy near the hot wall. Convection is the dominating mechanism for the cooling, which can be enhanced by the circulation zones and small vortices formed near the hot

wall. Fluid mixing controls the heat transfer and the cooling effectiveness.

The PE fan motions generate fluid flow that dominates heat transfer, the flow and heat transfer couple together. Diagrams of velocity vectors, streamline, and contours of temperature are also used to display the influences of the PE fan motions. Besides the instantaneous values, the mean surface Nusselt number and the mean temperature can evaluate the heat transfer characteristics of the piezoelectric fan.

4.3 Heat analysis of piezoelectric fans at different locations

The distance between the hot wall and the centre of the PE fan is set with two different distances, 0.02m and 0.35m, to investigate the effect of the location of piezoelectric fan on heat transfer. They stand for two different situations: the "near" location and the "middle" location, in terms of the distance between the fan and the hot wall. The flow field varies with the fan's location at the inlet boundary. The diagrams of velocity vectors coloured by velocity magnitude are shown in Figure 4.2, while the contours of temperature (K) are shown in Figure 4.3.

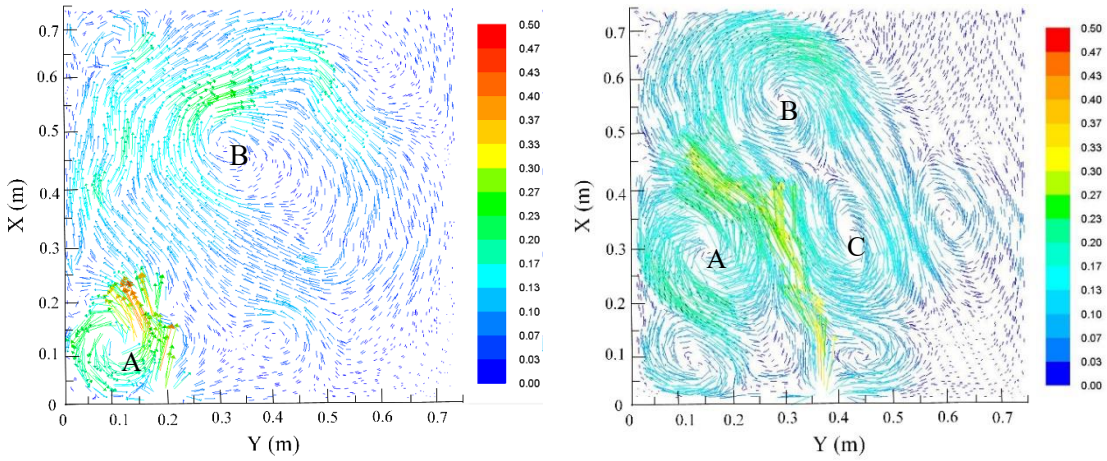

(a) Near location (b) Middle location

Figure 4.2: Velocity vectors coloured by velocity magnitude (m/s) at different fan locations when f=10 Hz, A=0.02m and k=2 at 500T (T is the oscillating period)

When the fan is located close to the hot wall (referred to as the "near location" case), a large circulation zone 'B' is located in the middle of the flow field. When the fan is located in the middle of the inlet (referred to as the "middle location" case), the corresponding circulation zones 'A' and 'B' are close to the hot wall, leading to circulations smaller than those of the near location case. Large circulation zones enhance the fluid

mixing. It means that the near location case helps to mix the fluid; accordingly, this configuration may enhance the process of heat transfer. Similarly, the contours of temperature in Figure 4.3 also show that the heat transfer is much improved when the location of the PE fan is close to the hot wall.

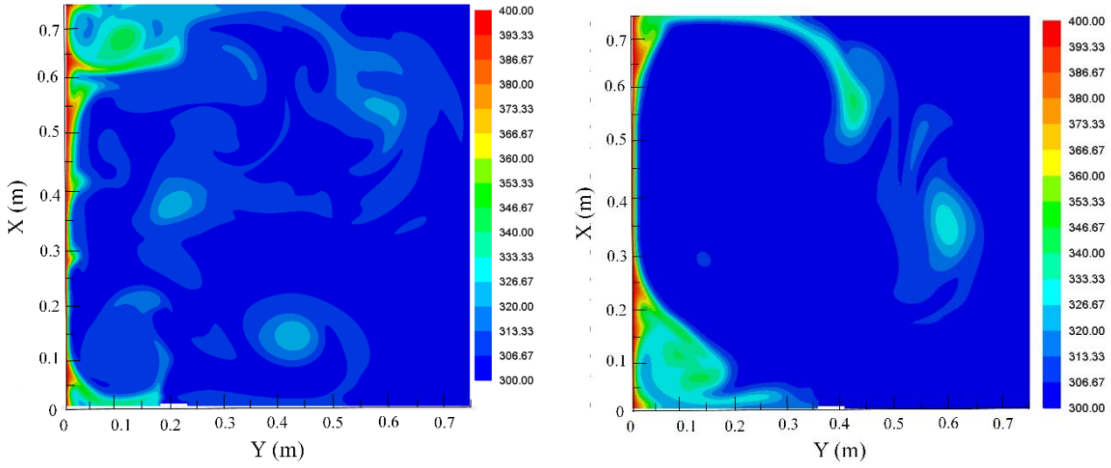

(a) Near location (b) Middle location

Figure 4.3: Contours of temperature (K) at different fan locations when f=10 Hz, A=0.02m and k=2 at 500T

When the location of the PE fan varies, the mean surface Nusselt number and mean temperature are shown in Figure 4.4 and Figure 4.5 respectively. For the case of 'near location', the mean surface Nusselt number has two peaks, which is displayed in Figure 4.4 (a). However, in Figure 4.4(b), three peak values appear in the case of 'middle location'. Compared with the results in Figure 4.2, it can also be observed that the Nusselt number peak corresponds to the location of the circulation zone. Besides, in these two figures, the peak at the downstream location is much more significant.

At the near location, the maximum value of mean surface Nusselt number is around 240, which is larger than 140, the maximum value of the case with middle location. This phenomenon is also demonstrated in Figure 4.5, where the mean temperature is shown. It can be seen that the large mean surface Nusselt number corresponds to the low temperature. All these results show that the distance between the PE fan and the hot wall has a significant influence on the heat transfer.

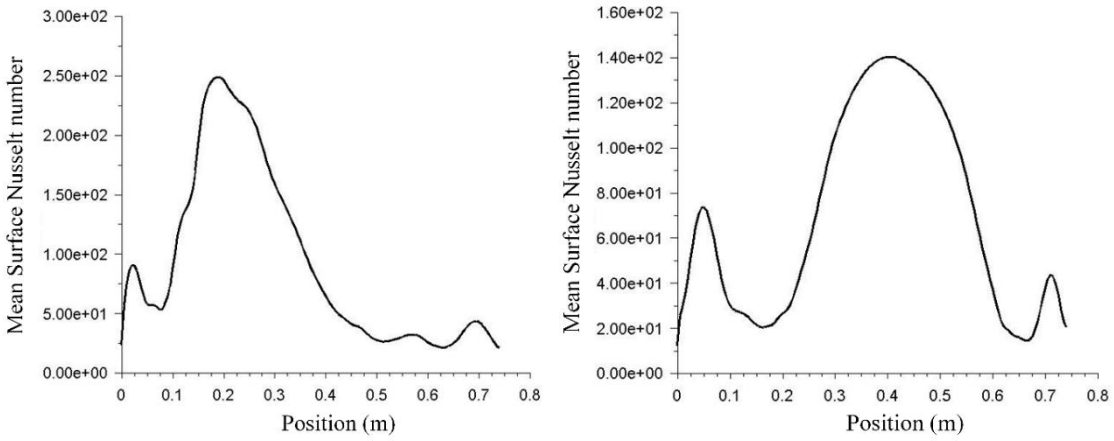

(a) Near location (b) Middle location

Figure 4.4: Mean surface Nusselt numbers for different fan locations when f=10 Hz, A=0.02 m and k=2

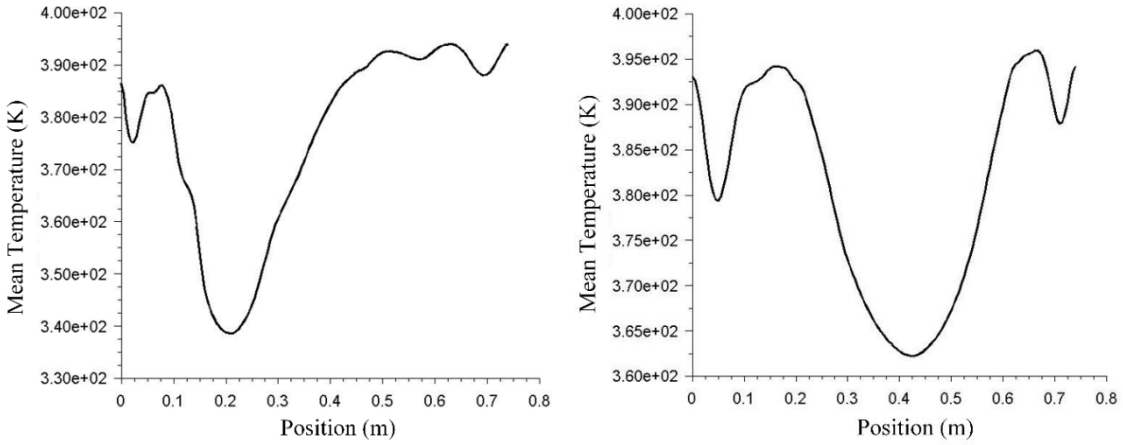

(a) Near location (b) Middle location

Figure 4.5: Mean temperature (K) for different fan locations when f=10 Hz, A=0.02 m and k=2

4.4 Effects of oscillating frequency of piezoelectric fan on heat transfer

Under the same amplitude 0.02 m and the same wave number k=2, three different oscillating frequencies, 5 Hz, 10 Hz and 20 Hz, are selected to compare the influence on the heat transfer of the PE fan. In Figure 4.6, the velocity of fluid flow in the computational domain are strongly affected by the fan's oscillating frequency. For example, when the oscillating frequencies are 5 Hz, 10 Hz and 20 Hz, the maximum velocities are around 0.25

m/s, 0.50 m/s and 1.10 m/s respectively.

In Figure 4.6, the distribution of circulation zones with different sizes and locations vary with the oscillating frequencies. At 5Hz, the circulation zones are mainly located at the left side of computational domain. The circulation zone “B” is the largest, and “A” is smaller than “B”. At 10Hz, two circulation zones are located on the left side of the PE fan, which are indicated as “A” and “B” in Figure 4.6 (b). However, there are mainly three large circulation zones when the oscillating frequency is 20 Hz. The largest circulation zone “C” can be observed in the middle of the flow field.

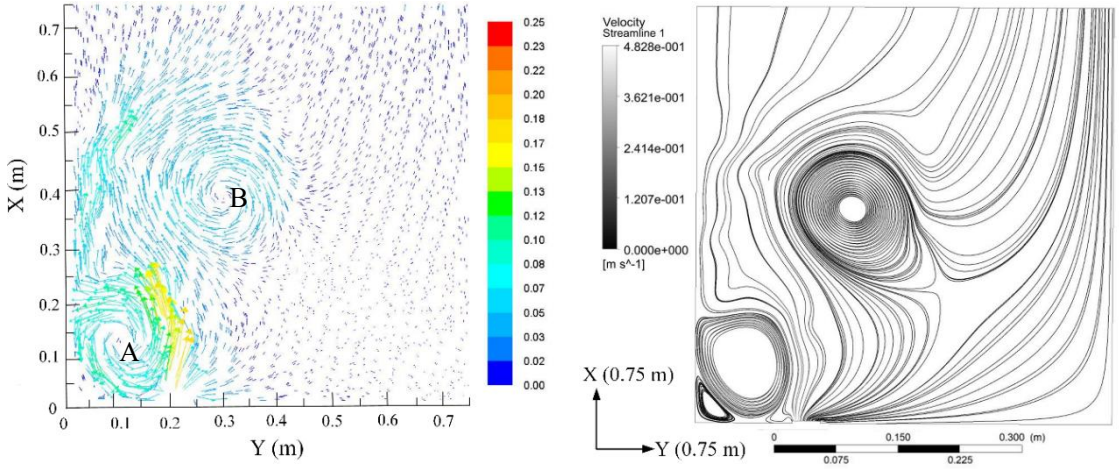

(a) Oscillating frequency 5 Hz

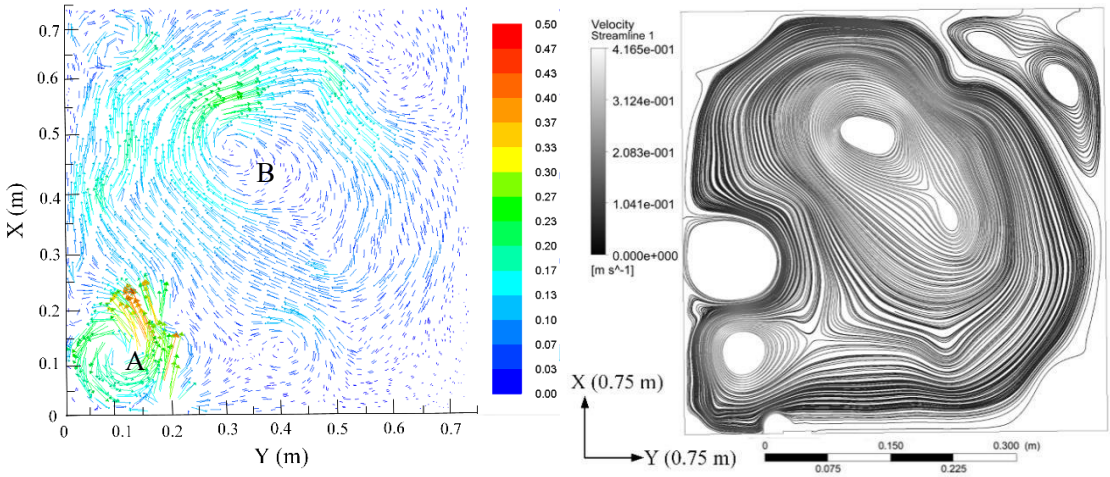

(b) Oscillating frequency 10 Hz

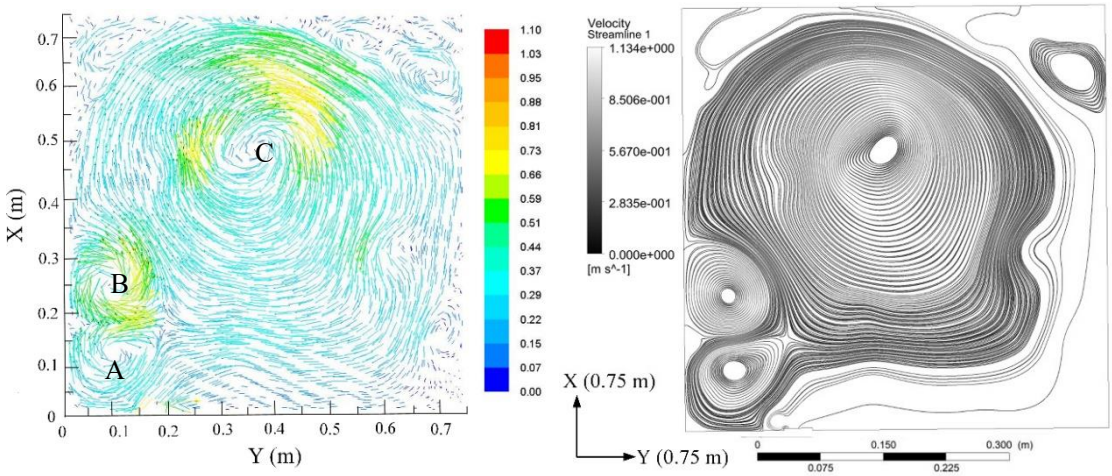

(c) Oscillating frequency 20 Hz

Figure 4.6: Velocity vectors coloured by velocity magnitude (m/s) at different oscillating frequencies when A=0.02 m and k=2 at 500T compared with the streamline diagrams

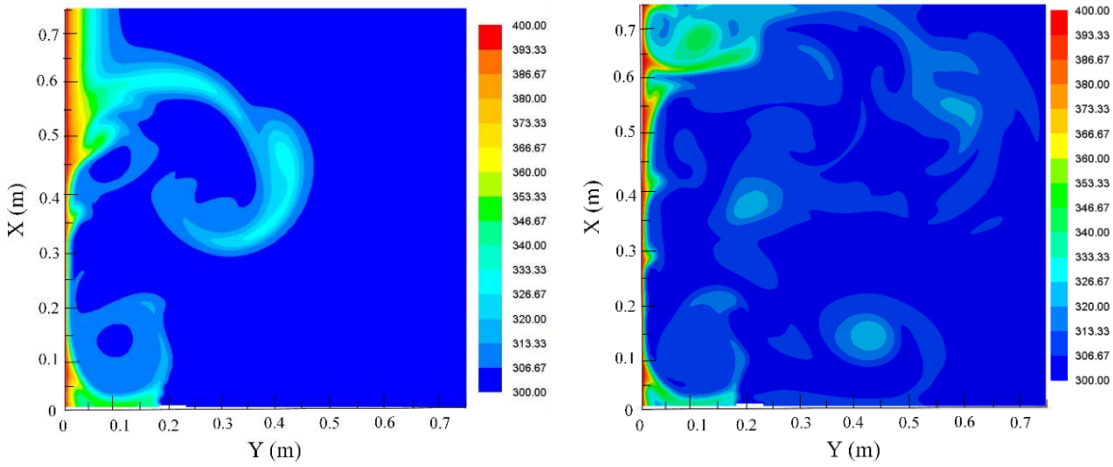

(a) Oscillating frequency 5Hz (b) Oscillating frequency 10Hz

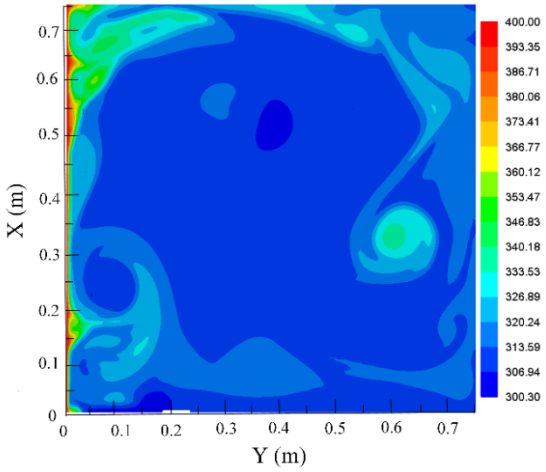

(c) Oscillating frequency 20 Hz

Figure 4.7: The contours of temperature (K) with different oscillating frequencies when A=0.02 m and k=2

The mean surface Nusselt number is displayed in Figure 4.8. When the oscillating frequencies are at 5 Hz, 10 Hz and 20 Hz, the maximum mean surface Nusselt numbers are around 170, 250 and 275 respectively. There are two peak values for 5 Hz and 10 Hz, but three peak values at 20 Hz. The number of peaks consists with the number of circulation zones in Figure 4.6. The changes of mean temperature are shown in Figure 4.9. These results also demonstrate that increasing the oscillating frequency can help improve the cooling performance of the PE fan.

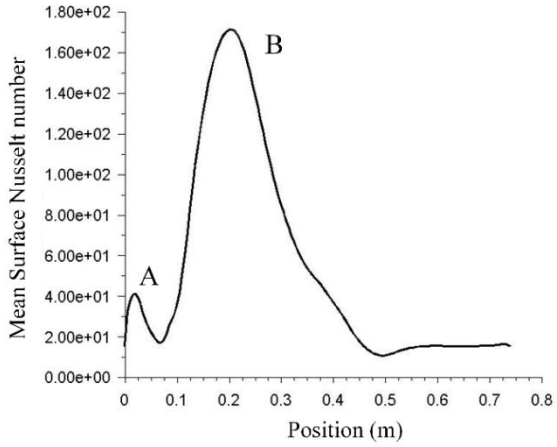

(a) Oscillating frequency 5 Hz

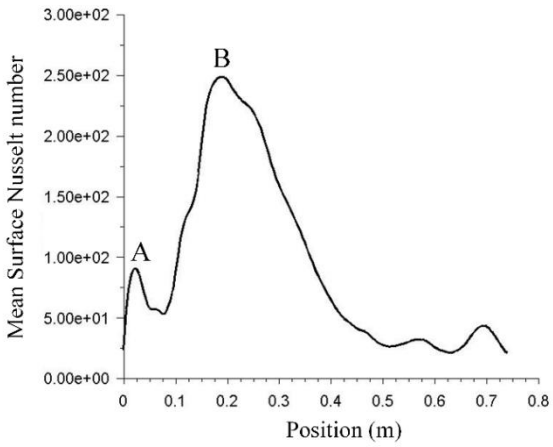

(b) Oscillating frequency 10 Hz

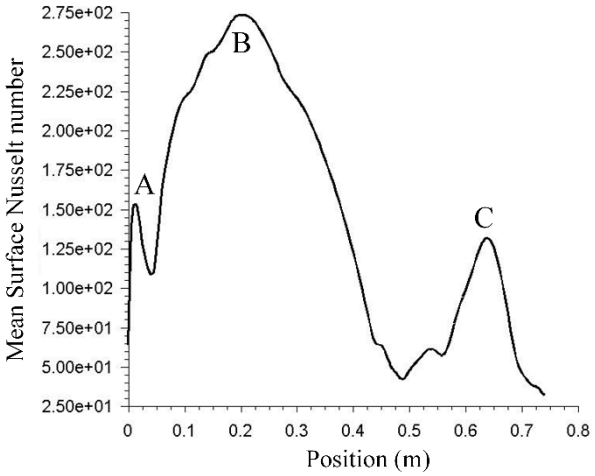

(c) Oscillating frequency 20 Hz

Figure 4.8: The mean surface Nusselt number with different oscillating frequencies when A=0.02 m and k=2

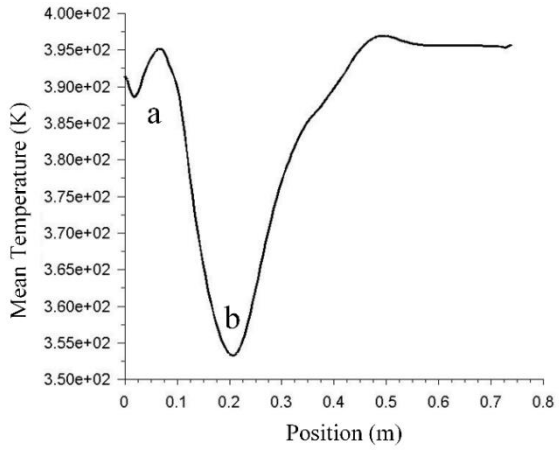

(a) Oscillating frequency 5 Hz

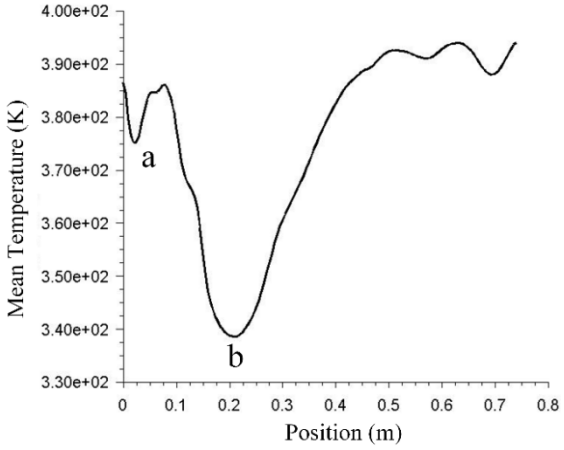

(b) Oscillating frequency 10 Hz

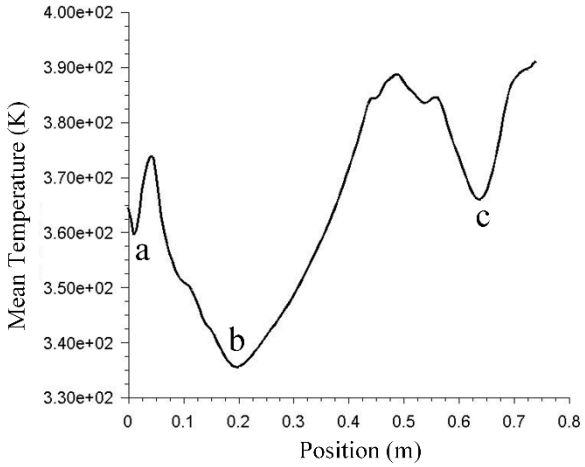

(c) Oscillating frequency 20 Hz

Figure 4.9: The mean temperature with different oscillating frequencies when A=0.02 m and k=2

Within one oscillation cycle at 500T, the velocity vector and the Nusselt number are shown in Figure 4.10 and Figure 4.11 respectively. These numerical results have the same inlet conditions, f=10 Hz, A=0.02 m and k=2. At different times, the size and location of circulation zones remain stable within one oscillating period. However, small variations are also shown in the velocity distribution and the surface Nusselt number. It means that when the main circulation pattern is formed, small vortices are also developed as shown in Figure 4.10. In Figure 4.11, the instantaneous curves of surface Nusselt numbers show very small variations within one oscillating period.

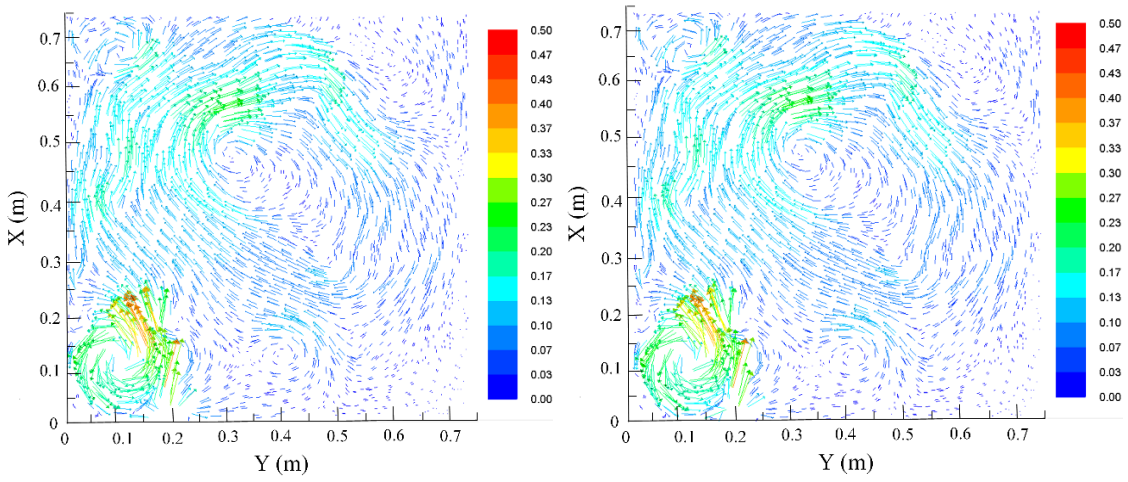

(a) t=500T+1/6T (b) t=500T+2/6T

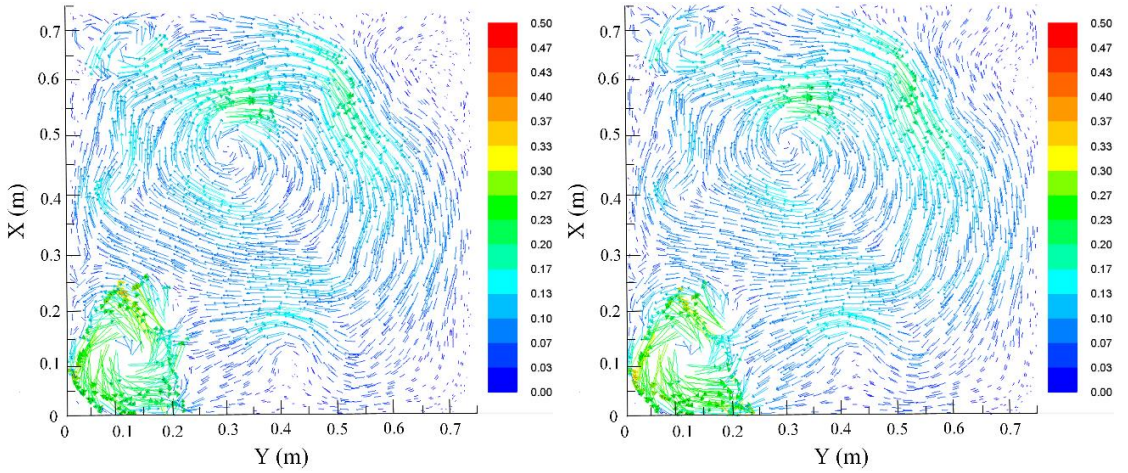

(c) t=500T+3/6T (d) t=500T+4/6T

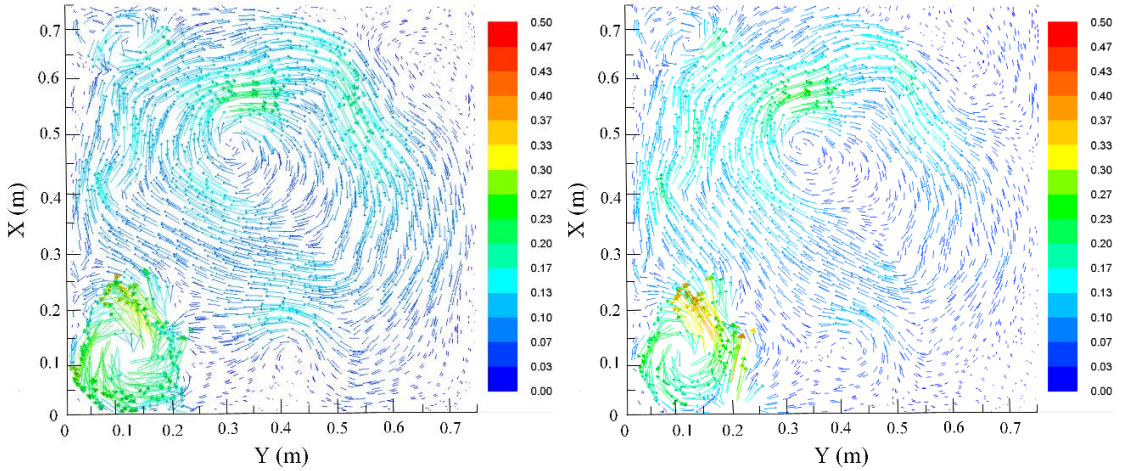

(e) t=500T+5/6T (f) t=500T+6/6T

Figure 4.10: Velocity vectors coloured by velocity magnitude (m/s) during one oscillating period when A=0.02m, f=10 Hz and k=2

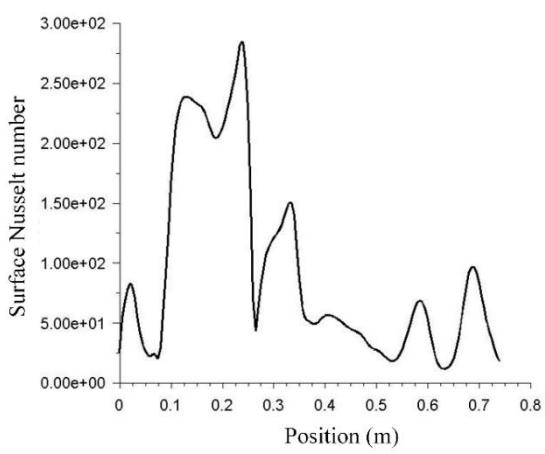

(a) t=500T+1/6T

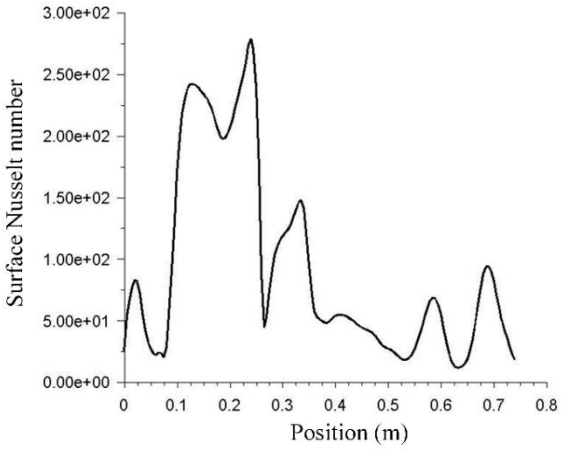

(b) t=500T+2/6T

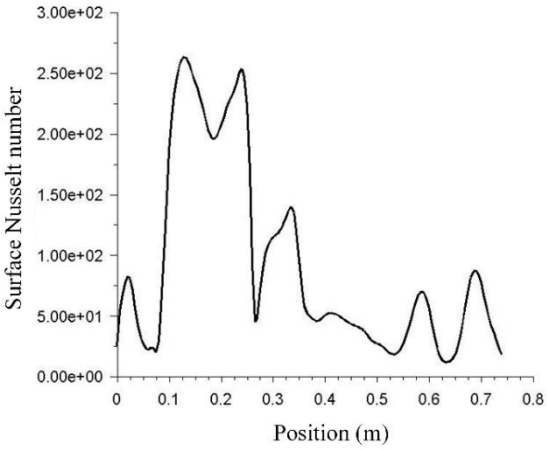

(c) t=500T+3/6T

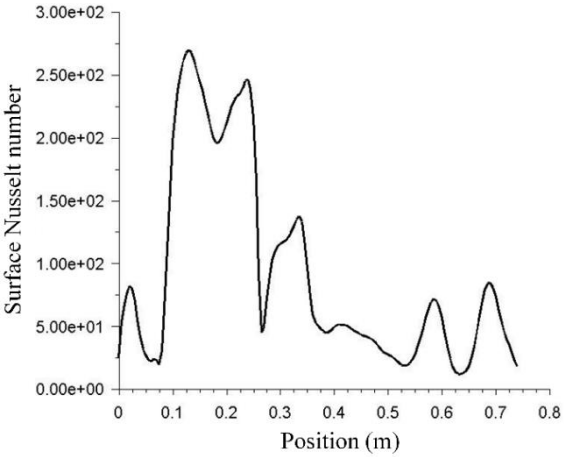

(d)t=500T+4/6T

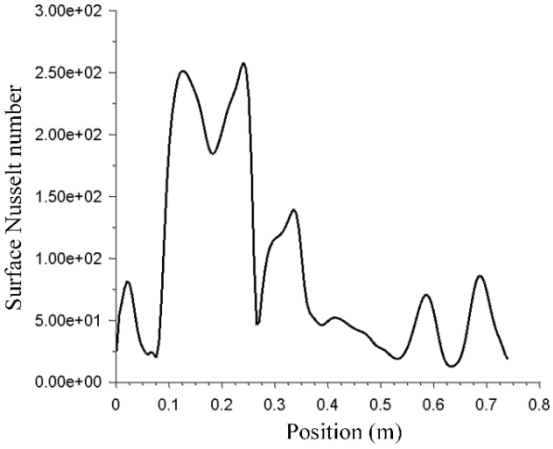

(e) t=500T+5/6T

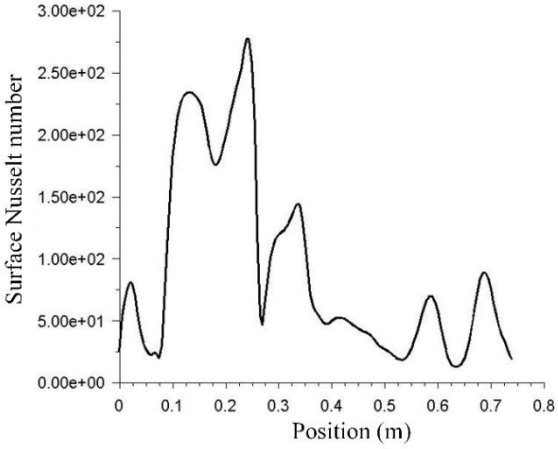

(f) t=500T+6/6T

Figure 4.11: The surface Nusselt number during one oscillating period when f=10 Hz, A=0.02 m and k=2

4.5 Effects of oscillating amplitude of piezoelectric fan on heat transfer

With the same frequency 10Hz and wave number k=2, the velocity vectors of the flow field vary with different oscillating amplitudes, 0.01m, 0.02m and 0.04m. In Figure 4.12, the diagrams of velocity vectors are coloured by velocity magnitude (m/s). With larger oscillating amplitude, more circulation zones are formed. The circulation zones play an important role in the local mixing, which controls the heat transfer and accordingly the cooling effectiveness of the PE fan. Besides, for different oscillating amplitudes, the contours of temperature are shown in Figure 4.13, which correspond to the velocity distributions in Figure 4.12.

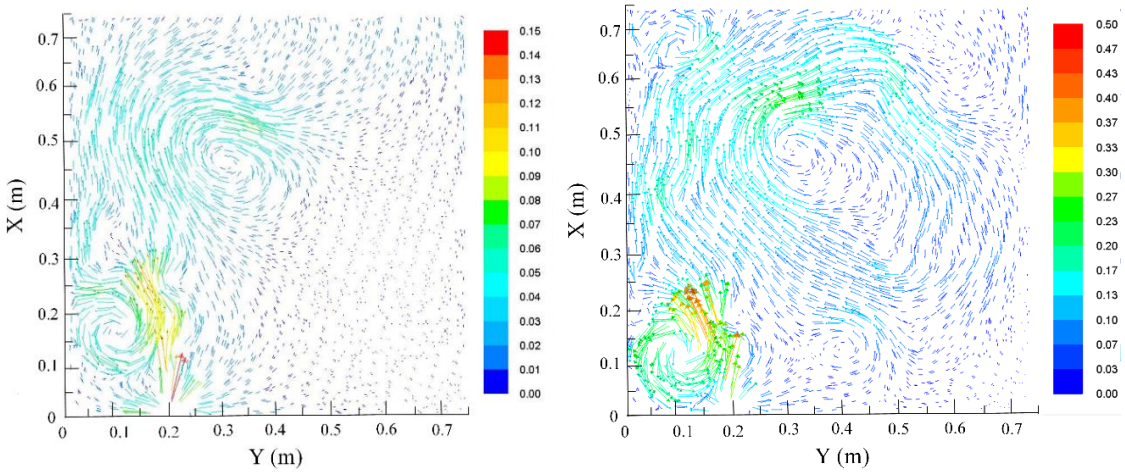

(a) Oscillating amplitude 0.01 m (b) Oscillating amplitude 0.02 m

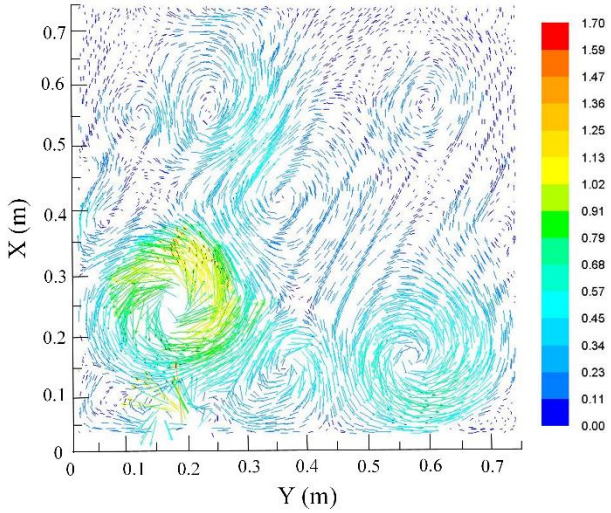

(c) Oscillating amplitude 0.04 m

Figure 4.12: Velocity vectors coloured by velocity magnitude (m/s) with different oscillating amplitudes when f=10 Hz and k=2.

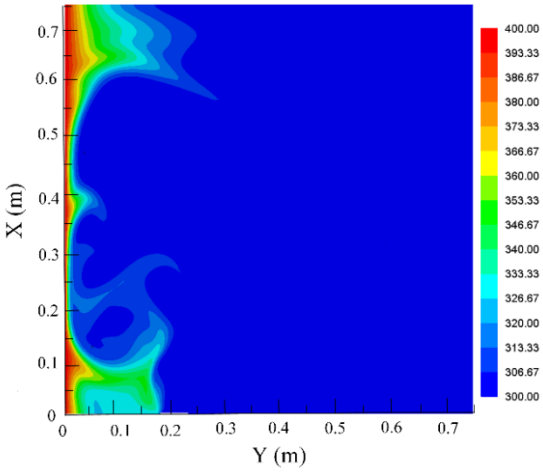

(a) Oscillating amplitude 0.01 m

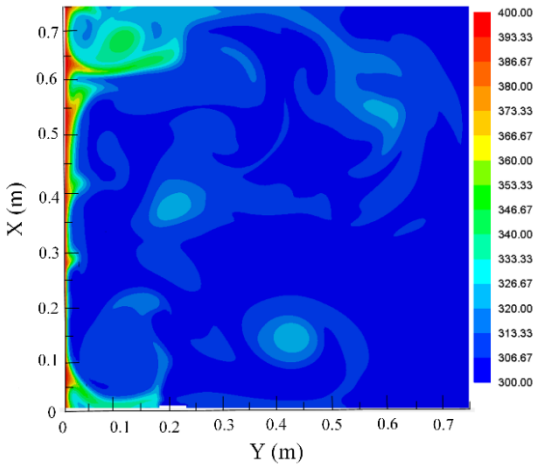

(b) Oscillating amplitude 0.02 m

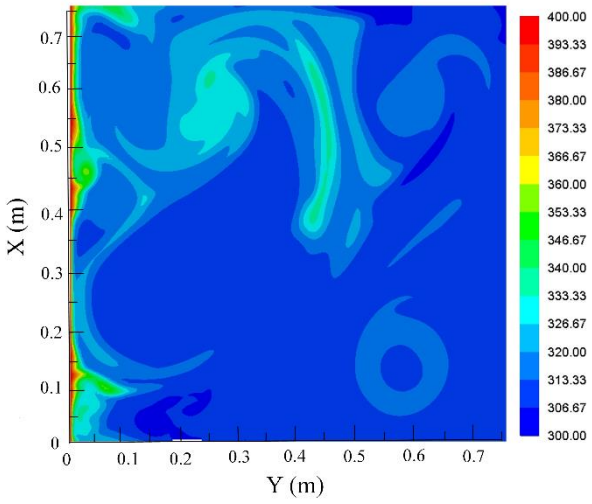

(c) Oscillating amplitude 0.04 m

Figure 4.13: The contours of temperature (K) with different oscillating amplitudes when f=10 Hz and k=2

With different oscillating amplitude, the changing pattern of the mean temperature and the mean surface Nusselt number are shown in Figure 4.14 and Figure 4.15 respectively. The oscillating amplitude has a significant impact on the temperature distribution. When the amplitude is 0.04m, the distribution of circulation zones in Figure 4.12 causes the complexity of variation trend of the mean temperature. Besides, the mean surface Nusselt number in Figure 4.15 increases with the amplitude. In Figure 4.15, there is a significant increase in the mean surface Nusselt number from around 120 to 250 when oscillating amplitude increases from 0.01m to 0.02m. Although when oscillating amplitude increases from 0.02m to 0.04m, there is still an increase in the mean surface Nusselt number but only a small increase from around 250 to 270. These trends correspond to the variation of the mean temperature drop.

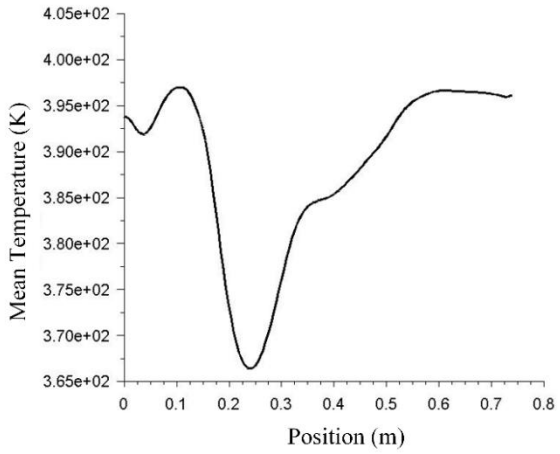

(a) Oscillating amplitude 0.01 m

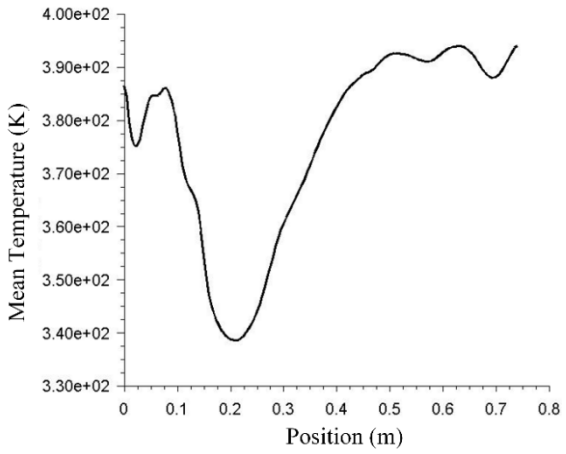

(b) Oscillating amplitude 0.02 m

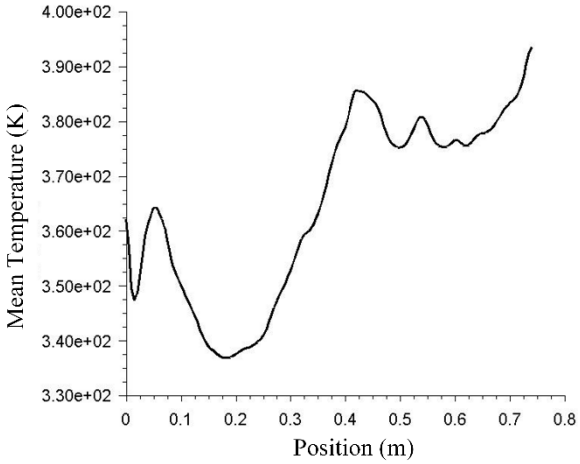

(c) Oscillating amplitude 0.04 m

Figure 4.14: The mean temperature (K) with different oscillating amplitude when f=10 Hz and k=2

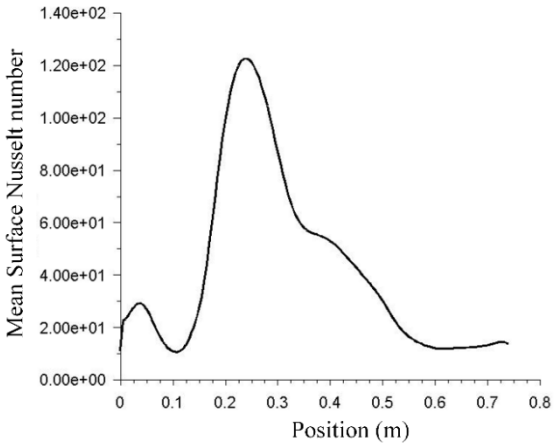

(a) Oscillating amplitude 0.01 m

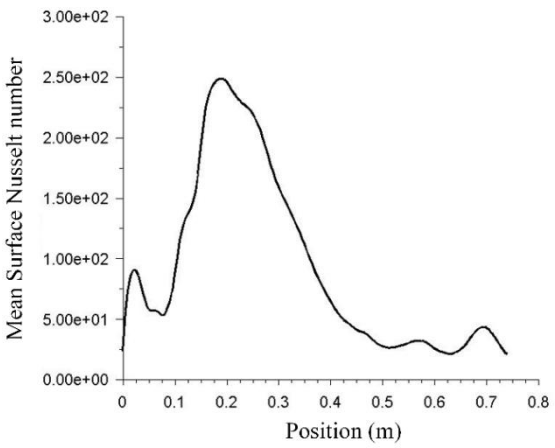

(b) Oscillating amplitude 0.02 m

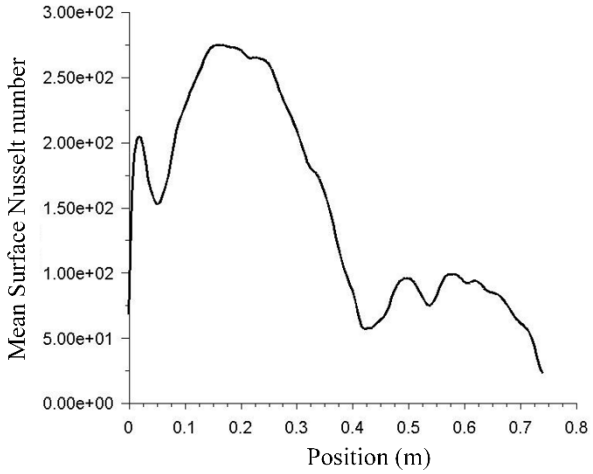

(c) Oscillating amplitude 0.04 m

Figure 4.15: The mean surface Nusselt number with different oscillating amplitude when f=10 Hz and k=2

When f=10 Hz, A=0.04 m and k=2, the changes of the velocity vector and the Nusselt number within one oscillating period are shown in Figure 4.16 and Figure 4.17 respectively. In general, the distribution of circulation zone remains stable, which is similar to Figure 4.10 and Figure 4.11. It indicates that the flow field within one oscillating period is largely stable. Compared with the results in Figure 4.10 and Figure 4.11, more circulation zones are formed when the amplitude increases, therefore, more oscillations in the curve of mean surface Nusselt number are observed in Figure 4.17.

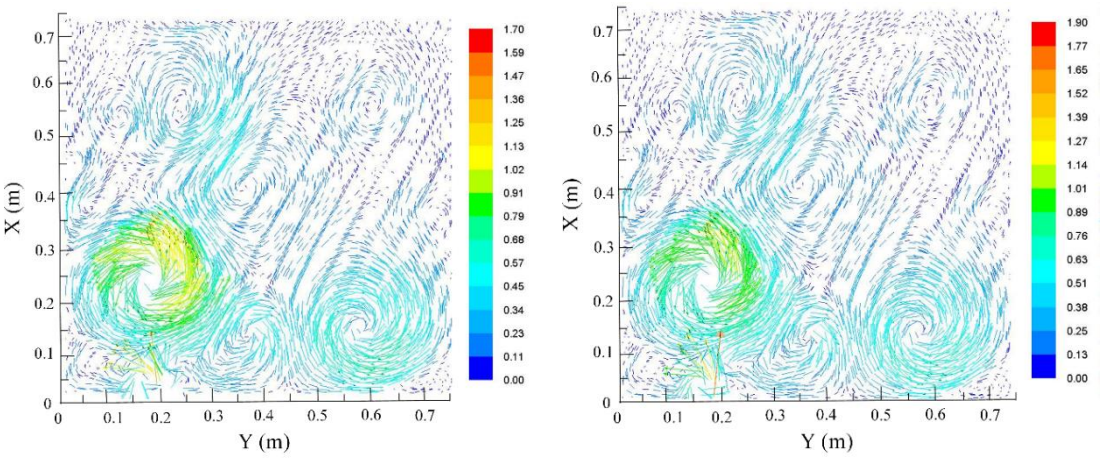

(a) t=500T+1/6T

(b) t=500T+2/6T

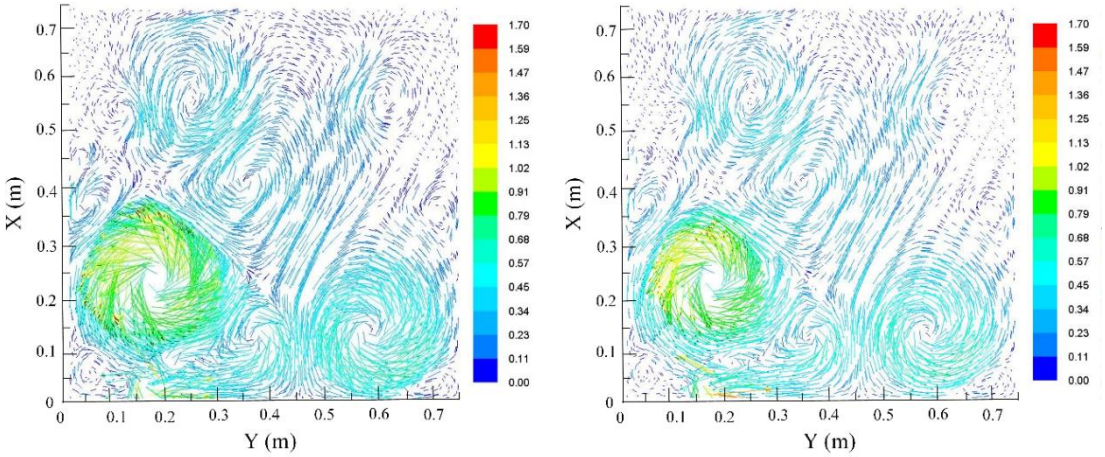

(c) t=500T+3/6T

(d)t=500T+4/6T

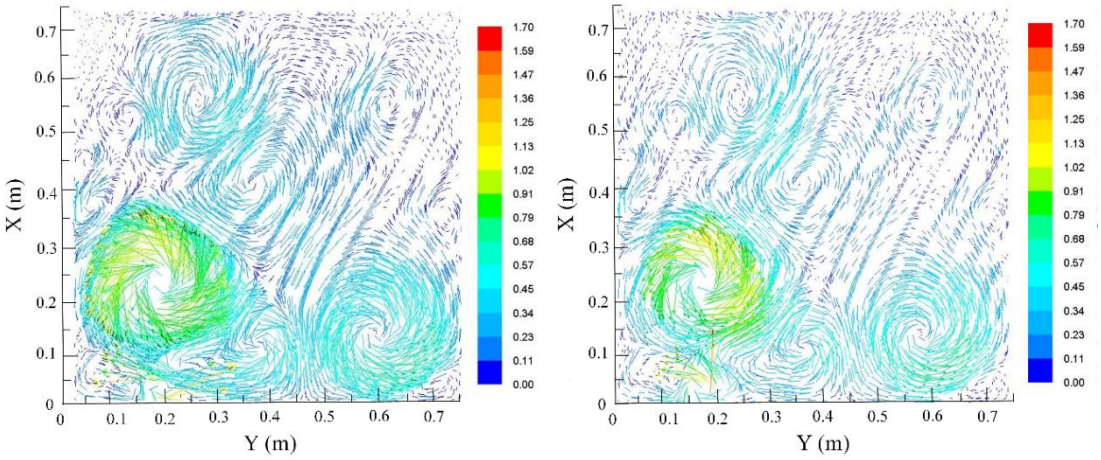

(e) t=500T+5/6T

(f) t=500T+6/6T

Figure 4.16: Velocity vectors coloured by velocity magnitude (m/s) within one oscillation cycle when f=10 Hz, A=0.04m and k=2

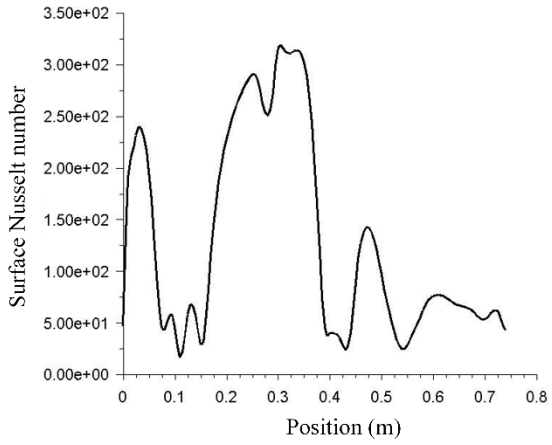

(a) t=500T+1/6T

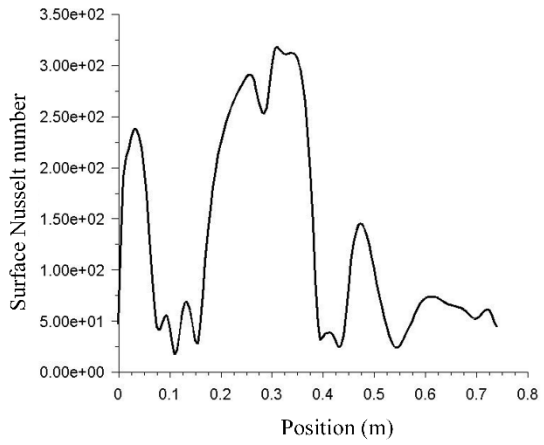

(b) t=500T+2/6T

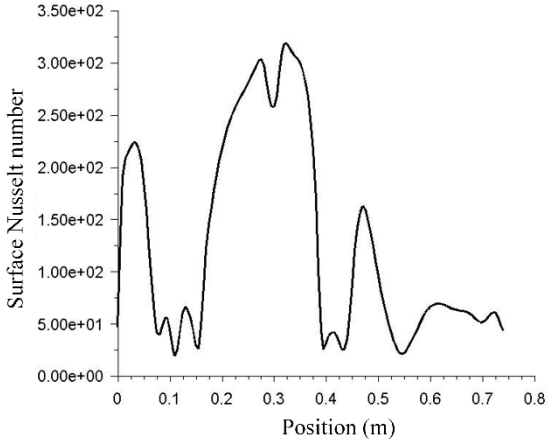

(c) t=500T+3/6T

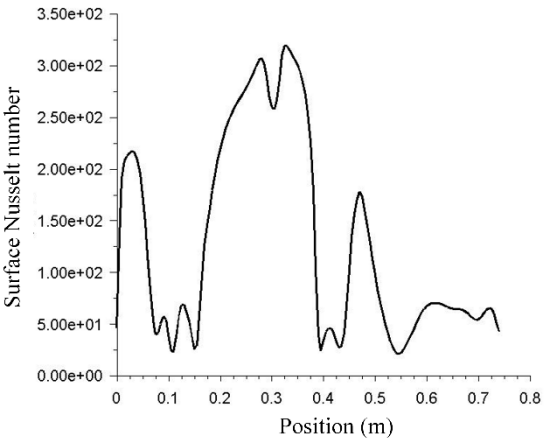

(d)t=500T+4/6T

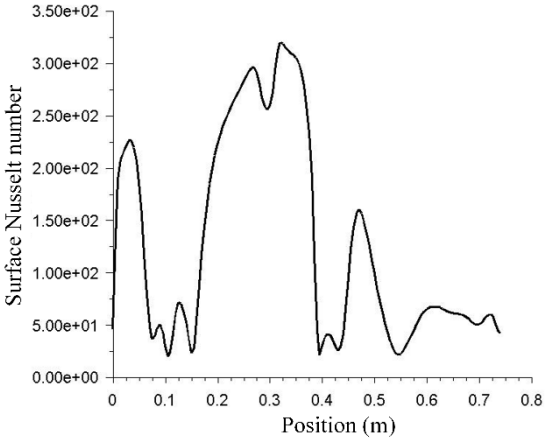

(e) t=500T+5/6T

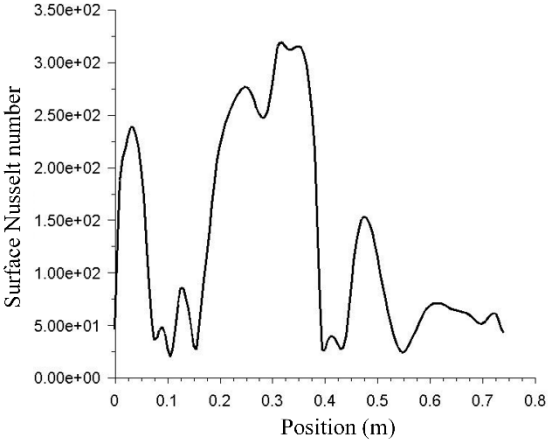

(f) t=500T+6/6T

Figure 4.17: The surface Nusselt number within one oscillation cycle when f=10 Hz, A=0.04 m and k=2

4.6 Effects of wave number of piezoelectric fan oscillation on heat transfer

Figure 4.18 shows the influences of PE fan motion on the velocity distribution for different wave numbers. When k=0, the motion of PE fan is a pure standing wave, and the largest velocity of fluid flow is around 0.25 m/s. Three circulation zones are formed, and they are named as 'A', 'B' and 'C'. This case k=0 is quite different from the other two cases with different wave numbers 2 and 7. In Figure 4.18(b) and Figure 4.18(c), when the wave number is 2 and 7, two circulation zones are formed, and the maximum velocity is about 0.5 m/s.

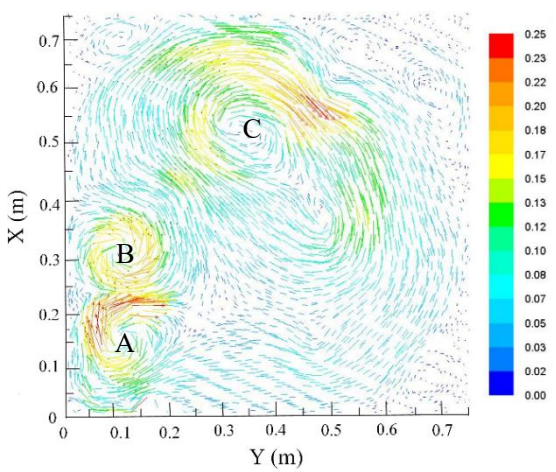

(a) Wave number 0

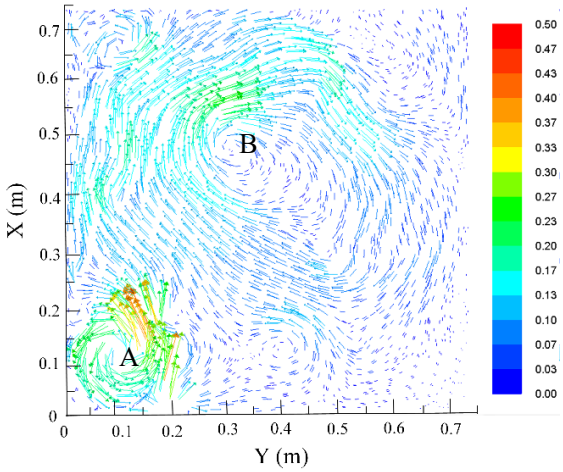

(b) Wave number 2

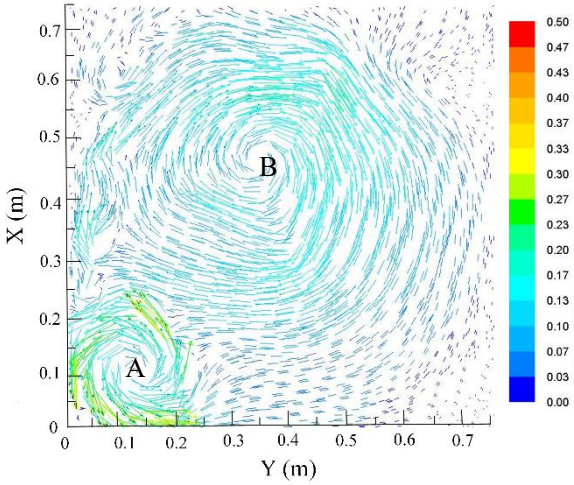

(c) Wave number 7

Figure 4.18: Velocity vectors coloured by velocity magnitude (m/s) with different wave numbers when f=10 Hz and A=0.02 m

The changes of mean surface Nusselt number and mean temperature are shown in Figure 4.19 and Figure 4.20 respectively. Compared with the cases with different amplitudes and frequencies, the wave number has a relatively small influence on the mean temperature and the surface Nusselt number. For different wave numbers 0, 2 and 7, the maximum surface Nusselt numbers are around 180, 250 and 270 respectively. When the wave number is 0, the mean surface Nusselt number is the smallest, although three circulation zones with low velocity are formed. Thus, an increase in the wave number also increases the Nusselt number.

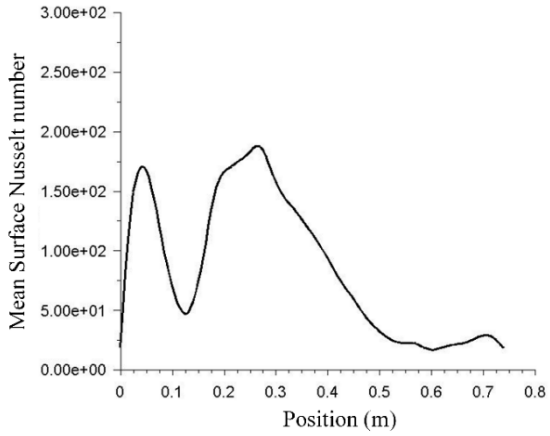

(a) Wave number 0

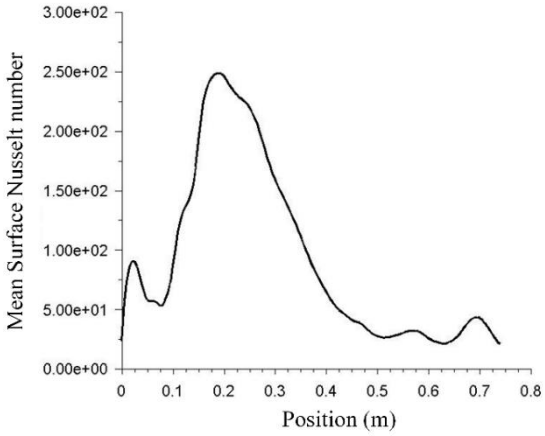

(b) Wave number 2

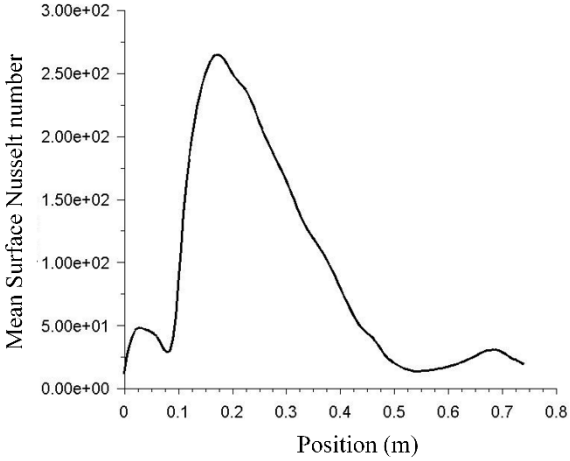

(c)Wave number 7

Figure 4.19: Mean surface Nusselt number with different wave number when f=10 Hz and A=0.02 m

In the flow field of the PE fan, both the velocity distribution and the circulation zones affect the surface Nusselt number and the mean temperature. All these characteristics of

flow field are affected by the kinematic parameters of the PE fan, i.e. the oscillating frequency, the amplitude, and the wave number. Overall, the results show that the effects of frequency and amplitude are more significant than the wave number in terms of affecting heat transfer.

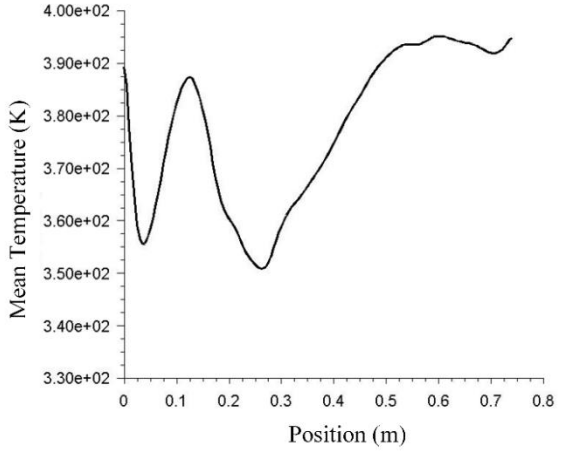

(a) Wave number 0

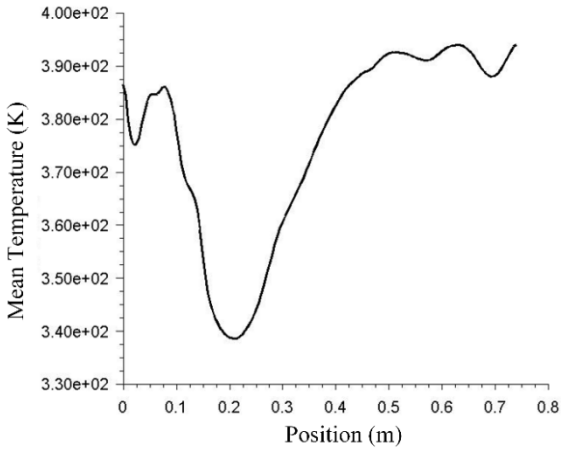

(b) Wave number 2

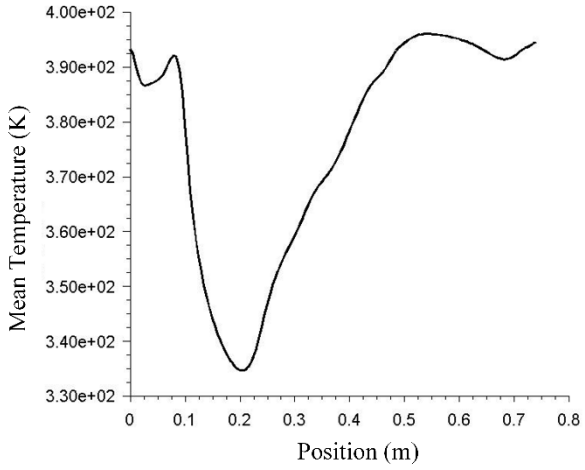

(c) Wave number 7

Figure 4.20: The mean temperature (K) with different wave number when f=10 Hz and A=0.02 m

4.7 Summary

In this chapter, a heat source with constant temperature 400K is added into the CFD model of the piezoelectric fan to study the heat transfer of the PE fan cooling system. When the movements of the PE fan generate airflow in the ambient, different types of circulation zones are formed to mix the local fluid, which are closely related to the heat transfer. The

motions of the PE fan generate fluid flow that dominates heat transfer. A parametric study involving several cases explains the characteristics of heat transfer, in which the motions of the PE fan vary with the fan location, the oscillating frequency, the oscillating amplitude, and the wave number. The heat transfer is evaluated by the mean surface Nusselt number and mean temperature.

The results show that:

(1) Heat transfer of the PE fan cooling system is affected significantly by the location of the PE fan at the inlet boundary. When the distance between the PE fan and the hot wall is small which is the case of near location, a large circulation zone is formed in the flow field, leading to circulations larger than those of the case with longer distance at middle position. Large circulation zone helps to mix the fluid and enhance the process of heat transfer. Meanwhile, the location of the circulation zone corresponds to the Nusselt number peak value. At the near location, the value of the maximum mean surface Nusselt number is almost twice than that at the middle location.

(2) The oscillating frequency has a strong influence on the distributions of circulation zone and the velocity magnitude of fluid flow. The temperature contours and velocity vectors are more uniformly distributed when the oscillating frequency increases. The mean surface Nusselt number increases with the oscillating frequency, and the peak value of Nusselt number also consists with the number of circulation zones. In one oscillating period, small variations are found in the velocity distribution and the surface Nusselt number. The results demonstrated that increasing the oscillating frequency could improve the cooling performance of the PE fan.

(3) The oscillating amplitude has a significant impact on the temperature distributions. The number of circulation zones increases with the oscillating amplitude, which also affects the local mixing and controls the heat transfer. The mean Nusselt number and temperature drop have a dramatic variation when amplitude increase from 0.01m to 0.02m but a relatively small change when amplitude increase from 0.02m to 0.04m. Another case of one oscillating period result with condition of f=10Hz, A=0.04m, k=2 is shown which indicates within one oscillating cycle, the flow field is largely stable.

(4) The wave number has a relatively small influence on the mean temperature and the surface Nusselt number compared to the cases with different amplitude and frequency. The results still show the trend of an increase in the Nusselt number when the wave number increases. Compared with the change of wave number from 2 to 7, the increase in the

Nusselt number is more significant when the wave number increases from 0 to 2.

Overall, all these results laid a foundation for optimising the heat transfer through optimising the kinematic parameters of the PE fan motions. These results can also help design the PE fan cooling systems.

Chapter 5

Optimisation Analysis of Heat Transfer of Piezoelectric Fan

5.1 Introduction

As discussed in the previous Chapter, piezoelectric fans can generate unsteady periodic flows with circulation zones. The movements of piezoelectric fan affect the fluid flow, which, in turn, affect the heat transfer. Accordingly, the cooling effectiveness varies with the oscillating frequency, the oscillating amplitude, the wave number and other geometrical parameters. However, due to the complexity of combining these influencing factors, it is difficult to define the best performance of piezoelectric fan regarding its operational parameters. It would be costly to run a large number of tests to determine the optimal operational parameters. Therefore, it is necessary to adopt optimisation methodology to identify the best operational parameters.

In this chapter, the response surface methodology (RSM) helps explore the relationships between the performance of piezoelectric fan and several variables controlling the fan movements, including the oscillating frequency, the oscillating amplitude and the wave number. The optimisation objective is to determine the operational parameters leading to the best performance of heat transfer, which is evaluated by the Nusselt number in this chapter; the influencing factors are the frequency, the amplitude and the wave number.

The geometric characteristics are fundamental parameters in design optimisation, along with blade material properties. The piezoelectric fans with different geometrical parameters (including the length, width and thickness) and materials (including the plastics and metals) are investigated to obtain the desired resonant frequency, which is closely related to the fan dynamics, the associated fluid flow and heat transfer. Understanding the effects of these factors is crucial for the design of piezoelectric fan.

From practical perspectives, there are limitations in determining the optimal operational parameters, which are closely related to the geometrical parameters such as the

blade geometry. In reality, theoretical optimal operational parameters may not be achievable under the constraints of geometrical parameters and materials choices. This important aspect is also discussed in this chapter.

5.2 The response surface methodology (RSM)

The response surface methodology (RSM) is one of the surrogate optimisation methods, which is commonly used in engineering field. It is firstly proposed by Box and Wilson (1951). Normally, when an outcome of an engineering project cannot be simply and directly measured, then a surrogate model of the outcome is used in order to substitute. However, the computational costs can be very high for many engineering problems, such as the CFD simulation of piezoelectric fan. It might take many hours or even days to complete each case. As a result, the routine tasks, such as design optimisation, design space exploration and sensitivity analysis, become impossible since they require hundreds or even thousands of simulations.

Constructing approximation models is one of the approaches to alleviating this burden, which is known as response surface models. Such models mimic the behaviour of simulation model as closely as possible with much lower computational costs. A model is constructed based on modelling the response of the simulator to a limited number of intelligently chosen data points. When only a single design variable is involved, the process is known as curve fitting. In the RSM-based optimisation, the relations between optimal factors and optimal objects are explored, and the experiments are designed to reduce the number of tests to explore the optimal operating conditions.

The RSM-based optimisation represents a class of optimisation methods that can locate the local or global optima quickly. The optimisation framework is provided, in which the conventional optimisation algorithms, e.g. gradient-based or evolutionary algorithms are used for sub-optimisation. For piezoelectric fan performance, RSM-based optimisation techniques can significantly improve the design efficiency and help identify global optima, filter numerical noise and realise design optimisation.

5.2.1 Types of RSM Model

There are different types of surrogate models, such as RSM, kriging, Gradient-Enhanced Kriging (GEK), support vector machines, space mapping, and artificial neural

networks. In this chapter, two popular techniques are discussed: First-Order RSM and polynomial RSM (Second-Order RSM) (Box and Wilson, 1992). RSM-based model is essentially a polynomial approximation model, in which the sampled data is fitted by a least-square regression technique.

For an m-dimensional problem, the prediction of the output with high-fidelity is assumed, and it is correspondent to an unknown function y: $\mathbb{R}^m \to \mathbb{R}$. By running the CFD code, y is observed at n sites:

$$\mathbf{S} = [\mathbf{x}^{(1)}, \mathbf{x}^{(2)}, \dots, \mathbf{x}^{(n)}]^{\mathrm{T}} \in \mathbb{R}^{n \times m}, \mathbf{x} = [x^{(1)}, x^{(2)}, \dots, x^{(n)}]^{\mathrm{T}} \in \mathbb{R}^m \quad (5\text{-}1)$$

with the corresponding responses:

$$\mathbf{y}_s = [y^{(1)}, \dots, y^{(1)}]^{\mathrm{T}} = [y(\mathbf{x}^{(1)}), \dots, y(\mathbf{x}^{(n)})]^{\mathrm{T}} \in \mathbb{R}^n \quad (5\text{-}2)$$

The pair $(\mathbf{S}, \mathbf{y}_s)$denotes the sampled data sets in the vector space. With the above descriptions and assumptions, the objective is to build a RSM-based model for predicting the output for any untried site x based on the sampled data sets $(\mathbf{S}, \mathbf{y}_s)$ to achieve the desired accuracy.

The RSM can be written in the following form:

$$\mathrm{y}(\mathbf{x}) = \hat{y}(\mathbf{x}) + \varepsilon, \mathbf{x} \in \mathbb{R}^m \quad (5\text{-}3)$$

where $\hat{y}(\mathbf{x})$ is the polynomial approximation, and ε is the random error. In RSM-based optimisation, the data is assumed to be normally distributed with mean value of zero, and the variance is σ^2 (Han and Zhang, 2012). At each observation, the error ε is independent and identically distributed.

(1) First-order response surface method

Before the peak of the response surface is reached, a small local experiment is conducted to assess the local terrain. If the local experiment is not in the vicinity of the peak, then a first-order regression model provides an approximation to the local response surface. For m factors, the standard first-order model is a first-order polynomial regression model:

$$\hat{y}(\mathbf{x}) = \beta_0 + \sum_{i=1}^{m} \beta_i x_i \quad (5\text{-}4)$$

The parameter β_i is a measure of the local linear effect of the ith factor (i = 1,2,..m). A design for estimating the parameters of a first-order model is called a first-order design. A first-order design should allow (i) efficient estimation of each linear effect β_i, (ii) a test for lack of fit of the first-order model, and (iii) be expandable to a good second-order design.

As long as no significant model lack of fit exists with significant linear effects, the

fitted first-order model can be used to estimate the path of steepest ascent. If there is significant lack of fit of the first-order model, then additional observations may be collected to augment the first-order design so that a second-order polynomial regression model can be fitted to the data.

If there is no significant model lack of fit and also no significant linear effects, then it requires more data to increase the precision of the parameter estimators. Alternatively, the experimenters may need to change the factors under study or increase the range of levels.

(2) Quadratic response surface method

In RSM-based optimisation applications, it can smooth out the various scales of numerical noise in the data while capturing the global trend of the variation, which makes it very robust and thus well suited for optimisation problems in engineering design (Han and Zhang, 2012). Compared with the first order or higher order polynomial models, the "quadratic" polynomial model serves as a compromise between the modelling accuracy and the computational cost. In particular, the quadratic RSM predictor $\hat{y}(\mathbf{x})$ is defined as:

$$\hat{y}(\mathbf{x}) = \beta_0 + \sum_{i=1}^{m} \beta_i x_i + \sum_{i=1}^{m} \beta_{ii} x_i^2 + \sum_{i=1}^{m} \sum_{j \geq i}^{m} \beta_{ij} x_i x_j, \tag{5-5}$$

where β_0, β_i, β_{ii} and β_{ij} are unknown coefficients. In Eq. (5-5), there are totally $p = (m+1)(m+2)/2$ unknown coefficients, and it requires at least p sample points to build a quadratic RSM with m factors. Let $\boldsymbol{\beta} \in \mathbb{R}^p$ be the column vector contains these p unknown coefficients. The least square estimator of $\boldsymbol{\beta}$ is:

$$\boldsymbol{\beta} = (\mathrm{U}^{\mathrm{T}}\mathrm{U})^{-1}\mathrm{U}^{T}\boldsymbol{y_s}, \tag{5-6}$$

Where:

$$\mathrm{U} = \begin{bmatrix} 1 & x_1^{(1)} & \cdots & x_m^{(1)} & x_1^{(1)}x_2^{(1)} & \cdots & x_{m-1}^{(1)}x_m^{(1)} & \left(x_1^{(1)}\right)^2 & \cdots & \left(x_m^{(1)}\right)^2 \\ \vdots & \vdots & \ddots & \vdots & \vdots & \ddots & \vdots & \vdots & \ddots & \vdots \\ 1 & x_1^{(n)} & \cdots & x_m^{(n)} & x_1^{(n)}x_2^{(n)} & \cdots & x_{m-1}^{(n)}x_m^{(n)} & \left(x_1^{(1)}\right)^2 & \cdots & \left(x_m^{(n)}\right)^2 \end{bmatrix} \in \mathbb{R}^{n \times p}.$$

The approximated response $\hat{y}$ at any untried $\mathbf{x}$ can be predicted by Eq. (5-5), only when the coefficients in $\boldsymbol{\beta}$ are determined (Han and Zhang, 2012).

5.2.2 Application of RSM Model

In RSM-based optimisation, an initial surrogate is constructed using some of the available simulations. The remaining simulations are to determine the most promising surrogate model prediction. In Figure 5.1, the process usually takes the form of the

following iterative procedure. In the RSM-based optimisation, the cost function is a function to be maximum or minimum, and the Nusselt number is chosen in the present study. In the optimisation problems of piezoelectric fan, the values of several variables, such as the oscillating frequency, oscillating amplitude and wave number, are mapped onto a real number intuitively, representing some "cost" associated with the heat transfer characteristics.

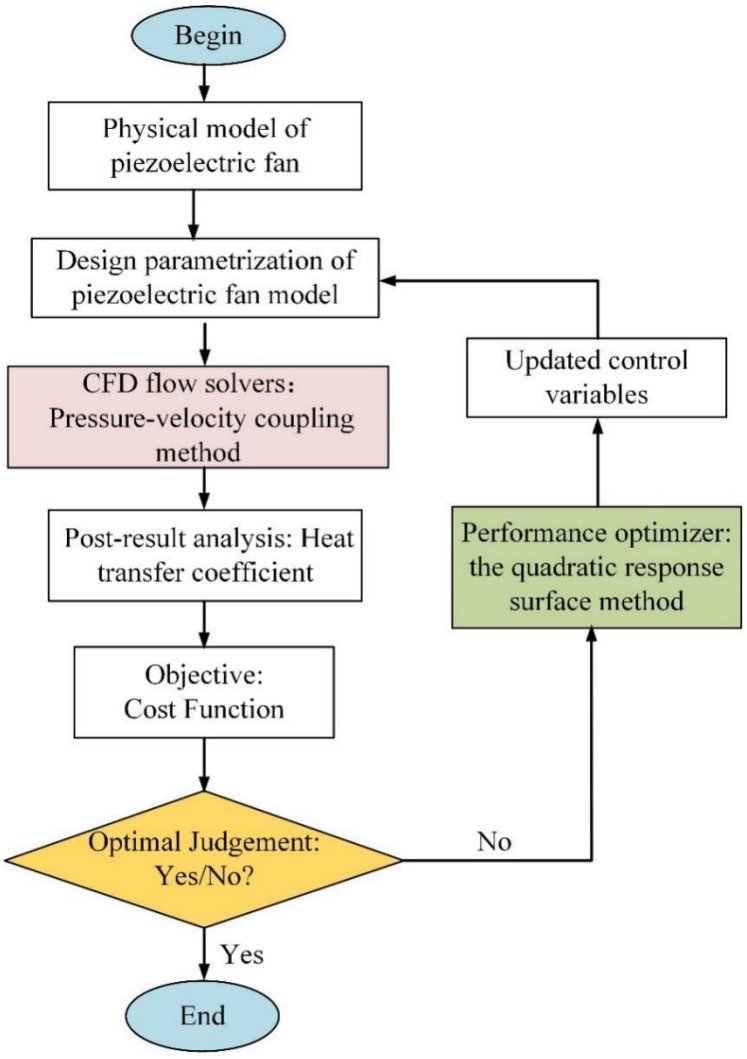

Figure 5.1: Optimisation loop of piezoelectric fan based on the response surface method

5.3 RSM-based optimisation of oscillating frequency

5.3.1 The gradient ascend method

The optimisation based first-order RSM, i.e. the method of gradient ascend, is then

used to analyse the performance of heat transfer. Gradient ascend is a first-order iterative optimisation algorithm for locating the maximum of a function. If the function $F(x)$ is differentiable in a neighbourhood of a point a, and $F(x)$ increases fastest if one goes from a in the direction of the positive gradient of F at a, then the gradient ascent is $\nabla F(a)$. If

$$a_{n+1} = a_n + \gamma \nabla F(a_n) \tag{5-7}$$

for γ small enough, then $F(a_n) \leq F(a_{n+1})$. The term $\gamma \nabla F(a)$ is subtracted from a, moving against the gradient, toward the maximum. Therefore, a guess x_0 is selected for a local maximum of F, and then the sequence x_0, x_1, x_2, …is built, such that:

$$x_{n+1} = x_n + \gamma_n \nabla F(x_n), n \geq 0. \tag{5-8}$$

Then it has,

$$F(x_0) \leq F(x_1) \leq F(x_2) \leq \cdots, \tag{5-9}$$

where the sequence (x_n) converges to the desired local maximum. To converge to a local maximum, the value of step size γ at each iteration is expressed as:

$$\gamma_n = \frac{(x_n - x_{n-1})^T [\nabla F(x_n) - \nabla F(x_{n-1})]}{\|\nabla F(x_n) - \nabla F(x_{n-1})\|^2} \tag{5-10}$$

When the function F is concave, all local maxima are global maxima, so the gradient ascent can converge to the global solution.

In Figure 5.2, this process is illustrated and F is assumed to be defined on the plane, and its graph has a bowl shape. The blue curves are the contour lines, and the values on these lines are constant. A black arrow originating at a point shows the direction of the positive gradient at that point. Note that the gradient at a point is orthogonal to the contour line going through that point. The gradient ascent leads to the bottom of the bowl, that is, to the point with the maximal value of the function F.

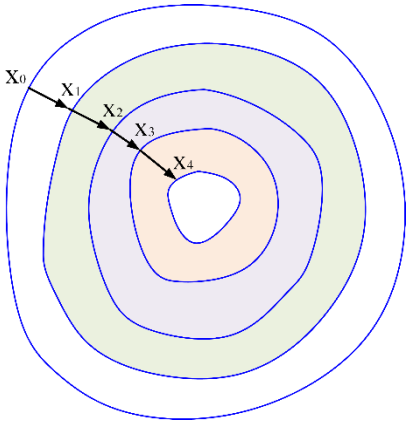

Figure 5.2: Illustration of gradient descent on a series of level sets

5.3.2 Optimisation analysis of the first-order RSM

In Figure 5.3, when the oscillating frequency changes from 2 Hz to 25 Hz, the mean Nusselt number changes approximately as a quadratic polynomial function. When the oscillating frequency increases, the flow field experiences more variations. Accordingly, there is a stronger interaction among the large circulation zones, and more small circulation zones are generated to mix the local fluids. Therefore, increasing the oscillating frequency can improve the performance of heat transfer.

The positive gradient of Nusselt number decreases with the frequency, which means that the heat transfer of piezoelectric fan cannot be improved as quickly as is desired when increasing the oscillating frequency further.

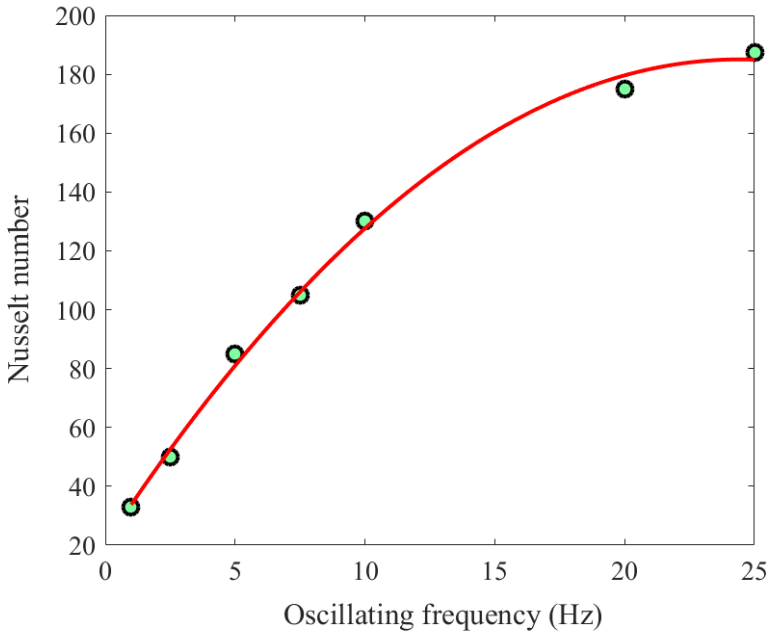

Figure 5.3: The Nusselt number varied with the oscillating frequency when A=0.02m and k=2

In Figure 5.4, the Nusselt number increases with the oscillating amplitude, and then reaches to a steady state. When the oscillating amplitude is close to 0.04 m, a slight decrease appears. It suggests that when the oscillating amplitude reaches a certain value, the performance of heat transfer cannot be further improved.

The numerical results show that the oscillating amplitude also has an influence on the number, sizes and locations of circulation zones, and the velocity of fluid flow increases with the amplitude. The growth potential of Nusselt number is relatively small when

compared with optimising the factor of oscillating frequency. The results indicate that the approach of increasing the frequency outperforms the amplitude in improving the performance of the PE fan. However, there are practical limitations under discussion subsequently.

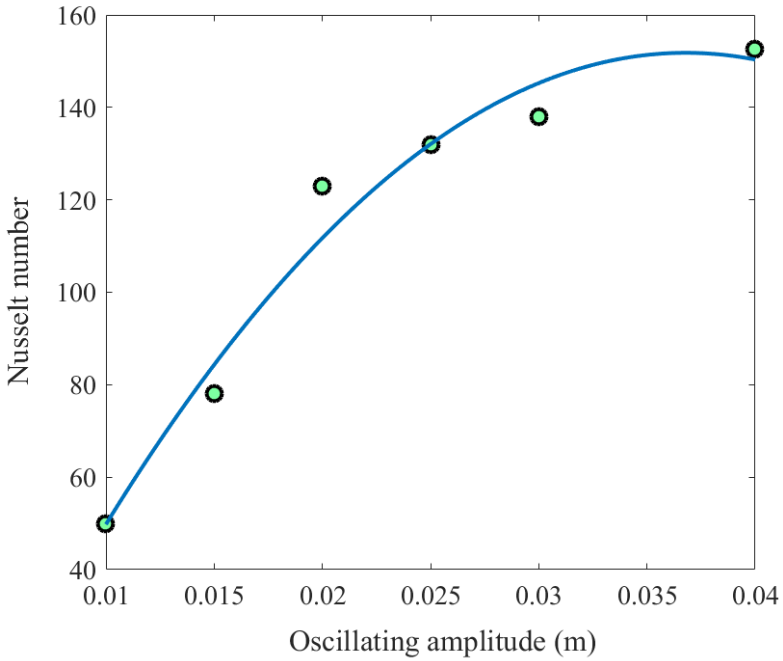

Figure 5.4: The Nusselt number varied with the oscillating amplitude when f=10 Hz and k=2

In Figure 5.5, a parabolic curve is used to express the relationship between the Nusselt number and the wave number. With the increase of wave number, the Nusselt number increases at first, and then decreases. It can be observed that a peak value appears when the wave number is around 8.

When the wave number changes from zero to non-zero value, the distribution of circulation zone locations turns from symmetrical to asymmetrical, and the tendency of flow transition to turbulence may be enhanced. However, when the wave number continues to increase, the fan deforms seriously, and the performance of heat transfer decreases. The large deformation of the fan blade associated with large wave numbers will induce fluid flow that demotes the fluid mixing near the hot surface, leading to weakened heat transfer.

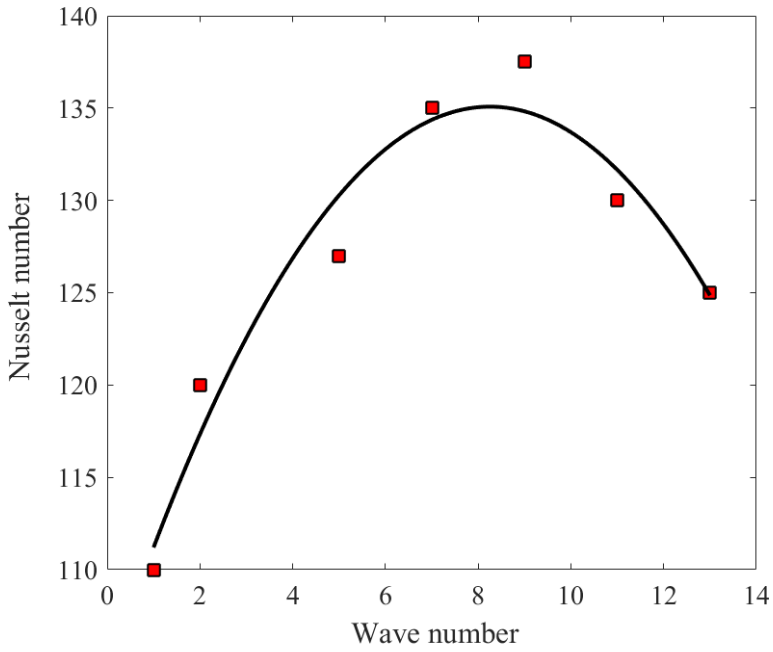

Figure 5.5: The Nusselt number varied with wave number when f=10 Hz and A=0.02m

5.4 Design of piezoelectric fan with geometry and materials

In terms of design optimisation and blade material properties, the geometric characteristics are the fundamental parameters. They govern the operational characteristics: frequency, amplitude and wave number. For optimal performance of the PE fan cooling, it seems that both oscillation frequency and amplitude should be maximised for a typical application. Achieving this, however, may be difficult and a compromise may be required.

Yoo et al. (2000) define the resonant frequency of piezoelectric fan, f_r, which is shown below:

$$f_r = G\frac{t_h}{L^2}\sqrt{\frac{E}{12\rho(1-\sigma^2)}} \tag{5-11}$$

where ρ is the density of fan material;

σ is the Poisson's ratio of fan material;

E is the Young's modulus of fan material;

L is the length of piezoelectric fan;

t_h is the thickness;

G is a coefficient, theoretically equal to 0.125π.

From the Eq. (5-11), it can be observed that the width of piezoelectric fan is independent of the oscillating frequency, which also has been verified experimentally by

Kimber and Garimella (2009b). The blade width varied in two otherwise identical piezoelectric fans by 400%. The respective blades' resonant frequencies varied by 0.6%. Different from that, the resonant frequencies of viscoelastic fan are analysed in this study in terms of fan geometry and materials.

5.4.1 The geometry of piezoelectric fan

In the present study, a piezoelectric fan made of the material of PZT-5 (one type of Piezo Ceramics) (Yoo et al., 2000) is selected to study the relations between resonant frequency and geometrical parameters. The parameters of piezoelectric fan are listed in Table 5-2.

Table 5-1 The geometrical parameters of piezoelectric fan made of PZT-5 (Yoo et al., 2000)

Length (mm)	60
Density (kg/m^3)	7.5×10^3
Young's modulus (N/m)	0.66×10^{11}
Thickness (mm)	0.3-0.35
Poisson's ratio	0.35

In Figure 5.6, the resonant frequency of piezoelectric fan decreases with the fan length. Acikalin et al. (2004) showed this benefit of shorter blades outweighed the increased volume of air displaced by a longer blade through each oscillation cycle. A trial of two blades, 76.2mm and 68.6mm in length, with respective oscillation frequencies of 62Hz and 103Hz, yielded a displaced air volume performance differential of 10-20% in favour of the latter. Therefore, the piezoelectric fan with shorter length is widely considered to be more effective, where resonant frequencies are significantly greater.

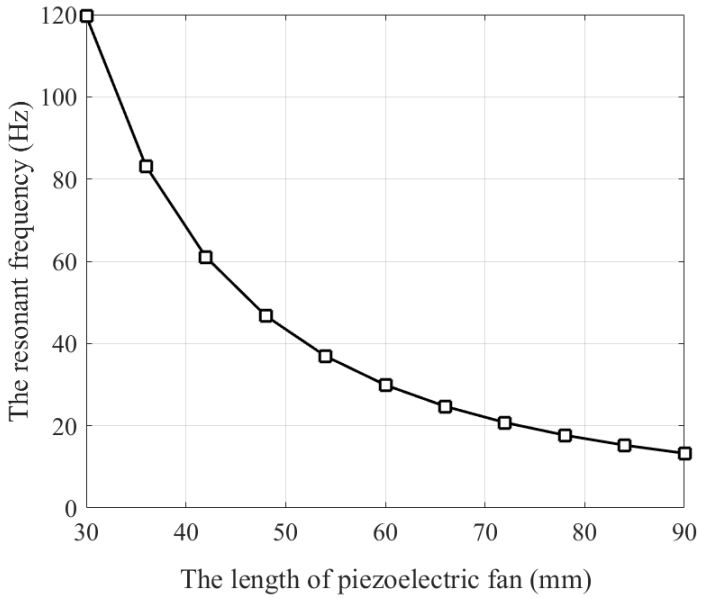

Figure 5.6: The rations between the resonant frequency and the length of piezoelectric fan

In Figure 5.7, it can be seen that the resonant frequency increases with fan thickness. Toda (1978) verified that blade width shared a proportional relationship with downstream airflow generation. Doubling width is shown to increase the average air velocity in the near and far field 110% and 105% respectively.

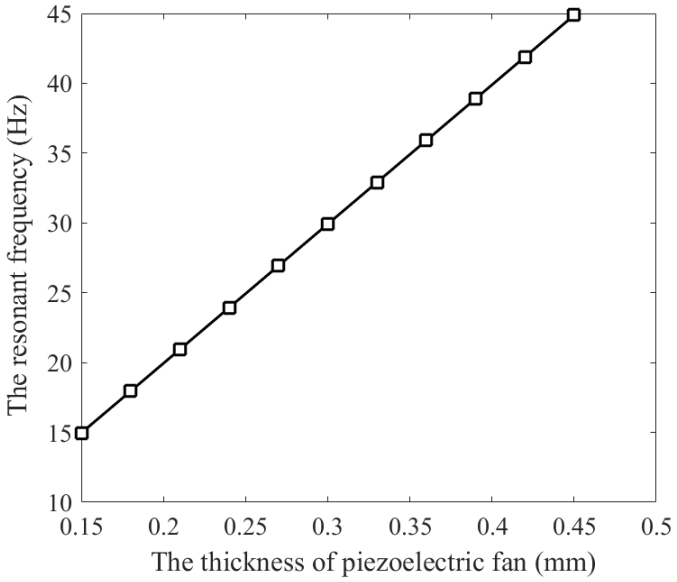

Figure 5.7: The rations between resonant frequency and the thickness of piezoelectric fan

Lin et al. (2016) proposed a simple geometry of piezoelectric fan, which is shown in Figure 5.8. It is described by four parameters: the full length of piezoelectric fan L, the

PZT length L_{PZT}, the full width of piezoelectric fan W and the PZT width W_{PZT}.

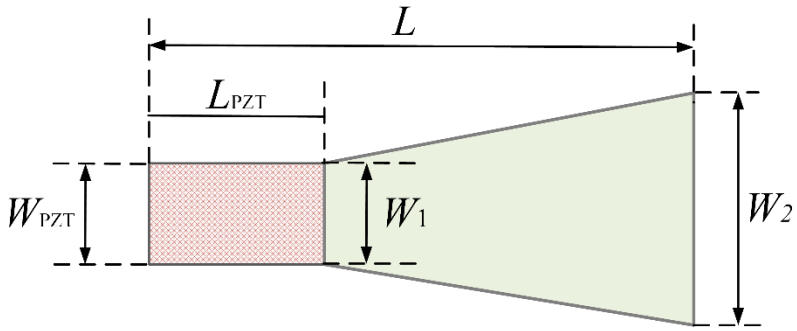

Figure 5.8: The geometry of piezoelectric fan proposed by Lin et al. (Lin et al., 2016)

Lin et al. (2016) considered several geometries of piezoelectric fan in Table 5-1. The results showed that the fan E had the highest resonant frequency, and the fan number D the lowest. When the width ratio, *W2/W1*, is less than unity, the mass of the blade creates a non-uniformly distributed load weighted towards the clamped end, and as such resonant frequency is increased (Liu et al., 2013; Gere and Timoshenko, 1997). Returning to blade shape considerations, Blade D required less power to achieve the same amplitude as Blade B, which has an equivalent face surface area. They also demonstrated that downstream airflow increases with oscillation frequency (Lin et al., 2016). It was observed that 17.3%, 36.7% and 47.7% increases in frequency induced a 22.4%, 49.3% and 97.0% increases in volume flow rate respectively.

Table 5-2 Dimensions of piezoelectric fan used by Lin et al. (2016)

Fan number	L/mm	L_{PZT}/mm	W_{PZT}/mm	W_1/mm	W_2/mm
A	76	29	12.7	12.7	12.7
B	76	29	12.7	19.1	19.1
C	76	29	12.7	25.4	25.4
D	76	29	12.7	12.7	25.4
E	76	29	12.7	25.4	12.7

5.4.2 The materials of piezoelectric fan

Material properties are also of great importance to the piezoelectric fan design optimisation, and density, Young's modulus, and Poisson's ratio can each be found in Eq. (5-11). Shyu and Syu (2014) found that the blade materials have a significant bearing on the performance of the piezoelectric fan. Heat transfer was enhanced by 225% when the mylar blade was used, but by just 105% and 60% for the aluminium and stainless-steel blades respectively.

Some metals and alloys are used for the PE fan, such as stainless steel, brass, bronze, phosphor bronze, phosphor copper and aluminium. The properties of some metals are shown in Table 5-3.

Table 5-3 Material properties of piezoelectric fan made of metals (Yoo et al., 2000)

PE fan	Density (kg/m^3)	Poisson's ratio	Young's modulus (N/m^2)
Brass	8.5×10^3	0.35	1.006×10^{11}
Aluminium	2.7×10^3	0.345	0.703×10^{11}
Bronze	8.8×10^3	0.33	1.078×10^{11}

Table 5-4 summarises the piezoelectric fan properties, while the distribution of resonance frequency is displayed in Figure 5.9. The PE fan should be light and flexible. Plastics available as foils can be suitable for this purpose. Metals like stainless steel are heavier due to higher density under the same geometry compared to plastics, but they can be processed into very thin blades.

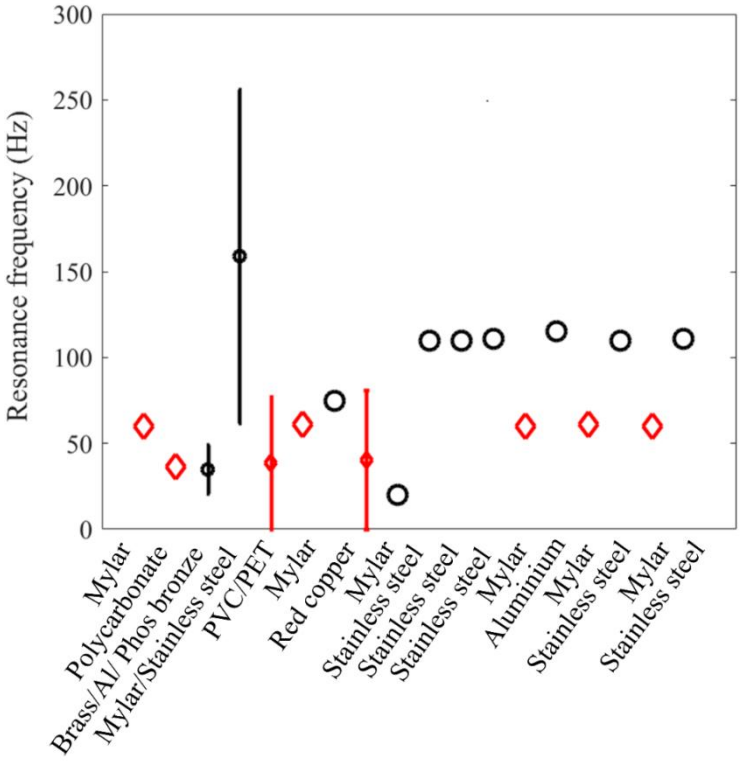

Figure 5.9: The resonance frequency of piezoelectric fan made of various materials in Table 5-4 from top to the bottom (red colour: plastic material; Black colour: metal material; The vertical bar means the changing range of resonant frequency)

Table 5-4 A summary of the reviewed piezoelectric fan properties and characteristics. NB: n/g: not given; PVC: polyvinyl chloride; PET: poly(ethylene) terephthalate. (Hales and Jiang, 2018b)

L, mm	W, mm	t_{BL}, mm	Material	L_{PZT}, mm	f_r, Hz	A, mm
64	12.7	n/g	Mylar	n/g	60	7.5
75	12.7	0.3	Polycarbonate	29	36.15	7.94
60.6-81	12-22	0.08-0.15	Brass/Al/ Phos bronze	32-35	10-60	5.5
14.9-36.5	6.35-25.4	n/g	Mylar/Stainless steel	n/g	61.7-256.2	2.5
76	12.7-25.4	0.2-0.5	PVC/PET	29	23.2-53.9	6.35
68.5	12.7	0.27	Mylar	32	61	4
20	n/a	0.1	Red copper	n/a	75	2.5
61-75	12-37	0.188-0.25	Mylar	n/g	28-53	3
50-63.5	10	0.076-0.13	Brass/ Stainless steel	n/g	20	15
47	12	0.4	Stainless steel	24	110	n/g

47	12	0.4	Stainless steel	24	110	4
47	12	0.4	Stainless steel	24	111	4.5
64	12.7	n/g	Mylar	n/g	60	6.35
47	12	0.4	Aluminium	n/g	115	n/g
68.5	12.7	0.27	Mylar	32	61	4
72	12.5	0.075	Stainless steel	24	110	6.25
64	12.7	n/g	Mylar	n/g	60	10
47	12	0.4	Stainless steel	24	111	5.01

The mechanical properties of fan material are described by three parameters: density, Poisson's ratio and Young's modulus. The piezoelectric fan with constant length 60mm and constant thickness 0.3mm can also help explore the relations between the resonance frequencies and the mechanical properties (Yoo et al., 2000).

In Figure 5.10, the results show that the resonant frequency decreases with the density of piezoelectric fan. It suggests that the piezoelectric fan should be designed as light as possible.

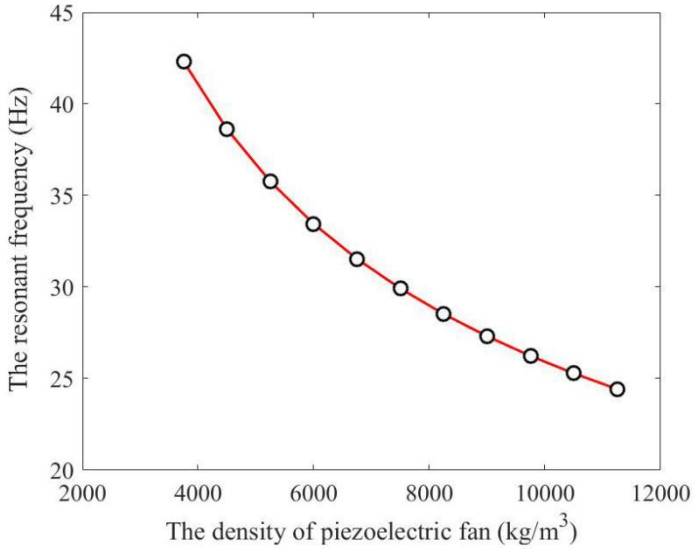

Figure 5.10: The rations between the resonant frequency and the density of piezoelectric fan

In Figure 5.11, the resonant frequency increases with the Poisson's ratio of fan materials, but the influence is relatively weak. For different types of materials, the Poisson's ratio has a small difference, which is also shown in Table 5-3. Therefore, the Poisson's ratio can be regarded as a secondary factor for designing a piezoelectric fan.

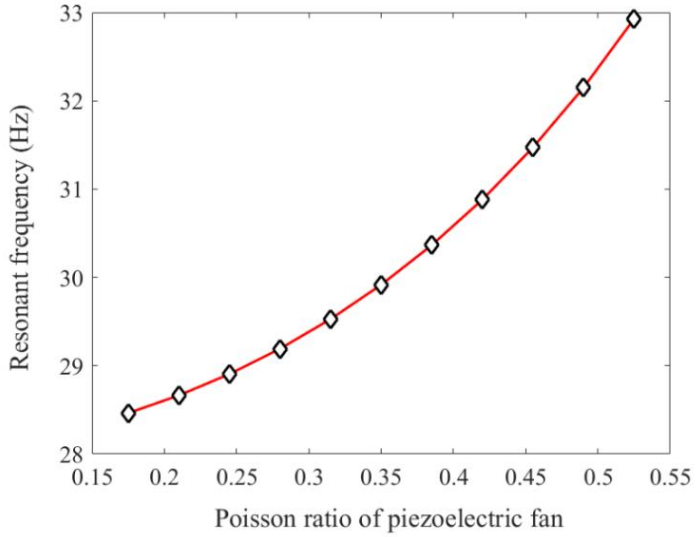

Figure 5.11: The rations between the resonant frequency and the Poisson's ratio of piezoelectric fan

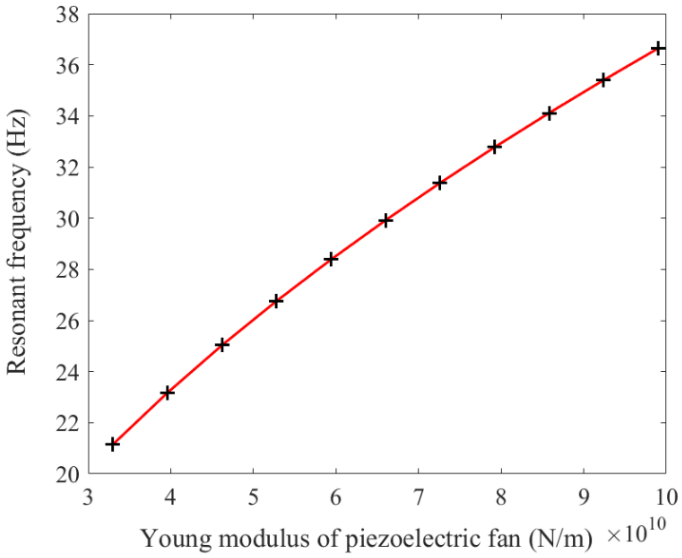

Figure 5.12: The rations between the resonant frequency and Young's modulus of piezoelectric fan

The influence of Young's modulus on the resonant frequency is shown in Figure 5.12. The resonant frequency increases with the Young's modulus of fan material. In general, taking metal materials as an example, the resonant frequency varies significantly with the Young's modulus, rather than the Poisson's ratio and the density, as shown in Table 5-3. It suggests that the Young's modulus of fan material is the primary factor for designing the piezoelectric fan.

5.4.3 Other geometrical considerations

The discussions on piezoelectric fan so far are mainly limited to a single blade. In practical applications, single blade fans can be effective in cooling of hot spots. In many practical applications, PE fans with multiple blades may be necessary if the cooling requirements are more demanding or more complex. In the present time, axial fans which can generate a volumetric airflow to transfer the heat of power electronics are regarded as the state-of-the-art in industry. The design and development of PE fans naturally aim at replacing these axial fans directly. When implemented into electrical components, the axial fans are often encased in cuboidal outer shells with limited space (Ihara and Watanabe, 1994; Yamada et al., 1988). In a multiple PE fan array, the separation distance from one fan to the next is defined by pitch, which is determined by their adjacent faces (face-to-face orientation, where the PE fan blades are parallel) or edges (edge-to-edge orientation, where the PE fan blades are in-line). The previous literature showed that face-to-face orientation is suitable for confining the array boundaries to a volume of comparable height and width, but that edge-to-edge orientation is preferable for minimising either the height (Sufian et al., 2014; Kimber et al., 2006).

The face-to-face orientation is preferable to replace a single axial fan. Stacked edge-to-edge orientation can also provide an alternative design with equivalent geometry to a face-to-face array containing a larger number of individual fans. For instance, a 3×3 stacked edge-to-edge array may be preferable in a certain situation to a face-to-face array containing nine blades adjacent to one another. The specific case of computer cooling usually presents a situation of confinement due to the base and lid walls.

The blade edges are confined regarding face-to-face orientation. The air is less able to move around the blade edges, from the leading to trailing face during oscillation. Such confinement may enhance the airflow generation along with the power required to drive the fan to the same amplitude of oscillation (Eastman and Kimber, 2014b; Eastman and Kimber, 2014a). There is an ample supply of air which can be driven downstream, because the blade's faces are unconfined. For the operation of face-to-face array, the air supply is severely inhibited as the blade's faces are effectively confined by the adjacent blades in an array. Thus, oscillation phase, plays a critical role in designing clamps and mounts as air must be supplied solely from the upstream direction.

For edge-to-edge orientation, the blade's faces are confined by the top and bottom

walls of the cooling space. Previous studies show that it will be more detrimental to performance than edge confinement (Acikalin et al., 2004). When the blade's faces were closely confined, performance was recorded to be just 20% compared to an equivalent array performing in unconfined conditions (Kimber et al., 2009b). Additionally, utilising available volume of the cooling space would require the stacked edge-to-edge orientation or a very large oscillation amplitude. Stacked edge-to-edge orientation may be preferable to edge-to-edge orientation, but still requires confinement of blade faces.

Phase of adjacent blades must be considered regarding face-to-face orientation. In terms of the generated airflow, two blade arrays with differing pitches can be divided into oscillating in-phase (IP) and counter-phase (CP). The previous literature showed that IP oscillation of all the blades is optimal in a face-to-face array (Ihara and Watanabe, 1994). However, the air supply to fan blades is the factor limiting array performance. It is evident that CP oscillation outperforms IP regarding all pitches trailed (Hales and Jiang, 2018a). The CP model outperformed the comparative IP setup, and CP oscillation will be solely considered during the optimisation. For the edge-to-edge orientation, the CP oscillation is optimal for maximising blade tip amplitude (Kimber et al., 2009a).

Besides, minimalising the number of fans also generates great benefits to the manufacture. Producing fewer blade-type air-movers will reduce time for manufacture and material and labour costs. A two-blade array will theoretically demand a slightly greater power input. Initial calculations suggest reducing the fan number by 33% increases the power demand by 4.2%. The primary aim of design optimisation is to generate the maximum volumetric airflow from a given geometric volume.

The design objective of PE fans is to replace the currently used axial fans, achieving massive reduction in energy consumption as well as reduction in noise generation. Previous studies suggested they can save over 90% energy for the thermal management system (Hales and Jiang, 2018a). An issue to manufacture a prototype array is air entrapment between adjacent blades, which inhibits the performance of the array. The effect of air entrapment can be reduced by ensuring a strong passage for airflow from the upstream direction. There are many issues that need to be considered in practical design, which has to accommodate various influencing factors present in the specific application.

5.5 Summary

In this chapter, the response surface methodology (RSM) explores the optimal

performance of heat transfer. Based on the analysis of the relationships among Nusselt number and several variables of fan movements, results show that the performance of piezoelectric fan can be improved through increasing the frequency and amplitude, but the trend diminishes at a later stage at higher values. Different from that, when the wave number varies from 0 to 13, the changing pattern of Nusselt number is approximately a parabolic function.

To obtain different resonant frequencies of piezoelectric fan, some design principles are discussed regarding the geometry and materials. For the geometry of PE fan, the resonant frequency of piezoelectric fan decreases with the fan length but increases with the thickness. For the fan material, the results show that the resonant frequency increases with Young's modulus of fan material and Poisson's ratio, but decreases with the density. These principles are also applicable in guiding the design of piezoelectric fan with desired resonant frequency, which are closely related to the characteristics of heat transfer.

The optimisation of PE fan performance is a complex task. The study performed in this Chapter can be considered as a first step towards this task. Further optimisation will have to involve multiple parameters with their interactions taken into consideration as well as linking the theoretical optimisation with the practical limitations associated with geometrical and materials aspects.

Chapter 6

Conclusion and Future work

6.1Conclusion

Energy consumption worldwide is increasing, especially for power electronics such as computers and servers. The energy consumed for cooling already accounts for a large proportion of the total energy consumption. Thus, the thermal management for energy use becomes ever more relevant. The piezoelectric fan has a huge advantage in low energy consumption compared with the currently used air movers such as traditional axial fans, which reduces the energy consumption by more than 90% (Sauciuc and Gupta, 2012). However, there is no ready-made PE fan products for power electronics cooling. There is also a lack of understanding on the cooling mechanism. As piezoelectric fans generate air flow via an intrinsic oscillation of the blades, energy consumption drops sharply. This advantage makes PE fan potentially an alternative and effective cooling technology, especially for computers and data centres. In spite of its huge potential in cooling power electronics, the mechanisms of the PE fan have not been fully understood and there is no mature product available in the market for the cooling of electronic devices of compact size. Thus, investigating and studying the movements of PE fan, the fluid flow and heat transfer associated with the PE fan motions are essential and urgent due to the increasing energy consumption of power electronics. Although the motions of piezoelectric are complex, the dynamics can be analysed theoretically. Chapter 2 presents a theoretical analysis of PE fan motions. The piezoelectric fan is simplified as a viscoelastic beam in this thesis, and its deformation motions are further decomposed into the pure travelling wave and the pure standing wave by the method of complex orthogonal decomposition. The travelling index is to analyse the curvature of the deformed piezoelectric fan. Further, a CFD model of vibrating piezoelectric fan is to investigate the fluid flow and heat transfer characteristics. The CFD study is based on the LES approach, to better account for the unsteadiness in the fluid flow. The simulations have focused on investigating the effects of the PE fan vibrating frequency, the vibrating amplitude and the travelling index. Finally, the quadratic response surface method (RSM) helps analyse the influence of these factors

and optimise the heat transfer of piezoelectric fan. As the theoretical optical parameters may not be achievable in practical applications, the optimisation study also tries to link the theoretical optimisation with the practical aspects of PE fans.

6.2 The new contribution to knowledge of the thesis

This section summarises the new contribution in the thesis, concluded from the previous Chapters:

(1) The piezoelectric fan is simplified as a homogeneous viscoelastic beam with uniform cross-section. The added mass models the interaction between fan and surrounding air-flow. The results show that: (1) when the dynamic model of piezoelectric fan is a proportional damping system, the standing wave is generated from the real mode of vibration modal; (2) when the dynamic model is a non-proportional damping system, the travelling wave is produced from the complex mode of vibration modal. The motions of piezoelectric fan are decomposed into the travelling and standing components by the method of complex orthogonal decomposition (COD). The travelling index is to evaluate the curviness of piezoelectric fan.

(2) A three-dimensional CFD model of piezoelectric fan serves the purpose of investigating the interactions between the movements of piezoelectric fan and the surrounding air-flow, using the LES method. To avoid the complex re-meshing process, the displacement of piezoelectric fan is replaced by its velocity profile, which is described by the frequency, the amplitude and the wave number. The numerical results suggest that the large circulation zones and the small vortices in the flow field are significantly affected by the motions of piezoelectric fan, which are also closely related to the mixing in the flow field. It provides some insight into the fluid flow that drives the heat transfer.

(3) A heat source with constant temperature 400K is added into the CFD model of piezoelectric fan to study the heat transfer of the cooling system. When the fan's movements taking place in ambient air, different types of recirculation zones are formed to mix the local fluid, which are closely related to the heat transfer. The heat transfer characteristics are studied in terms of the fan location, the oscillating frequency, the oscillating amplitude and the wave number, and evaluated by the averaged surface Nusselt number and the average temperature.

The results show that:

(a) The Nusselt number and the temperature are determined by the fluid flow

especially the circulation zones, which are closely related to the movements of the PE fan;

(b) The fan location at the inlet boundary has a significant influence on the heat transfer characteristics;

(c) The heat transfer has a strong dependence on oscillating frequency and amplitude, which can be enhanced by increasing the oscillating frequency or the oscillating amplitude for the parameter ranges under investigation. However, the wave number has a relatively weak influence.

(4) The response surface method (RSM) is demonstrated to optimise the heat transfer of piezoelectric fan. In the method, the sampled data is fitted by a least-square regression technique, and the polynomial model is applied in the RSM-based optimisation applications. RSM can smooth out the various scales of numerical noise in the data while captures the global trend of the variation, which makes it very robust and thus well suited for optimisation problems.

(5) Moreover, the influence of geometric optimisation and materials are also investigated. For the geometry of the PE fan, the resonant frequency of piezoelectric fan decreases with the fan length but increases with the thickness. For the fan material, the results show that the resonant frequency increases with Young's modulus of fan material and Poisson's ratio, but decreases with the density.

6.3 Future work

This thesis focuses on understanding the motions of piezoelectric fan and analysing the characteristics of heat transfer numerically. More could be done in the future for the development of the PE fan cooling system.

(1) Experiments of piezoelectric fan.

After the theoretical and numerical analyses of the PE fan, the optimised PE fan could be built and tested to further develop this novel cooling system. Moreover, the dynamic analysis of piezoelectric fan demonstrates that the deformed motions of piezoelectric fan can be regarded as the complex modal shapes of the vibrating beam. In designing experiments, the motions of piezoelectric fan could be controlled by adjusting the geometry parameters, the viscoelastic properties of fan materials (the elastic and viscosity) and the actuation conditions. Only when the desired motion is obtained, the best performance of heat transfer or cooling may be achieved for the cooling system.

(2) Multiple piezoelectric fan system.

A single piezoelectric fan is studied in this thesis, in terms of its dynamics and heat transfer characteristics. Hot-spot cooling is one of the applications for single PE fan. In practical applications, multiple fan arrays may enjoy wide application, when considering the cooling of more complex systems. The multiple piezoelectric fans involve more geometrical parameters compared with single piezoelectric fan; accordingly, the fluid flow and heat transfer can be more complex. The mechanisms of fluid flow and heat transfer of multiple piezoelectric fan system for cooling have not been well investigated. In addition, the fluid-structure interactions among the multiple piezoelectric fans have not been well understood.

(3) Further optimisation of piezoelectric fan.

With optimisation in Chapter 5, there will be an optimal result of best combination of oscillating frequency, oscillating amplitude and wave number. Moreover, based on the design optimisation discussion in Chapter 5, if the best combination could not be reached due to the limitations in practice such as the available space for installation, blade geometries and orientations and materials, then there is still need for the optimisation exercise to identify the practical optimal values after considering all the practical restrictions.

Bibliography

Acikalin, T., Garimella, S. V., Petroski, J. & Raman, A. Optimal design of miniature piezoelectric fans for cooling light emitting diodes. Thermal and Thermomechanical Phenomena in Electronic Systems, 2004. ITHERM'04. The Ninth Intersociety Conference on, 2004. IEEE, 663-671.

Acikalin, T., Garimella, S. V., Raman, A. & Petroski, J. 2007. Characterization and optimization of the thermal performance of miniature piezoelectric fans. *International Journal of Heat and Fluid Flow,* 28(4), 806-820.

Acikalin, T., Raman, A. & Garimella, S. V. 2003. Two-dimensional streaming flows induced by resonating, thin beams. *The Journal of the Acoustical Society of America,* 114(4), 1785-1795.

Acikalin, T. 2007. *Thermal and fluidic characterization of piezoelectric fans.* Purdue University.

Acikalin, T., Wait, S. M., Garimella, S. V. & Raman, A. 2004. Experimental investigation of the thermal performance of piezoelectric fans. *Heat Transfer Engineering,* 25(1), 4-14.

Agency, I. E. 2010. *Key world energy statistics 2010*: OECD Publishing.

Balay, S., Gropp, W. D., McInnes, L. C. & Smith, B. F. 1997. Efficient management of parallelism in object-oriented numerical software libraries. *Modern software tools for scientific computing.* Springer.

Basak, S. & Raman, A. 2007. Hydrodynamic coupling between micromechanical beams oscillating in viscous fluids. *Physics of Fluids,* 19(1), 017105.

Bergman, T. L., Incropera, F. P., DeWitt, D. P. & Lavine, A. S. 2011. *Fundamentals of heat and mass transfer*: John Wiley & Sons.

Bidakhvidi, M. A., Vanlanduit, S., Shirzadeh, R. & Vucinic, D. Experimental and Computational Analysis of the Flow Induced by a Piezoelectric Fan. Proceedings of the 15th International Symposium on Flow Visualization, Minsk, Belarus, 2012.

Box, G. E. P. & Wilson, K.B. 1951. On the Experimental Attainment of Optimum Conditions (with discussion). *Journal of the Royal Statistical Society* Series B 13(1):1–45.

Box, G. E. & Wilson, K. B. 1992. On the experimental attainment of optimum conditions. *Breakthroughs in statistics.* Springer.

Burmann, P., Raman, A. & Garimella, S. V. 2002. Dynamics and topology optimization of piezoelectric fans. *IEEE Transactions on Components and Packaging Technologies,* 25(4), 592-600.

Cengel, Y. A. & Pérez, H. 2004. Heat transfer: a practical approach. transferencia de calor.

Challa, V. R., Prasad, M., Shi, Y. & Fisher, F. T. 2008. A vibration energy harvesting device with bidirectional resonance frequency tunability. *Smart Materials and Structures,* 17(1), 015035.

Choi, M., Cierpka, C. & Kim, Y.-H. 2012. Vortex formation by a vibrating cantilever. *Journal of Fluids and Structures,* 31, 67-78.

Curie, J. & Curie, P. 1880. Sur l'électricité polaire dans les cristaux hémièdre à faces inclinées. Présentée par M. Desains. *Comptes rendus de lAcadémie des sciences,* 91, 383-386.

Deardorff, J. W. 1970. A numerical study of three-dimensional turbulent channel flow at large Reynolds numbers. *Journal of Fluid Mechanics,* 41(2), 453-480.

Dimarogonas, A. D. 1996. *Vibration for engineers*: Prentice Hall.

Eastman, A. & Kimber, M. L. 2014a. Aerodynamic damping of sidewall bounded oscillating cantilevers. *Journal of Fluids and Structures,* 51, 148-160.

Eastman, A. & Kimber, M. L. 2014b. Flow shaping and thrust enhancement of sidewall bounded oscillating cantilevers. *International Journal of Heat and Fluid Flow,* 48, 35-42.

Feeny, B. 2008. A complex orthogonal decomposition for wave motion analysis. *Journal of Sound and Vibration,* 310(1-2), 77-90.

Feeny, B. 2013. Complex modal decomposition for estimating wave properties in one-dimensional media. *Journal of Vibration and Acoustics,* 135(3), 031010.

Gartner, I. September 29, 2010. Stamford, CT. *Press release*.

Gautschi, G. 2002. Piezoelectric sensors. *Piezoelectric Sensorics.* Springer.

Gere, J. & Timoshenko, S. 1997. Mechanics of materials, 1997. *PWS-KENT Publishing Company, ISBN 0,* 534(92174), 4.

Germano, M., Piomelli, U., Moin, P. & Cabot, W. H. 1991. A dynamic subgrid-scale eddy viscosity model. *Physics of Fluids A: Fluid Dynamics,* 3(7), 1760-1765.

Gilson, G. M., Pickering, S. J., Hann, D. B. & Gerada, C. 2013. Piezoelectric fan cooling: A novel high reliability electric machine thermal management solution. *IEEE Transactions on Industrial Electronics,* 60(11), 4841-4851.

Hales, A. & Jiang, X. 2018a. Geometric Optimisation of Piezoelectric Fan Arrays for Low Energy Cooling. *In 20th International Conference on Applied Energy*.

Hales, A. & Jiang, X. 2018b. A review of piezoelectric fans for low energy cooling of power electronics. *Applied Energy,* 215, 321-337.

Han, Z.-H. & Zhang, K.-S. 2012. Surrogate-based optimization. *Real-world applications of genetic algorithms.* InTech.

Horvath, A. & Masanet, E. 2007. An analysis of measures to reduce the life-cycle energy consumption and greenhouse gas emissions of California's personal computers.

Ihara, A. & Watanabe, H. 1994. On the flow around flexible plates, oscillating with large amplitude. *Journal of Fluids and Structures,* 8(7), 601-619.

Kim, B.-J., Rho, J.-S. & Jung, H.-K. 2005. Optimal design of piezoelectric cantilever fan by three-dimensional finite element analysis. *KIEE International Transactions on Electrical Machinery and Energy Conversion Systems,* 5(1), 90-94.

Kim, J. & Moin, P. 1985. Application of a fractional-step method to incompressible Navier-Stokes equations. *Journal of computational physics,* 59(2), 308-323.

Kim, Y.-H., Wereley, S. T. & Chun, C.-H. 2004. Phase-resolved flow field produced by a vibrating cantilever plate between two endplates. *Physics of fluids,* 16(1), 145-162.

Kimber, M. & Garimella, S. V. 2009a. Cooling performance of arrays of vibrating cantilevers. *Journal of Heat Transfer,* 131(11), 111401.

Kimber, M. & Garimella, S. V. 2009b. Measurement and prediction of the cooling characteristics of a generalized vibrating piezoelectric fan. *International Journal of Heat and Mass Transfer,* 52(19-20), 4470-4478.

Kimber, M., Garimella, S. V. & Raman, A. An experimental study of fluidic coupling between multiple piezoelectric fans. Thermal and Thermomechanical Phenomena in Electronics Systems, 2006. ITHERM'06. The Tenth Intersociety Conference on, 2006. IEEE, 333-340.

Kimber, M., Lonergan, R. & Garimella, S. 2009a. Experimental study of aerodynamic damping in arrays of vibrating cantilevers. *Journal of Fluids and Structures,* 25(8), 1334-1347.

Kimber, M., Suzuki, K., Kitsunai, N., Seki, K. & Garimella, S. V. 2009b. Pressure and flow rate performance of piezoelectric fans. *IEEE transactions on components and packaging technologies,* 32(4), 766-775.

Kimber, M. L. & Garimella, S. V. Local heat transfer characteristics of flows induced by multiple piezoelectrically actuated vibrating cantilevers. ASME/JSME 2007 Thermal Engineering Heat Transfer Summer Conference collocated with the ASME 2007 InterPACK Conference, 2007. American Society of Mechanical Engineers, 149-158.

Koomey, J. 2011. Growth in data center electricity use 2005 to 2010. *A report by Analytical Press, completed at the request of The New York Times,* 9

Koomey, J. G. 2008. Worldwide electricity used in data centers. *Environmental research letters,* 3(3), 034008.

Li, X.-J., Zhang, J.-z. & Tan, X.-m. 2017. Convective heat transfer on a flat surface induced by a vertically-oriented piezoelectric fan in the presence of cross flow. *Heat and Mass Transfer,* 53(9), 2745-2768.

Lienhard IV, J. & Lienhard, J. 2008. A Heat Transfer Textbook. Phlogiston Press, Cambridge, MA.

Lighthill, M. J. 1971. Large-amplitude elongated-body theory of fish locomotion. *Proc. R. Soc. Lond. B,* 179(1055), 125-138.

Lilly, D. K. 1992. A proposed modification of the Germano subgrid-scale closure method. *Physics of Fluids A: Fluid Dynamics,* 4(3), 633-635.

Lin, C.-N., Jang, J.-Y. & Leu, J.-S. 2016. A Study of an Effective Heat-Dissipating Piezoelectric Fan for High Heat Density Devices. *Energies,* 9(8), 610.

Liu, S.-F., Huang, R.-T., Sheu, W.-J. & Wang, C.-C. 2009. Heat transfer by a piezoelectric fan on a flat surface subject to the influence of horizontal/vertical arrangement. *International Journal of Heat and Mass Transfer,* 52(11-12), 2565-2570.

Liu, T. J.-C., Chen, Y.-S., Ho, H.-Y., Liu, J.-T. & Lee, C.-C. 2013. Notes on vibration design for piezoelectric cooling fan. *World Academy of Science, Engineering and Technology-International Journal of Mechanical, Industrial Science and*

Engineering, 7, 798.

Ma, H., Chen, B., Lan, H., Lin, K. & Chao, C. Study of an LED device with vibrating piezoelectric fins. Semiconductor Thermal Measurement and Management Symposium, 2009. SEMI-THERM 2009. 25th Annual IEEE, 2009. IEEE, 267-272.

Ma, H., Liao, S., Li, Y., Li, Y. & Liu, C. The application of micro multiple piezoelectric-magnetic fans (m-MPMF) on LEDs thermal management. Semiconductor Thermal Measurement and Management Symposium (SEMI-THERM), 2014 30th Annual, 2014a. IEEE, 159-163.

Ma, H., Liu, C., Su, H. & Ho, W. Study of a cooling system with a piezoelectric fan. Semiconductor Thermal Measurement and Management Symposium (SEMI-THERM), 2012 28th Annual IEEE, 2012a. IEEE, 243-248.

Ma, H., Luo, W. & Su, H. A multiple vibrating-fan system using interactive magnetic force and piezoelectric force. Semiconductor Thermal Measurement and Management Symposium (SEMI-THERM), 2012 28th Annual IEEE, 2012b. IEEE, 238-242.

Ma, H., Su, H., Liu, C. & Ho, W. 2012c. Investigation of a piezoelectric fan embedded in a heat sink. *International Communications in Heat and Mass Transfer,* 39(5), 603-609.

Ma, H., Su, H. & Luo, W. 2013. Investigation of a piezoelectric fan cooling system with multiple magnetic fans. *Sensors and Actuators A: Physical,* 189, 356-363.

Ma, H., Tan, L., Li, Y. & Liu, C. 2014b. Optimum thermal resistance of the multiple piezoelectric–magnetic fan system. *International Communications in Heat and Mass Transfer,* 55, 77-83.

Maaspuro, M. 2016. Piezoelectric oscillating cantilever fan for thermal management of electronics and LEDs—A review. *Microelectronics Reliability,* 63, 342-353.

Manbachi, A. & Cobbold, R. S. 2011. Development and application of piezoelectric materials for ultrasound generation and detection. *Ultrasound,* 19(4), 187-196.

Meirovitch, L. 1967. *Analytical methods in vibrations*: Macmillan New York.

Meneveau, C. 2010. Turbulence: Subgrid-scale modeling. *Scholarpedia,* 5(1), 9489.

MIDE Technology. 2016. *Forced Convection with Solid State Piezoelectric Fan.* Available at: https://www.mide.com/collections/piezo-cooling-overview. (Accessed: 26 August 2017)

Orlanski, I. 1976. A simple boundary condition for unbounded hyperbolic flows. *Journal of computational physics,* 21(3), 251-269.

Park, J. & Kim, E. A Numerical Analysis In Piezoelectric Fan Systems For Cooling Of Electronic Devices. 2011 International Conference on Chemistry and Chemical Process IPCBEE vol. 10 (2011)©(2011) IACSIT Press, Singapore, 2011.

Petroski, J., Arik, M. & Gursoy, M. 2010. Optimization of piezoelectric oscillating fan-cooled heat sinks for electronics cooling. *IEEE Transactions on Components and Packaging Technologies,* 33(1), 25-31.

Pope, S. B. 2001. Turbulent flows. IOP Publishing.

Ramananarivo, S., Godoy-Diana, R. & Thiria, B. 2013. Passive elastic mechanism to mimic fish-muscle action in anguilliform swimming. *Journal of The Royal Society Interface,* 10(88), 20130667.

Ramananarivo, S., Godoy-Diana, R. & Thiria, B. 2014. Propagating waves in bounded elastic media: Transition from standing waves to anguilliform kinematics. *EPL (Europhysics Letters),* 105(5), 54003.

Sauciuc, I. & Gupta, A. April 25-26, 2012. Electronics cooling advancements, challenges and innovation needs: System/chip level thermal management. *In: 2nd Workshop on thermal management in telecommunication systems and data centers in Santa Clara, CA*.

Schmidt, R. Local and average transfer coefficients on a vertical surface due to convection from a piezoelectric fan. Thermal Phenomena in Electronic Systems, 1994. I-THERM IV. Concurrent Engineering and Thermal Phenomena., InterSociety Conference on, 1994. IEEE, 41-49.

Schmidt, R. 2005. Liquid cooling is back. *Electronics Cooling,* 11(3), 34-38.

Sheu, W.-J., Huang, R.-T. & Wang, C.-C. 2008. Influence of bonding glues on the vibration of piezoelectric fans. *Sensors and Actuators A: Physical,* 148(1), 115-121.

Shyu, J.-C. & Syu, J.-Z. 2014. Plate-fin array cooling using a finger-like piezoelectric fan. *Applied Thermal Engineering,* 62(2), 573-580.

Skoog, D. A., Holler, F. J. & Crouch, S. R. 2017. *Principles of instrumental analysis*: Cengage learning.

Smagorinsky, J. 1963. General circulation experiments with the primitive equations: I. The basic experiment. *Monthly weather review,* 91(3), 99-164.

Sri-Jayantha, S. M., McVicker, G., Bernstein, K. & Knickerbocker, J. U. 2008. Thermomechanical modeling of 3D electronic packages. *IBM Journal of Research and Development,* 52(6), 623-634.

Su, H., Liu, C., Pan, T. & Ma, H. Investigation of a multiple-vibrating fan system for electronics cooling. Semiconductor Thermal Measurement and Management Symposium (SEMI-THERM), 2013 29th Annual IEEE, 2013. IEEE, 110-115.

Sufian, S., Fairuz, Z., Zubair, M., Abdullah, M. & Mohamed, J. 2014. Thermal analysis of dual piezoelectric fans for cooling multi-LED packages. *Microelectronics Reliability,* 54(8), 1534-1543.

Timoshenko, S., Young, D. & Weaver, J. 1974. Vibration Problems in Engineering. *John Wiley and Sons, New York*.

Toda, M. 1978. Theory of air flow generation by a resonant type PVF2 bimorph cantilever vibrator. *Ferroelectrics,* 22(1), 911-918.

Toda, M. 1981. Voltage-induced large amplitude bending device-PVF2 bimorph-its properties and applications. *Ferroelectrics,* 32(1), 127-133.

Toda, M. & Osaka, S. 1979. Vibrational fan using the piezoelectric polymer PVF 2. *Proceedings of the IEEE,* 67(8), 1171-1173.

Turner, V., Bigliani, R. & Ingle, C. 2009. Reducing greenhouse gases through intense use of Information and Communication Technology: Part 1. *International Data Corporation (IDC). Retrieved August,* 2, 2014.

Yamada, Y., Fujimoto, K. & Inoue, J. 1988. Piezoelectric fan. Google Patents.

Yole Développement, 2016. Data Center Market and Technology Trends Power Electronics presentation held at APEC 2016 from Yole Développement. Available at: https://www.slideshare.net/Yole_Developpement (Accessed: 23 August 2017).

Yoo, J. H., Hong, J. I. & Cao, W. 2000. Piezoelectric ceramic bimorph coupled to thin metal plate as cooling fan for electronic devices. *Sensors and Actuators A: Physical,* 79(1), 8-12.

Yoo, J. H., Hong, J. I. & Park, C. Y. Characteristics of piezoelectric fans using PZT ceramics. Properties and Applications of Dielectric Materials, 1997., Proceedings of the 5th International Conference on, 1997. IEEE, 1075-1081.

Zhang, K., Xiao, D. G., Zhang, X., Fan, H., Gao, Z. & Yuen, M. M. Novel cooling solutions

for LED solid state lighting. Electronic Packaging Technology and High Density Packaging (ICEPT-HDP), 2011 12th International Conference on, 2011. IEEE, 1-5.